ΠΑΝΕΠΙΣΤΗΜΙΟ ΚΡΗΤΗΣ
UNIVERSITY OF CRETE

Τμήμα Χημείας
Πανεπιστήμιο Κρήτης
Department of Chemistry
University of Crete

Investigating the Occurrence and Fate of Metal Nanoparticles in Seawater Systems Using Single Particle Inductively Coupled Plasma - Mass Spectrometry

~ ~

Μελέτη της Παρουσίας και του Γίγνεσθαι Μεταλλικών Νανοσωματιδίων σε Θαλάσσια Συστήματα με τη Χρήση της Φασματομετρίας Μάζας - Επαγωγικά Συζευγμένου Πλάσματος Μεμονωμένων Σωματιδίων

Chronakis Michail Ioannis

Master's Degree Thesis

Supervising Professor: Spiros A. Pergantis

Contents

1. Abstract

1.1. Abstract

The use of Inductively Coupled Plasma – Mass Spectrometry (ICP – MS) in the analysis of metal content, in a wide range of different samples and matrices, is both widespread and well-known for decades. In cases of suspensions containing relatively low particle concentrations (~10^6 particles/ml), single particles can be detected as a result of the system's capability for very short reading time per datapoint. This parameter is called dwell time, and the technique is also known in the literature as single particle Inductively Coupled Plasma – Mass Spectrometry (sp – ICP – MS).

The following thesis is a presentation of the further development of a method for studying the presence and fate of metal – containing nanoparticles in seawater samples. This approach was subsequently applied on samples acquired for the needs of two different studies: First, from a mesocosm experiment in 2019, as part of a larger experiment taking place in Cretacosmos, the Greek branch of Aquacosm (EU network of mesocosms facilities). And second, from Santorini island, as part of a program investigating the occurrence and nature of nanoparticles in the proximity of islands (NanoIsland, ELIDEK) during different times throughout the year. For the needs of these analyses, in addition to the inductively coupled plasma mass spectrometry system, and the application of the single particle detection technique, an on-line dilution system was also incorporated.

For the mesocosm experiment two different types of samples have been investigated, spiked with low ppt concentrations of Ag nanoparticles and ionic Ag respectively. Also, two different dwell times have been used, and three different threshold criteria for the identification of particles have been applied. For the analysis of samples from seawater tanks spiked with Ag nanoparticles, analyzed using 10 ms dwell time, the μ + 3std threshold criterion proved suitable. ''μ'' stands for the average intensity value and std for the standard deviation of the dataset, after a process that is well documented in literature. For the analysis of samples from seawater tanks spiked with Ag nanoparticles, analyzed using 75 μs dwell time, a different kind of threshold has been proven more reliable. It is equal to $\mu + 2.71 + 3.29 * \sqrt{\mu}$, where ''μ'' stands for the mean intensity of the dataset, as it was mentioned before. For the analysis of samples from seawater tanks spiked with Ionic Ag, analyzed using 10 ms dwell time, both the μ + 3std and μ + 5std threshold criteria performed similarly well. And finally, for the analysis of samples from seawater tanks spiked with Ionic Ag, analyzed using 75 μs dwell time, the μ + 5std threshold proved sufficient. During the analysis of the samples from the ionic Ag spiked tanks, pulse events usually associated with particles were observed, whose nature and origin are addressed.

Regarding the NanoIsland samples, an investigation of temporal and spatial variations has been conducted, focusing on the occurrence and Cu content of Cu containing nanoparticles. The data processing of these samples incorporated a developing, python – based coding script, specifically made for the needs of this project. The processing revealed generally higher particle concentration in sites associated with boats activity during the

summer period. Also, particles with higher Cu content were generally found in deeper waters, while there have been indications about their precipitation, beginning around the same period as the high particle concentrations observed.

Finally, the system itself also exhibited sufficient ruggedness and the capability of continuous analysis for more than 10 hours of continuous operation, for a number of months, without significant equipment downtime, despite the aggressive seawater matrix.

1.2. Περίληψη

Η χρήση της φασματομετρίας μάζας επαγωγικά συζευγμένου πλάσματος (Inductively Coupled Plasma – Mass Spectrometry, ICP – MS) στην ανάλυση μετάλλων σε δείγματα πάσης φύσεως είναι ευρέως διαδεδομένη, και γνωστή εδώ και δεκαετίες. Σε περιπτώσεις σχετικά αραιών αιωρημάτων (~10^6 σωματίδια/ml), και εκμεταλλευόμενοι την δυνατότητα πολύ μικρών χρόνων καταγραφής, είναι δυνατόν να ανιχνευθούν μεμονωμένα σωματίδια (single particles). Η τεχνική αυτή είναι επίσης γνωστή στη βιβλιογραφία ως φασματομετρία μάζας επαγωγικά συζευγμένου πλάσματος μεμονομένων σωματιδίων (single particle – ICP – MS).

Στην παρούσα εργασία καταγράφεται η περαιτέρω ανάπτυξη μιας μεθόδου μελέτης της παρουσίας και κατά περίπτωση του γίγνεσθαι σωματιδίων που περιέχουν μέταλλα σε δείγματα θαλασσινού νερού. Η προσέγγιση αυτή ακολούθως εφαρμόστηκε σε δείγματα που ελήφθησαν από δύο διαφορετικές μελέτες: Πρώτον, από ένα πείραμα μεσοκόσμων το 2019, ως μέρος ενός μεγαλύτερου πειράματος που λάμβανε χώρα στο Cretacosmos, το ελληνικό τμήμα του Aquacosm (δίκτυο εγκαταστάσεων μεσοκόσμων της ευρωπαϊκής ένωσης). Και δεύτερον, απο τη Σαντορίνη, ως μέρος ενός προγράμματος που μελετά την παρουσία και τη φύση νανοσωματιδίων κοντά σε νησιά (NanoIsland, ΕΛΙΔΕΚ), σε διαφορετικές χρονικές περιόδους. Για τις ανάγκες των αναλύσεων αυτών, πέραν του συστήματος της φαματομετρίας μάζας επαγωγικά συζευγμένου πλάσματος και της εφαρμογής της τεχνικής της ανίχνευσης μεμονομένων σωματιδίων, χρησιμοποιήθηκε και ένα σύστημα εισαγωγής αραίωσης εντός ροής (on – line dilution).

Κατά το πείραμα των μεσοκόσμων, αναλύθηκαν δύο διαφορετικοί τύποι δειγμάτων, όπου είχε γίνει προσθήκη χαμηλών συγκεντρώσεων (ppt) νανοσωματιδίων αργύρου, και ιόντων αργύρου αντίστοιχα. Επιπλέον, χρησιμοποιήθηκαν δύο διαφορετικοί χρόνοι ανά καταγραφή (dwell times) και εφαρμόστηκαν τρία διαφορετικά κριτήρια για τον διαχωρισμο και την ταυτοποίηση σημάτων ως νανοσωματίδια. Για την ανάλυση των δειγμάτων θαλλασινού νερού, από τις δεξαμενές όπου είχε προστεθεί νανοσωματιδιακός άργυρος, και είχε χρησιμοποιηθεί 10 ms χρόνος ανά καταγραφή, το κριτήριο μ + 3std αποδείχτηκε κατάληλο. Το ''μ'' αντιστοιχεί στη μέση τιμή έντασης και το std στην τυπική απόκλιση του συνόλου των δεδομένων, όπως προκύπτουν μετά από ευρέως γνωστή στη βιβλιογραφία. Για την ανάλυση των δειγμάτων θαλλασινού νερού, από τις δεξαμενές όπου είχε προστεθεί νανοσωματιδιακός άργυρος, και είχε χρησιμοποιηθεί 75 μs χρόνος ανά καταγραφή, χρησιμοποιήθηκε ένα διαφορετικό κριτήριο, ίσο με $\mu + 2.71 + 3.29 * \sqrt{\mu}$, όπου ''μ'' είναι η μέση τιμή της έντασης του συνόλου των δεδομένων, όπως και πριν. Για την ανάλυση των δειγμάτων θαλλασινού νερού, από

τις δεξαμενές όπου είχαν προστεθεί ιόντα αργύρου, και είχε χρησιμοποιηθεί 10 ms χρόνος ανά καταγραφή, τα κριτήρια μ + 3std και μ + 5std ανταπεξήλθαν εξίσου καλά στην περιγραφή των δεδομένων. Και τέλος, Για την ανάλυση των δειγμάτων θαλλασινού νερού, από τις δεξαμενές όπου είχαν προστεθεί ιόντα αργύρου, και είχε χρησιμοποιηθεί 75 μs χρόνος ανά καταγραφή, το κριτήριο μ + 3 std αποδείχθηκε επαρκές. Κατά την ανάλυση των δειγμάτων από τις δεξαμενές όπου είχε προστεθεί μόνο ιοντικός άργυρος, εμφανίστηκαν παλμοί οι οποίοι συνήθως συσνετίζονται με την παρουσία σωματιδίων, των οποίων παλμών η φύση και προέλευση επίσης εξετάζονται.

Όσον αφορά τα δείγματα του NanoIsland,διενεργήθηκε μια τοπική και χρονική μελέτη γύρω από την παρουσία και το περιεχόμενο σωματιδίων που περιείχαν χαλκό. Η επεξεργασία των αποτελεσμάτων αυτών των δειγμάτων έγινε μέσω ενός αναπτυσσόμενου κομματιού κώδικα python, ειδικά φτιαγμένου για τις ανάγκες αυτής της εργασίας. Τα αποτελέσματα κατέδειξαν γενικά μεγαλύτερη σωματιδιακή συγκέντρωση σωματιδίων που περιέχουν χαλκό σε περιοχές που σχετίζονται με τη δραστηριότητα πλοίων, κατά την καλοκαιρινή περίοδο. Επιπλέον, σωματίδια με υψηλότερες ποσότητες χαλκού βρέθηκαν σε μεγαλύτερα βάθη, ενώ υπάρχουν ενδείξεις για καθίζηση τους, η οποία δείχνει ότι θα μπορούσε να ξεκνάει την ίδια περίοδο με την παρατήρηση των υψηλών σωματιδιακών συγκεντρώσεων.

Τέλος, το σύστημα φάνηκε να είναι ικανό για συνεχόμενη ανάλυση άνω των 10 ωρών, επί σειρά μηνών, χωρίς αξιοσημείωτη φθορά του εξοπλισμού, παρά την συνήθως σημαντικά επιζήμια μήτρα του θαλασσινού νερού.

2. Introduction

2.1. Nanomaterials

Nanomaterials occupy a prominent position in modern society and industry due to their many, varied and occasionally tuneable properties. This simple fact has understandably caused a rising interest in both their use, and consequently the study of their properties and effects under different circumstances.

2.1.1. Definition of Nanomaterials

''Nanomaterial'' seems like a self – explanatory term when it comes to everyday communication. However, in scientific literature, there is a much higher need for precision. That has led to a wide range of different definitions for ''nanomaterials''. Some of these terms refer to their size as a whole, while others only examine one or more of their dimensions. Other terms take into account weather the structure consists of discrete parts whose dimensions fall into the nano scale, accepting aggregates and agglomerates of nanoscale moieties as nanomaterial, regardless of their actual size. Moreover, the ''nanoscale'' itself is not well-defined, as the limits seem to change according to the needs of the study[1]. It is generally accepted, that any moiety that is 100 nm or less in one or more dimensions can be identified as ''nanomaterial'', while the lower limit is still somewhat unclear (from atomic level to 2 nm). Kreyling et al. (2010)[2] summarized the widely accepted terms and limits for nanomaterials, and even proposed a complementary definition based on volume specific surface area (VSSA), to clarify the nano- or larger materials' classification. As of 2011, the European Union has adopted the definition of ''nanomaterial as ''a natural, incidental or manufactured material containing particles, in an unbound state or as an aggregate or as an agglomerate and where, for 50 % or more of the particles in the number size distribution, one or more external dimensions is in the size range 1 nm -100 nm''.
In this study, any moiety smaller than 1 μm will be referred to as ''nano-''. In different parts of the study, the materials of interest will either be *engineered* (man – made, crafted for a specific purpose), *incidental* (their formation was man – facilitated, but their occurrence in the environment is unintentional) or *natural* (spontaneously formed through natural processes)[3].

2.1.2. Applications of Nanomaterials

Due to the wide variety of their properties, and their occasional superiority against other forms or species, more than one branches of modern life are incorporating, or even depend on, nanomaterials.
To start with, medicine, the cornerstone of human health and well – being, has benefitted greatly from advances in nanomaterial science (*Figure 1*).

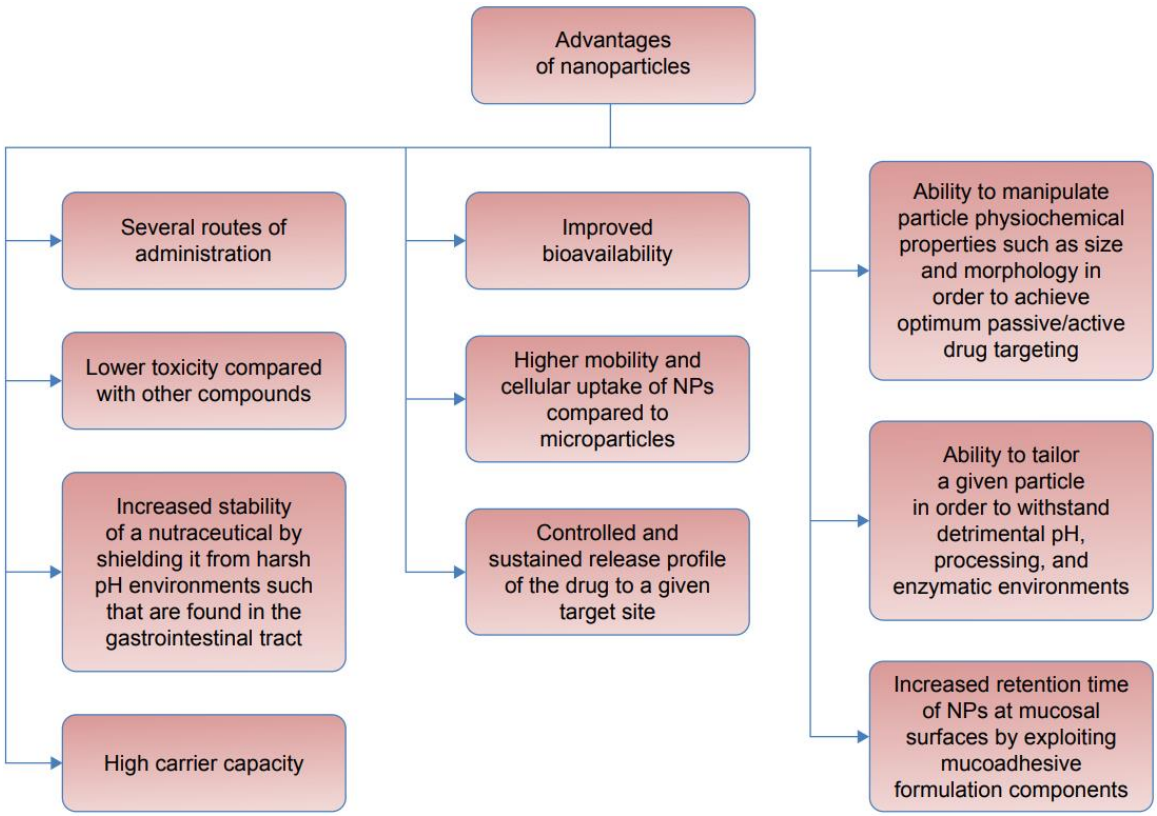

Figure 1. Advantages of Nanoparticles in Medicine.[4]

Selenium nanoparticles, along with a wide range of different coatings to tune their properties, have been thoroughly examined as chemotherapeutic agents.[4–8] They have, on occasions, been found superior to other selenium forms, or other known and widely used anticancer agents. They are also reported to prevent metastasis, have fewer side effects[6], and there are even reports that they can be co-administered with cis – platin to counter some of its side effects (CIS – induced reproductive toxicity)[4]. Platinum complexes have also been under the microscope, due to their known anticancer capabilities, and the nano-functionalization (nano-sized carriers for the drugs) of platinum(II) and platinum(IV) appears to have some very interesting prospects.[9] Some promising steps have also been taken in the nanomaterial - facilitated cancer diagnostic detection, again through the use of self -assembled selenium nanoparticles.[10]

The contribution of nanomaterials to medicine does not, of course, stop with anticancer treatment and diagnosis. Biosynthesized selenium nanoparticles have been reported as protective agents against DNA damage caused by UV- radiation.[11] Titanium dioxide particle interactions with specific proteins have been exploited to promote burned tissue healing and regeneration[12], while silver-, gold-, and zinc- containing nanomaterials are being explored for their antimicrobial and antibacterial properties[4,13–15]. And as far as diagnostics go, the intrinsic fluorescence of selenium – containing nanoparticles has been explored as a means for cellular imaging[16], while other elements, such as gold, are also examined as potential molecular imaging agents[9].

Beyond medicine, several fields have taken advantage of the nanomaterials' properties. Gold nanoparticles have been found to have catalytic properties the bulk material did not possess[17], while selenium (being robust direct band – gap semiconductor) is also examined as a potential catalysts for the incarceration of mercury vapours,

and more[18]. Some of the other, less known applications of selenium nanoparticles include the construction of optical devices, and the functionalization of photovoltaic solar cells and photo – assisted direct methanol fuel cells. It has also been incorporated in the making of selective and reliable chemical sensors.[18] And of course, the food industry has taken advantage of advances in nanotechnology to improve the products' processing and packaging procedures, and increase their nutritional value and shelf-life[19], while the cosmetics industry exhibits an ever - rising interest in the nanotechnological applications[20].

2.1.3. Nanomaterials in Environmental samples

Due to the fortunate rise of environmental concern, nanomaterial occurrence and properties in environmental samples have also been put under the microscope. The interest usually revolves around the potential toxicity they can induce on the flora and fauna of the ecosystems they are found in[21–25], while they can also play a major role in the alteration of soil[26–30] and atmospheric[31–34] systems as well. Their origin is also a point of interest, as nanoparticles can be naturally occurring[35,36], incidental[3,37] (unwilling by-products of anthropogenic activities), or engineered (created on purpose by humans for a specific purpose)[38,39].

Due to the nature and objectives of this study, its focus will be on samples of marine ecosystems (seawater). Nanoparticulate moieties interacting with the complex matrix of seawater can severely affect both on the analytical process, and the physicochemical characteristics of the moieties themselves.[40]There have been reports regarding the effects of seawater (or its constituents) on particle stability[41], the kinetics of their aggregation[42–44], or the alteration of their surface chemistry[45,46]. As far as the analytical process is concerned, seawater is a challenging matrix at two different levels: On the first hand, the complex composition of the sample could lead to signal interference. Different concentrations of dissolved organic matter and/or dissolved solids may in some cases affect the nanoparticles' transport efficiency and the sample's flow rate. On the other hand, the usually unavoidable salt residue pileup could be detrimental to the instrumentation, causing damage to the equipment and hampering the analysis.[47,48]

2.1.4. Detection and Characterization of Nanoparticles

While studying the occurrence of nanomaterials is a major field of interest, modern instrumentation and know – how with great potential are still in development. The properties of the detected nanomaterials, their size, composition, homogeneity of their population etc., can be studied at many different levels. Towards that end, an incredible array of analytical methods and techniques have been applied.[49]

Utilization of Scanning and Transmission Electron Microscopy (SEM/TEM)[50–54] and Dynamic Light Scattering (DLS)[50,53–57] imaging allows for the nanoparticle shape and size (or hydrodynamic size) characterization. Hydrodynamic size, in particular, has also been determined on occasion through Nanoparticle Tracking Analysis (NTA)[54]. The study of their morphology allows for the statistical analysis of their populations' size

distribution, that could reveal possible polydispersity. In addition, transmission mode - Fourier Transform InfraRed spectroscopy (FTIR) has been used to discern the biomolecular composition of their surface[52]. UV – Vis and micro – Raman spectroscopic methods have also been applied in the detection and elemental composition analysis of metalliferous particles[51,58,59]. X-ray Diffraction (XRD/XEDS) enables the identification of different material phases[49,51,54] as well, and thusly the study of probable crystalline solids, while dispersive X – ray spectroscopy (EDS) is used to determine the nanoparticle elemental composition[60]. Even flow cytometry, along with dark field microscopy, has been reported for indirect observation of the effects of TiO_2 nanoparticles on ARPE-19 cells.[50]

As far as the study of inorganic nanomaterials is concerned, atomic spectroscopy has provided the analytical process with very efficient tools. Techniques like Electrothermal Atomic Absorption spectroscopy (ET – AAS), Inductively Coupled Plasma – Optical Emission Spectrometry (ICP – OES) and – Mass Spectrometry (ICP – MS) have been preferred due to their sensitivity, selectivity, low detection limits[49] and their adaptability when coupled with other techniques.

Coupling the ICP – MS online to Reversed Phase High Performance Liquid Chromatography (RP HPLC) [56,57,61] or Hydrodynamic Chromatography[62], has been a common practice in the analysis of an array of samples, including nanomaterials. Sedimentation and Asymmetrical Flow – Field Flow Fractionation (SedFFF and AF^4) have also successfully been coupled online with ICP – MS for the detection and characterization of inorganic nanoparticles[55,63,64]. And Ion Mobility Spectrometry (IMS) has been coupled on-[65] and offline[66] with ICP – MS for the determination of nanoparticle size and elemental composition. On occasion, Isotope Dilution Analysis (IDA) has been used in addition to previously mentioned techniques, in order to counter interference effects caused by the matrix and thus achieve acceptable analyte recoveries and limits of detection.[56,67]

2.1.5. Single Particle ICP – MS in the Analysis of Nanoparticles

Single particle ICP – MS (SP – ICP – MS) is one of the most widely used techniques for the study of nanomaterials at low levels and in complex sample types. This comes as no surprise, as the development of the technique focuses on the analysis of individual particles, and more specifically their detection and the quantification of their metal content[68]. It has been used for various purposes, like detecting semiconductor contaminations, monitoring engineered nanoparticles in sunscreen products etc[69]. The food industry has also invested in SP – ICP – MS analysis, studying specific products uptake of nanoparticles[69], tracking the presence of incidental[69] or engineered[70] particles in products, or monitoring the composition of various dietary supplements[69,71,72]. It can also be a powerful tool in the service of nanotoxicology[73], or generally the monitoring of the occurrence and fate of different particles in human blood or tissue[69]. SP – ICP – MS has been applied in the monitoring of biogenic nanomaterial as well[61]. And of course, it has been used in the study of environmental samples, either during quality control of drinking water[69], for the monitoring of the nanomaterial release into the environment[74], and their subsequent occurrence, fate and toxicity[69,75,76]. The technique is also quite useful in the monitoring of nanoparticle effect on marine ecosystems[77–79].

The principle of SP-ICP-MS operation (detecting single moieties, see section *2.2.3. Single Particle ICP – MS*), can also be applied for the analysis of single cells (*Single Cell ICP – MS*[80]), to count them and determine their metal content[81]. The uptake of various metal constituents by individual cells can also be determined this way[82,83], as well as the presence of different moieties on or within the cells[61,84].

2.2. Objectives

Owing to the wide range of their potentially either useful or harmful properties, the study of nanomaterials has never before been more important than in current years. Modern industry has been mass – producing and using engineered nanomaterials, a huge part of which will, willingly or incidentally, end up in the earth's crust, the aquifer or the world's reservoirs. More than a few of them are also able to alter the chemistry and behavior of the atmosphere. It is therefore imperative to find new, ever – evolving and adaptable techniques to monitor the occurrence of nanoparticles, and the interaction with their respective ecosystems, in order to be able to either predict or even prevent emissions that would prove detrimental to the environment.

Within the current study, an array of previously known techniques is being used, combined and optimized, in order to develop a method for seawater sample analysis that will allow for the detection and characterization of metal nanoparticles in such environmental samples. For the limits of the developed method to be realized, and pushed, different aspects of the ICP – MS instrumentation, introduction systems and analytical procedure are tested. Furthermore, more than one data processing tools are incorporated in the data processing, some of them less known, but more specialized. The objective is to provide the results, and any conclusions attained through the process, with high accuracy.

Operating within the significant capabilities of the *Inductively Coupled Plasma – Mass Spectrometry* technique (ICP – MS), two different dwell times (time per reading) in the ms or μs range are used (single particle analysis), in order for a comparative study to able to be conducted. Also, different thresholds for the identification of particles are applied in both dwell time cases. The objective is to determine which dwell time is better suited in each given situation, the differences between them, and which threshold application is better suited to examine the resulting data.

In conclusion, the purpose of the presented experimental work is to develop and apply a rapid, robust and reliable technique for the analysis of untreated seawater samples, for the study of the occurrence and fate of metal nanoparticles. The protection of the instrumentation is a necessary concern as well, as the natural seawater samples are usually detrimental to the system's interface, due to salt residue built – up. Towards that end, the on – line dilution sample introduction system is being evaluated. As an added element, new data processing tools are being used, in order to cross – reference the obtained results, solidify the reached conclusions, and evaluate their performance in terms of time and quality of outcome.

2.2.1. Objectives of Investigating the Fate of Silver Nanoparticles and Ionic Silver in Seawater Systems (Mesocosm Tanks)

This part of the study was conducted as part of a larger experiment, under the title ''Addressing the impacts of a low-dose addition of silver nanoparticles vs. silver ions in a coastal marine ecosystem''. It was conducted in ''CRETACOSMOS'', which is the Greek branch of ''Aquacosm'', a European network of mesocosm facilities. The objective of the extended experiment was to investigate the impact of low and stepwise addition of silver, in ionic or particulate form, in coastal marine ecosystems. Furthermore, a comparative study between the effects of the two different species would be facilitated, as well as a comparison with a similar experiment previously conducted in the same facility[85]. For that purpose, nine mesocosm tanks were incorporated, and treated as it is explained in *Section 3.3.1* of this study.

Regarding the part of that experiment conducted within this study, an on – line dilution introduction system was incorporated in the analysis of seawater samples from the aforementioned mesocosms. Using SP – ICP – MS, samples from the tanks that have been treated either with ionic or with particulate silver have been analysed on a daily basis, in order to monitor the occurrence of silver nanoparticles, and potential changes in their population and size (therefore, their *fate* in the seawater system).

Moreover, owing to the fact that the added silver amount in the system can be known at any given time, this series of experiments is also used for the evaluation of the on – line dilution system, the comparative study of two different dwell times, and the verification of the statistical significance of the application of different thresholds for the identification of nanoparticles (see *Section 3.3.2. Data Acquisition and Processing).*

2.2.2 Objectives of Investigating the Occurrence and Metal Content (Cu) of Copper – containing Particles in Seawater Samples from the Proximity of the Island of Santorini

2.2.2.1 Objective of the Experiment

The on – line dilution introduction system has also been incorporated in the analysis of seawater samples from the proximity of Santorini Island, for the detection of nanoparticles. The selection of this island was mainly the result of three factors: To begin with, it is a very popular touristic summer destination, elevating the anthropogenic factor for the nanoparticles' occurrence. Secondly, it is considered an active volcano, a state that has been closely associated with the formation of *hydrothermal vents* (see section *2.2.2.2. Hydrothermal vents*). And finally, the unique morphology of the seabed *within* the perimeter of the island is considered very likely to ''trap'' particles of any origin.

Within the periphery of the island, different sampling sites have been selected due to a number of factors (higher boat activity, proximity to known hydrothermal vent, deeper waters etc.). From those sites, samples were acquired from different depths (~0 m, 5m, 50m, 250m), and from different periods of the year within the span of two years. Due to this process, the temporal variability of the nanoparticles' population and metal content

can be determined, due to the presence or absence of touristic and/or boats' activity, as well as the differences from one sampling site to the other and the effect of the depth of the acquired sample. For the needs of the analysis, five different elements have been investigated (Pb, V, Ni, Cu, Fe). The results presented within this study will include the investigation of the occurrence and metal content of Cu nanoparticles.

2.2.2.2 Interest in Studying Hydrothermal Vents

Hydrothermal vents are naturally formed fissures found on the seafloor, from which geothermally heated water is emitted. They are responsible for the formation of hydrothermal deposits, and they can promote the growth of their surrounding area, due to the chemical composition of their emissions[86]. Depending on that composition, they are usually categorized as either black smokers (higher sulphur content) or white smokers (higher barium, calcium, silicon content).

Due to the unique conditions occurring in and around them, and their effect on the formation and fate of particulate analytes, they are of considerable interest. Depending on their type, due to the different chemical content, the hydrothermal vents can produce different types of nanoparticles. High sulfuric content, either due to the vent or the sulfide content of seawater (S^{2-})[87], leads to the formation of various types of sulfide clusters and nanoparticles.[21,58,88–91] Other types of particles, such as graphite[92], copper-containing aggregates[90], Barite, Calcite etc. have also been reported.

The composition of those particles, as expected, is rarely pure, due to the complexity of the matrix. They usually interact with other inorganic compounds or Natural Organic Matter (NOM) of various kinds[21], acting as a stabilization factor or a potential ligand[88].

2.3. Inductively Coupled Plasma Mass Spectrometry

2.3.1. ICP – MS Principle of Operation

The use of the Inductively Coupled Plasma ion source, coupled with a quadrupole mass analyzer, in the analysis of trace elements, has been proposed since 1980 by R.S. Houk et at.[93] Despite several upgrades and occasional targeted alterations, in order for the technique to adapt to the needs of each different analytical process, the fundamental principles remain the same to this day. While, over the years, the technique has adapted to the analysis of solids[94–96] and gases[97], the samples are usually in liquid form[98].

One of the most critical components of the ICP-MS is its *sample introduction system*, that essentially consists of two parts, the *nebulizer* and the *spray chamber*[99]. The introduction system is responsible for the delivery of the sample into the instrument in a suitable form. That includes the nebulizer turning the liquid sample into a fine aerosol, and the spray chamber usually rejecting droplets of higher volume. There is an array of different nebulizers and spray chambers available, depending on the needs of the analysis. For instance, some nebulizer - spray chamber systems do not need to reject droplets, leading to a higher transport efficiency (detected moieties to actual moieties in the sample ratio)[100].

After the sample has been properly transported into the instrument, it enters the *inductively coupled plasma.* The ICP includes the *torch* and the *RF coil* that create and sustain the plasma. When the instrument is turned on, the plasma region is filled with Ar gas, and then an electrical discharge ionizes the first Ar atoms. The RF field generated by the RF coil provides the ionized atoms with more kinetic energy, so they collide with other neutral atoms, ionizing them. The newly formed ions are then in turn accelerated by the RF field, creating more ions and that is how, through the constant supply of Ar gas and the RF field, the plasma is sustained. Due to the high energy of the Ar plasma (6000 – 10000 K), the sample is vaporized upon entering the chamber, the resulting gas is atomized, and the resulting atoms are ionized (plasma *ionization source)*[101]. A system of sampling cones (*Interface*), usually made from nickel, allows sufficient number of ions to go from the plasma region (~760 Torr), via an area of lower pressure (~2 Torr), into the high vacuum area (~10^{-8} Torr) of the ion focusing system and the mass analyzer while conserving their integrity.[102].

The *ion focusing system* consists of metallic cylinders or plates etc. that have voltages applied to them. Its purpose is to focus the ion beam, and prevent it from spreading due to the high vacuum. Also, the ICP – MS instrumentation usually suffers from matric effects, especially when the constituents of the matrix are heavier than the analytes. The ion focusing system is responsible for the transfer of the maximum number of analyte ions possible to the mass analyzer, while discarding as many of the matrix – related ions as possible.[103]

The *mass analyzer* is one of the most critical parts of the ICP – MS instrumentation, as it is the part where the selected ions are sorted out of the beam, in order to reach the detector, while the rest of the unwanted ions are discarded.[104] The original Mass Analyzer paired with the Inductively Coupled Plasma Ion source was the *Quadrupole Mass Analyzer*, and it is considered, up to this day, a very popular, relatively low cost and dependable choice. In principle, it consists of four, cylindrical or hyperbolic, parallel rods made of stainless steel or molybdenum, sometimes coated against corrosion, crosswise paired. The (+) pole of a direct current (dc) source is applying a dc field on one pair, and the (-) pole is applying a similar field on the other pair. Variable radiofrequency current (rf) is also applied on both pairs, with 180^{o} phase difference. The cumulative effect of dc and rf fields only allows ions with specific mass to charge ratio to reach the other end of the quadrupole (~15 – 20 cm), while the rest are rejected. Despite the universality of the quadrupole analyzer, there are nowadays more commercially available analyzers, like the *Double Focusing – Magnetic Sector Mass Analyzer*[105], the *Time of Flight Mass Analyzer*[38,106] etc.

The ions that do make it out of the Mass Analyzer reach the *detector.* The detector's role is to count the ions, by transforming them into an electrical signal. The intensity of the signal corresponds to the detected number of analyte ions. More than one types of detectors are of course available, including a *Faraday Cup* (essentially a metal electrode) and the *Channel Electron Multiplier* (or *Continuous Dynode Electron Multiplier*, semiconductor that generates multiple electrons upon the ions' impinging on its surface). Due to its superior dynamic range, the *Discrete Dynode Electron Multiplier (DDEM)* eventually dominated the field, operating under the same principle as the Channel Electron Multiplier, but using multiple, discrete dynodes for the amplification of the signal. Taking advantage of the flexibility of the discrete dynodes, the DDEM has the ability to switch between two different circuitries for the counting of the ions (*Dual Stage Discrete Dynode Detector)*.

The analog circuitry measures the signal in the midpoint dynode, and, depending on whether it is above a certain threshold or not, it is either measuring the analog signal right away (if the signal is higher than the threshold) or allows the beam to keep cascading through the rest of the dynodes, and be measured as a pulse signal (if the signal is lower than the threshold).[107]

2.3.2. Collision / Reaction Cell

The *Collision or Reaction Cell (CRC)* is a multipole cell located after the ion focusing system and before the mass analyzer. It provides an instrumental solution against isobaric and polyatomic interferences[108,109], by turning unwanted ions into something that the mass analyzer will eliminate immediately afterwards. It is usually operated in two different modes, either the *Kinetic energy Discrimination (KED)*, or the *Dynamic Reaction Cell (DRC)* mode. The KED approach, using a non – reactive gas (i.e., He) eliminates polyatomic interferences by taking advantage of their larger collision cross-section. The polyatomic ions collide more frequently than the analytes due to their higher cross – section, and are therefore eliminated based on an appointed energy threshold. The DRC approach, using a reactive gas (O_2, NH_3, CH_4), eliminates isobaric interferences by taking advantage of selective reactions. The cell gas either reacts with the interference, therefore changing its mass, and allowing the detection of the analyte at its isotopic mass to charge ratio (on-mass approach), or reacts with the analyte, therefore changing the analyte mass that will be analysed by the quadrupole (mass – shift approach)[110]. The same principle of operation has been later used in the development of a more efficient detection system, incorporating more than one quadrupole (Triple Quadrupole – ICP – MS).[96,111–113]

2.3.3. Single Particle – ICP – MS

As it was mentioned before, Single Particle ICP – MS is a very powerful tool for the analysis, or more precisely for the screening, of individual nanoparticles.[114,115] During the *Conventional* operating mode of the ICP - MS, intensity readings are integrated over a time window (or dwell time), averaged and transformed through a calibration function, to correspond to the analyte's concentration. In SP-ICP – MS, shorter dwell times are used per intensity reading, and are plotted individually as a function of time. As a result, the signal from the detection of dissolved analytes will remain steady, as the dissolved constituents will still be homogenously distributed in the solution, but will be significantly lower in intensity, since fewer ions will be detected per dwell time. In case of a suspension though, the analyte's atoms will not be homogeneously distributed in the sample due to the presence of particles, that consist of thousands of atoms. So, in principle, when a nanoparticle enters the plasma, its atoms will be ionized, creating a much more concentrated *cluster* of ions, that will move through the instrument more or less as a whole. This is also what happens upon the entrance of a *single cell* in the plasma chamber, that results in an ion cluster consisted of the metal atoms the cell contained. Upon reaching the detector, the cluster will cause the detection of a much higher ions per dwell time ratio, that will lead to a

detection ''spike'', or ''event'' .[68,116]

There are three important requirements for this technique to work: First, the sample should be dilute enough ($<10^6$ particles/ml), in order to reduce the possibility of pulses overlapping (the signal of one particle coinciding with the signal of another in the same detection window). Second, the dwell time should be adjusted, so that, on the first hand, it is representative of the individual particles' transient signal, and on the other hand, it is sufficient to acceptably reduce the background, lowering the limit of detection for the particles' size.[117,118] And third, the particles should be transported into the plasma as intact as possible, in order for their quantification to be accurate.[119,120]

Should the requirements be met, each individual event will correspond to the detection of a single particle, and therefore, the *frequency* of the events will directly relate to the *number concentration* of the particles in the sample. The *size* of each detected nanoparticle will also be proportionate to the event's *intensity* (height or area)[121], allowing for the of study the particle population's *size distribution*[75,122]. It is possible, if the dwell time is low enough (μs range), for a particle to be detected over multiple datapoints, and therefore for its duration *profile* to be acquired. In that case, a different approach should be used during the signal deconvolution, since every single particle's signal will stretch over more than one datapoint, therefore both the number and the size of the detected particles will need to be differently calculated.

2.4. Particle Identification, Dwell Times and Detection Thresholds

Looking into the particle identification procedure, the pulses that corelate with the detection of particles are essentially the outliers of a dataset, that is otherwise following a set of rules governed by statistics. So, in order to discriminate the particles from the background (or dissolved analyte, depending on whether that is a constituent of the sample or not), one has to realize the distribution of the background in a frequency versus peak area histogram, and apply the appropriate statistical analysis that will indicate the datapoints that do not follow the same behavior as the rest of the dataset. These datapoints are the ones that correspond to the detected particles.

While working in the ms range (typical dwell times are 1-10 ms), the background level is usually revolving around a mean value, closely resembling the Gaussian Distribution, or *Normal Distribution*. Per the Normal Distribution's statistics, 99.73% of the datapoints will be included within the $(\mu - 3\sigma, \mu + 3\sigma)$ range, where μ is the mean value of the dataset, and σ is standard deviation. Given the fact that, by the SP – ICP – MS principle, the particle – related datapoints will have *higher intensity* than the background, it is reasonable to assume (in fact, with 99.73% certainty), that any datapoints that have a peak area greater than the $\mu + 3\sigma$ threshold are very likely caused by the detection of a particle. Increasing the number of standard deviations added to that threshold, within reasonable boundaries, increases the confidence level, that the outliers are indeed particles. For instance, an $\mu + 5\sigma$ threshold is providing the analysis with a 99.999% confidence level. It is though very possible, that the addition of redundant standard deviations will lead to the exclusion of particle – related pulses.[75]

As it was briefly mentioned before, lowering the dwell time (in the μs range, usually 50 to 200) leads to lower

background and the acquisition of the particles' *time profiles.*[123] That becomes possible, when the dwell time is lower than the time required for the ion cloud to be detected. However, lowering the background level can cause the mean value of the dataset to creep closer to zero, and, since the lower detectable value for a datapoint is zero, the shape of the background distribution begins to change. This particular shape resembles the *Poisson* distribution, characterized by a very low mean value and high skewness. What's interesting, is that a Poisson Distribution with a higher mean value could adequately resemble a Gaussian Distribution (*Figure 2*, image from X – The Analysis Factor, by Karen Grace – Martin).

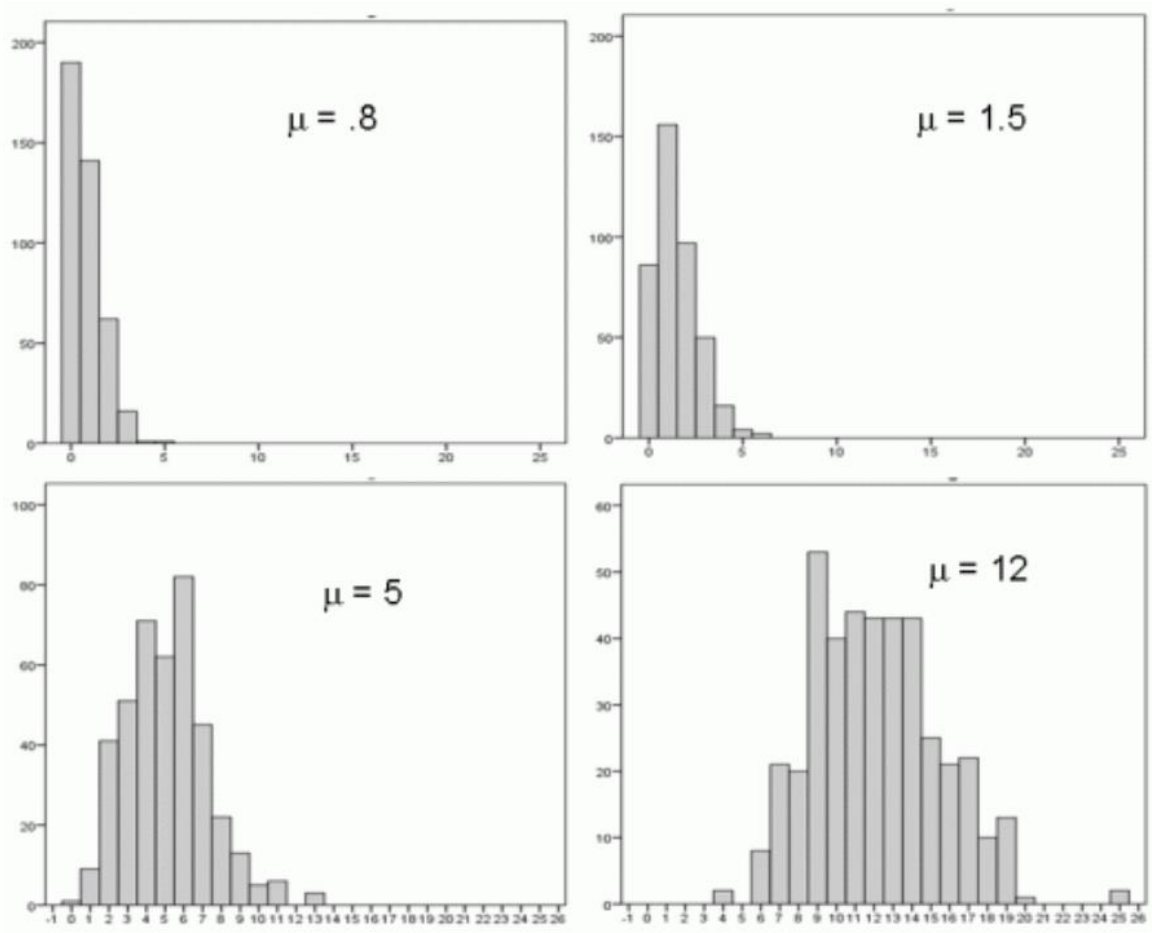

Figure 2. Poisson Distributions with gradually increasing mean values.

It becomes apparent, that when using lower dwell times, due to the lowering of the background signal per dwell time, the Poisson Statistics are preferable for outlier detection. The threshold for the detection of nanoparticles (Th), is in that case determined as the mean value of the dataset (μ) plus the detection limit derived from the Poisson statistics ($L_{D(Poisson)}$)[124].

$$Th = \mu + 2.71 + 3.29 * \sqrt{\mu}$$

The Poisson statistics have proven to be a valuable tool, that is being used in the low dwell time SP – ICP – MS more and more frequently.[114,125]

Dwell times in the 200 μs to 1 ms range are generally avoided, because there is a risk that a pulse could be only partially recorded. It is also recommended that dwell times lower than 50 μs be avoided, because they lead to

an incorrect recording of the signal, due to the very low number of ions reaching the detector during that time window, which leads to very high uncertainty values for the measurements.[123]

3. Experimental Part

3.1. Materials

3.1.1. Materials used for Investigating the Fate of Silver Nanoparticles and Ionic Silver in Seawater Systems (Mesocosm Tanks)

For the spiking of the Ag nanoparticle treated tanks, and the determination of the transport efficiency of the system, the BioPure Silver Nanospheres material was used (nanoComposix, Branched PolyEthylenImine coating, 60 nm diameter, 1 mg/ml in water concentration, product code: AGBB60-1M). The dissolved silver treated tanks were spiked with silver standard for ICP (TraceCert 10.000 mg/L Ag in 5% nitric acid, product code: 91543). Deionized water used throughout the experiment was provided by the Elga PureLab Ultra Genetic Water Purification System, and had a resistivity value of 18.2 MΩ·cm. Regarding the seawater used throughout the experiment, both for the mesocosm tanks and for the preparation of any necessary standard solutions, it was sampled from open water in the proximity of Gournes, Heraklion (Crete, Greece).

3.1.2. Material used for Investigating the Occurrence and Metal Content (Cu) of Copper – containing Particles in Seawater Samples from the Proximity of the Island of Santorini

For the determination of the transport efficiency, the aforementioned reference material was used (nanoComposix, Branched PolyEthylenImine coating, 60 nm diameter, 1mg/ml in water concentration, product code: AGBB60-1M). The deionized water that was used was also the same as the one mentioned in section 3.1.1., provided by the Elga PureLab Ultra Genetic Water Purification System, and had a resistivity value of 18.2 MΩ·cm. For the dissolved Cu standard preparation, a 3% NaCl solution was prepared each day (Sodium Chloride by Fluka, BioChemica, 71378). The Cu dissolved standard was from CPI International, Peak Performance certified reference material, Single – Element Copper standard (10.000 ± 30 μg/ml Copper in 4% HNO_3).

3.2. Instrumentation

3.2.1. Experimental Set – Up

The analysis was carried out using a NexION 300X® (upgraded to 350X) ICP-MS[126], from Perkin Elmer, whose operating conditions are summarized in Table 1. The introduction system that was used during the analyses is shown in *Figure 3.* and it is similar to the introduction system previously used by Toncelli et al[127].

Table 1. ICP – MS Instrument Conditions	
Description	**Value**
Nebulizer Gas Flow	0.88 – 0.91 l/min
Makeup Gas Flow	0.00 l/min
Auxiliary Gas Flow	1.50 l/min
Plasma Gas Flow	15.00 l/min
Deflector Voltage	-10.75
ICP – PF Power	1400.00
Analog Stage Voltage	-2350.00
Pulse Stage Voltage	1550.00
Quadrupole Rode Offset STD	0.00
Cell Rod Offset STD	-8.00
Discriminator Threshold	10.00
Cell Entrance/Exit Voltage	-4.00

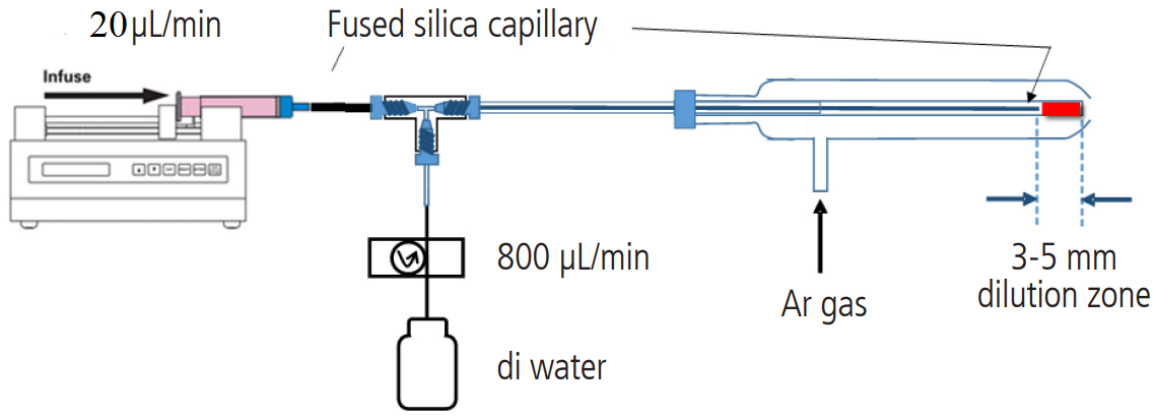

Figure 3. The introduction system used in the analysis of both experiments' samples[128].

A syringe pump (Cole – Palmer Single Syringe Infusion Pump, Cat.Number:78-9100C, 010A, 250V) introduces the sample into a fused silica capillary, though which it is transferred to the tip of the nebulizer (dilution zone), at a rate of 20 µl/min. It is met at this point by a make – up flow of ~800 µl/min of deionized water, introduced by a peristaltic pump, resulting in a ~40 fold dilution, thus eliminating the need for sample dilution prior to its analysis. As a result, not only is the analysis time reduced, but also the physicochemical characteristics of the analytes (especially particles) are mostly preserved, since their microenvironment and the ionic strength of the solution are only altered for a very small fraction of time (100-200 ms).

The nebulizer is a concentric, pneumatic, glass model from Meinhard Type C0.5, while a glass Cyclonic spray chamber from PerkinElmer was attached to it.

3.2.2. Data Acquisition and Processing

3.2.2.1. Data Acquisition and Processing for Investigating the Fate of Silver Nanoparticles and Ionic Silver in Seawater Systems (Mesocosm Tanks)

For the data acquisition, the PerkinElmer Syngistix™ software and its Nano Application software module were used. Two different dwell times, 75 μs and 10 ms have been used during the analysis of the Mesocosm Samples. There is usually a time period between two consecutive datapoint acquisitions, during which no signal is detected (dead time). Due to a firmware upgrade, this instrument is able to operate without this limitation.
The data analysis incorporated the Nano module results, as well as some post analysis handling by OriginPro and Microsoft Excel. GEOCHEM – EZ[129] was also incorporated for the simulated calculation of the silver species in the complex matrix of seawater. The nanoparticle detection thresholds that have been incorporated on occasion, in accordance with everything that was mentioned in Section 2.4., are 1) $Th = \mu + 3\sigma$ (hereafter referred to as the 3σ threshold), 2) $Th = \mu + 5\sigma$ (hereafter referred to as the 5σ threshold), and 3) $Th = \mu + 2.71 + 3.29 * \sqrt{\mu}$, (hereafter referred to as PG threshold).

3.2.2.2. Data Acquisition and Processing for Investigating the Occurrence and Metal Content (Cu) of Copper – containing Particles in Seawater Samples from the Proximity of the Island of Santorini

For the data acquisition, the PerkinElmer Syngistix™ software has been used, with a dwell time of 10ms. Due to severe polyatomic interferences[108], the CRC was also incorporated in KED mode, Using 3.75 ml/min of He flow.
The data analysis was carried out using the JupyterLab[130] Python notebook interface. The code that was developed for the need of this project is presented and explained in the Supplementary section of this Thesis (S*ection 2.2)*. For the identification of particles, the 5σ threshold was used, in the same manner as it was explained before.

3.3. Experimental Procedure

3.3.1. Experimental procedure for Investigating the Fate of Silver Nanoparticles and Ionic Silver in Seawater Systems (Mesocosm Tanks)

3.3.1.1. Sample Collection and Preparation

Sampling took place daily at the Hellenic Center for Marine Research (HCMR), where the Mesocosm project was conducted. Starting from Day 0, the samples were collected in sterilized containers, using silicon tubes,

that are permanently put in each of the mesocosm tanks (a total of nine) *prior* to the spiking. Subsequently, three of those tanks were spiked with 50 ppt of silver nanoparticles (AgNP treated tanks) and three of them were spiked with 50 ppt of ionic silver (Ag treated tanks), while three were control tanks. Each of the tanks was then lightly stirred with a dedicated paddle, in order for the spiked analytes to be dispersed. The procedure was repeated each day up to Day 11. Two hours after the first spiking, an extra set of samples was collected (D0 + 2H), in order to monitor the standard's interaction with the system.

3.3.1.2. Analytical Protocol for the Determination of Ag in Seawater

Prior to the samples' arrival the analytical laboratory (the HCMR is located 30 to 40 minutes away by car), the instrumentation was prepared:

- The instrument's performance check and optimization were conducted: A multielement solution (containing 1 ppb of each element) was used to monitor the instrumentation's response to Be, In, U, Ce, CeO/Ce ratio (oxides), Ce^{++}/Ce (double charged ions ratio) and Background (noise) at m/z 220. When the response values were within acceptable ranges, meaning the instrument was in good working condition, the ''Tune'' file was saved. In the case of any irregularity in the performance check, the instrument's response optimization would usually include the realignment of the torch, or the slight alteration of the nebulizer's gas flow. Rarely was any other intervention necessary, that would include changing of the peristaltic pump's tubing, or cleaning the nickel cones etc.
- After the performance check and optimization, the transport efficiency check and optimization were conducted. If the transport efficiency was within the acceptable range (>1.5%, the experiment was conducted with 1.70% – 2.94% efficiency), the procedure would resume. If not, the position of the fused silica capillary tip was re-adjusted, until an acceptable value was reached. Rarely was the capillary change necessary, either due to its clogging, or due to any residues from previous analysis, as there were no such cases reported.
- Following the optimization of the transport efficiency, the system's calibration was conducted, for both dwell times (75 μs and 10 ms), using standard solutions containing 0.5, 1.0 and 5.0 ppb of Ag, in seawater (from the control tanks).
- The calibration was then followed by a long (15 – 20 min) monitored cleaning step with 2% HNO_3 solution, until any residue of the standard solutions was eliminated from the system.

Mesocosm samples were analyzed as soon as they were delivered to the analytical laboratory at the University of Crete:

- Each sample was then analysed two times for 3 min each, using a 75 μs dwell time, and once for 6 min, using a 10 ms dwell time, through the previously described on-line dilution introduction system.
- Prior to each sample's first run, the syringe was washed with deionized water (18.2 MΩ) for 30 seconds, and then the system was conditioned (using the sample itself) for another 90 seconds.
- At the end of each sample analysis, the instrument's performance was checked again, and the whole system was rigorously washed with 2% HNO_3 solution (~25 min), while monitoring the washout signal with the ICP-MS.

This experimental procedure, as well as some of this study's results have been published in an application note,

in collaboration with PerkinElmer, Inc[128].

3.3.2. Experimental Procedure for Investigating the Occurrence and Metal Content (Cu) of Copper – containing Particles in Seawater Samples from the Proximity of the Island of Santorini

3.3.2.1. Sample Collection

Seawater samples were collected from around Santorini Island, over the span of two years. A total of five sample batches were collected, on July 2019, October 2019, January 2020, June 2020, and August 2020. After each sampling process, the samples were transferred to the analysis laboratory as soon as possible, where they were stored in a cold room (~4^{o}C) until analysis. The sampling procedure was carried out using a Niskin Bottle (~3 l), suspended by grappling hooks and / or pulleys. Each sample was filtered through 10 μm filters, with the aid of a portable vacuum pump. A small portion of the filtered sample was used to rinse the container of the sample, and then the container was filler with the filtered sample (~250 ml).

3.3.2.2. Analytical Protocol for Detecting Cu-containing Particles in Seawater

The protocol that was followed for their analysis each day was the following:

- The samples were taken out of the fridge and left at room temperature for about one hour.
- While waiting for the samples to reach room temperature, the instrument's performance check and optimization was conducted, in the same manner that was previously mentioned.
- Each bottle was then stirred and gently shaken, so that the potential nanoparticles' suspension is homogenised, and then a small portion of the solution (~5 ml) was poured into a new sterilized container.
- After the performance check and optimization, the transport efficiency check and optimization were conducted, in the same manner that was previously mentioned.
- Following the optimization of the transport efficiency, the analyte's calibration was conducted, using standard solutions with concentrations of 1.0, 5.0, 10.0 and 50.0 ppb in 3% NaCl, unless otherwise stated.
- The calibration was then followed by a long (15 – 20 min) monitored cleaning step with 2% HNO_3 solution, until any residue of the standard solutions was eliminated from the system.
- Each sample was then analysed three times for 5 minutes each, using a 10 ms dwell time, through the on-line dilution introduction system. The He KED flow was 3.75 ml/min. Prior to each sample's first run, the syringe was washed with deionized water (18.2 MΩ) for 30 seconds, and then the system was conditioned (using the sample itself) for another 90 seconds.
- At the end of the sample's analysis, the instrument's performance was again checked, and the whole system was rigorously washed with 2% HNO_3 solution (~25 min), while being monitored.

4. Results and Discussion

4.1. Results and Discussion for Investigating the Fate of Silver Nanoparticles and Ionic Silver in Seawater Systems (Mesocosm Tanks)

As it was previously mentioned in section *3.2.2 Data Acquisition and Processing*, the dwell times of 75 μs and 10 ms were used for the analysis of samples collected from the ionic silver (Ag^+) and silver nanoparticle (AgNP) treated seawater tanks. The use of 10 ms dwell time is well-documented in the literature for the analysis of nanoparticle-containing samples.[68]In this acquisition mode, the nanoparticle signal can be captured within a single dwell time, provided that the suspension is sufficiently dilute. The much shorter 75 μs dwell time is documented to produce lower background levels, and allows for the acquisition of the time profiles of the detected particles. The data acquired with 75 μs and 10 ms were processed using the commercial software, Nano Syngistix™ (Perkin Elmer) by applying 3 detection thresholds referred to as 3σ, 5σ, PG.

Through the use of the Nano Syngistix™ software, an array of metrics can be extracted for each sample. This includes the mean intensity, which is the average intensity of the pulse signals detected throughout the sample acquisition. Mean intensity is turned into mean size, i.e., the average diameter of nanoparticles in the sample, by using the mass calibration equation obtained through the aspiration of a nanoparticle reference material. The most frequent size, which is the most frequently observed nanoparticle diameter, can be determined through the use of (Gaussian, Log-Normal, Max Intensity) fitted to the obtained nanoparticle size distribution. The number of peaks, the total number of signal pulses obtained throughout the data acquisition for each sample, can be automatically converted into particle concentration by taking into account the transport efficiency of the ICP-MS introduction system. As is the case for mass calibration, the transport efficiency can be determined upon aspiration of a nanoparticle reference material of known NP number concentration. The software also provides the intensity of the dissolved Ag, which is the average intensity of the background after the pulse signals are separated and excluded from the original sample dataset. While the default procedure for the dissolved intensity calculation is carried out according to Pace et al (insert ref)[116], the software allows for the application of different threshold values and thus recalculation of the Dissolved Intensity. By performing a dissolved calibration, dissolved intensity is turned into Dissolved Ag concentration.

4.1.1. AgNP treated seawater tanks, analyzed using 10 ms dwell time detection

4.1.1.1. Ag mass balances for AgNP treated seawater tanks as determined using 10 ms dwell time detection

The following charts (*Fig. 4-6*) summarize the quantity of Ag detected, both as dissolved ionic Ag, as well as Ag nanoparticles (AgNPs), for each of the three thresholds applied. Each data point represents an average value that has resulted from the analysis of the three seawater tanks. The ''spiked'' values (yellow line) refer to the

cumulative amount of silver (Ag) added to each tank as AgNPs, i.e., 50 parts per trillion (ppt) Ag daily in the form of AgNPs. The trendline (red line) is a fit to the experimental data, whereas each numerical value given in the figures corresponds to an average value from the three tanks.

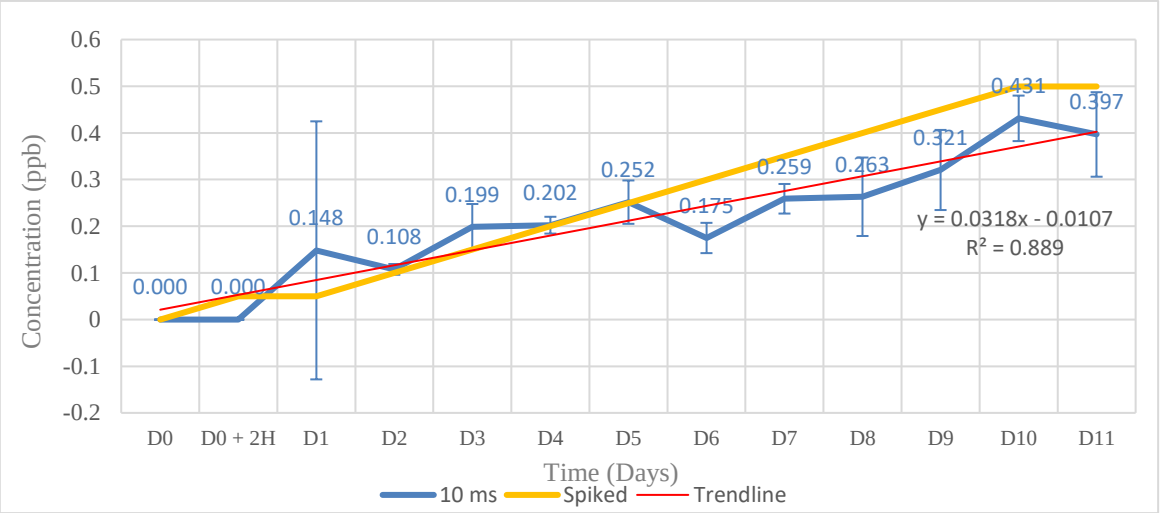

Figure 4. Mass balance for the AgNP treated seawater tanks, 10 ms dwell time, 3σ threshold.

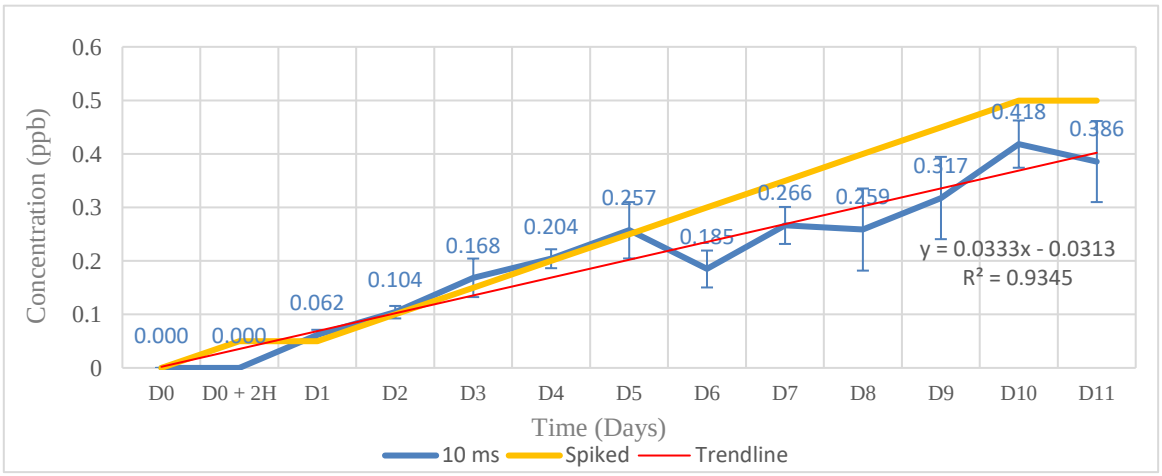

Figure 5. Mass balance for the AgNP treated seawater tanks, 10 ms dwell time, 5σ threshold.

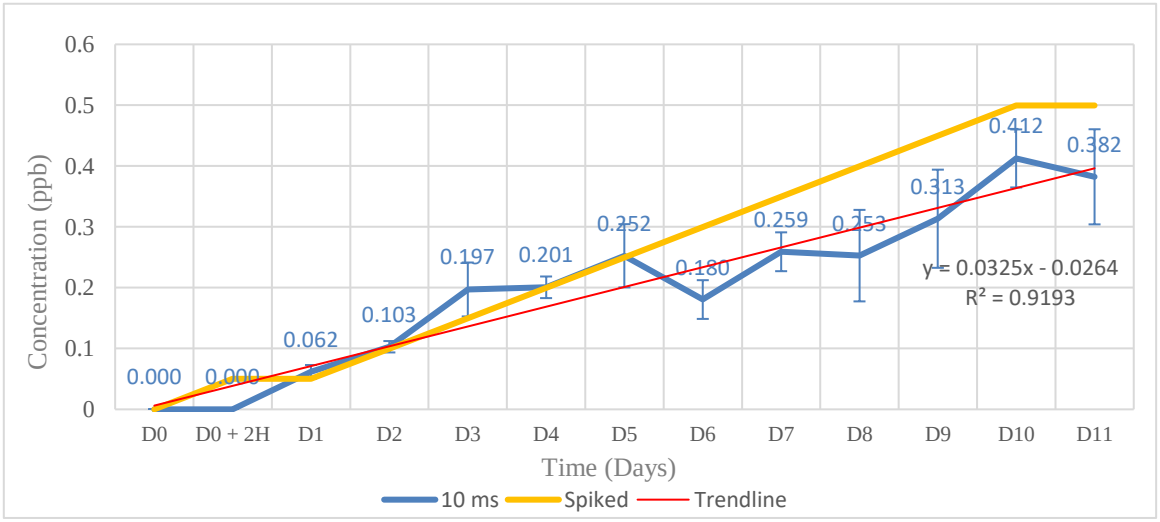

Figure 6. Mass balance for the AgNP treated seawater tanks, 10 ms dwell time, PG threshold.

Regarding the observed mass balances (sum of dissolved Ag and AgNP concentrations compared to the spiked concentrations of Ag NPs), there is little difference when using each of the three thresholds. This can probably be explained by the fact that the 10 ms dwell time is generally acceptable both for the quantitation of the element present in the form of nanoparticles and in a dissolved state, a fact validated by the high recovery values (3σ = 97.9%, ±66.6% standard deviation, 5σ = 81.7% ± 20.9% standard deviation, and PG = 82.2% ± 24.0 standard deviation). This means that any Ag amount not detected as a particle, is accounted for in its dissolved state. The 3σ obtained results are characterized by a significantly higher recovery value (97.9%). However, these results are also the least consistent among the three, as evidenced by their obviously larger uncertainty and the standard deviation of the percent recovery (66,6%), as well as the R^2 value (less good linear fitting). It is worth noticing that the difference between the PG and 5σ in terms of recovery, deviation of the recovery and uncertainty of the datapoints is insignificant. Despite them not being identical, their recovery values and respective uncertainties suggest that all three threshold criteria perform equally well in terms of determining Ag mass balances. The application of a different threshold, does not really change the dataset itself. It only affects the characterization of pulses as part of the dissolve, or as an outlier, (a pulse event). Therefore, the fact that the three different threshold criteria perform equally well, could be an indication that the difference between them is not significant enough to cause a substantial change in the discrimination of the Ag particles from the dissolved Ag. That may be suggesting that the detection of particles of a higher size, cannot be affected by a higher threshold. In the meantime, the lower threshold (3σ) might be suffering from the effects of false positive signals, that would falsely contribute to the overall mass balance. The case that those signals indeed correspond to smaller particles is also possible. s

Overall, , , all three of the applied thresholds seem to be performing equally well, depicting the expected increase in the total Ag amount, with time (both dissolved ionic Ag and AgNPs). That is evidenced by the recovery values, that is the ratio of the detected Ag amount in both forms, to the known cumulative spiked amount of Ag, in the form of AgNPs.

4.1.1.2. AgNP particle concentrations for AgNP treated seawater tanks as determined using 10 ms dwell time detection

Looking deeper into the nature of the Ag species in the seawater samples, the determined Ag particle concentration is shown in *Figures 7-9*, obtained using different threshold criteria. The actual numbers of detected peaks have also been presented in charts and can be found in *SS 1.1.1*, *Figures 1-3* of the present thesis. The results represent an average value that has resulted from the data obtained from all three tanks. The ''spiked'' values refer to the cumulative amount of silver (Ag) added as AgNPs daily at 50 parts per trillion (ppt) corresponding to 42125 particles per mL of seawater sample.

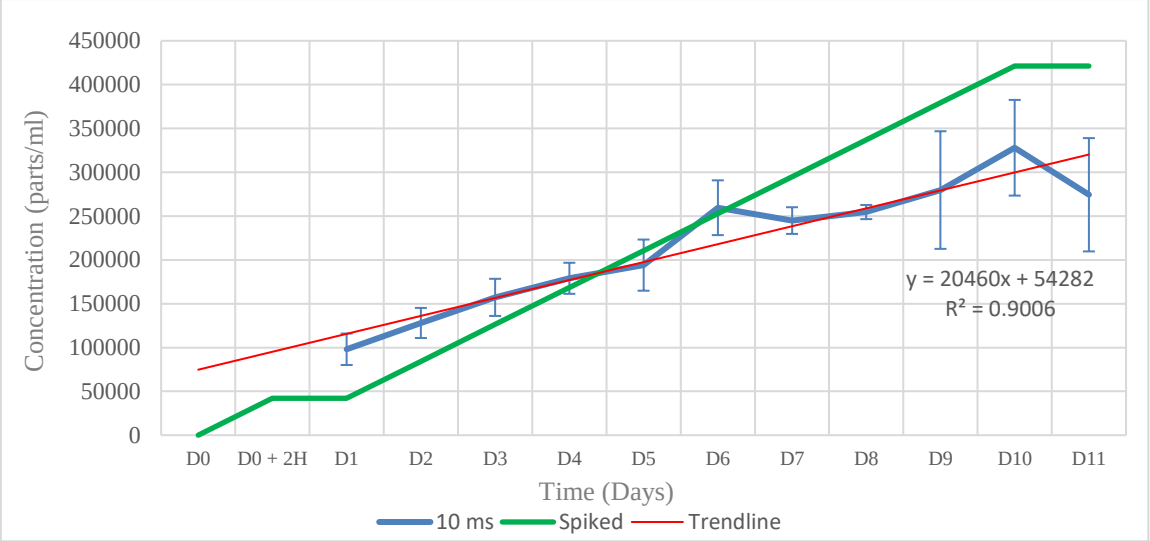

Figure 7. Particle concentration for the AgNP treated seawater tanks, 10 ms dwell time, 3σ threshold.

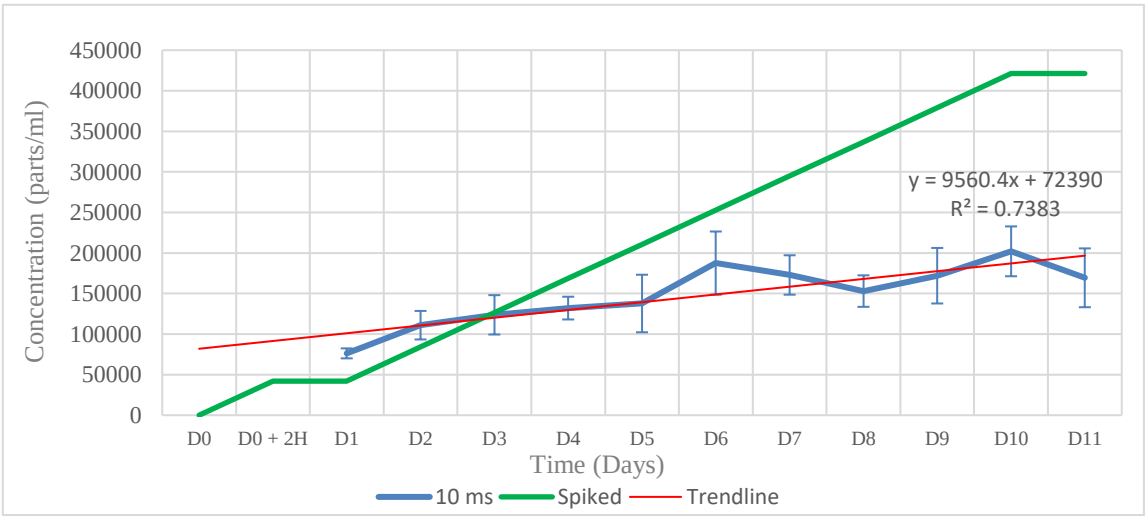

Figure 8. Particle concentration for the AgNP treated seawater tanks, 10 ms dwell time, 5σ threshold.

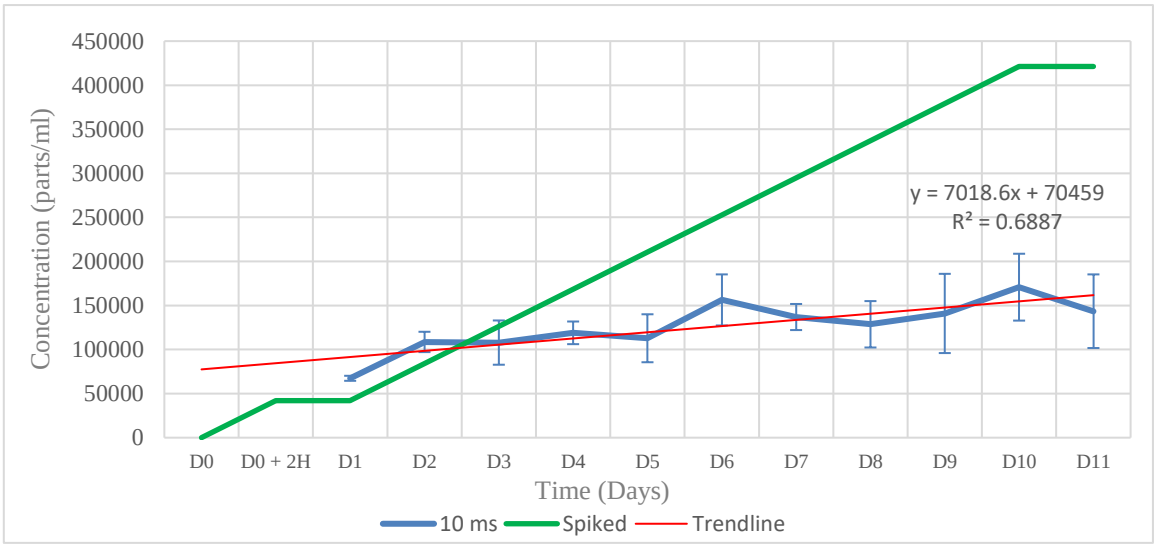

Figure 9. Particle concentration for the AgNP treated seawater tanks, 10 ms dwell time, PG threshold.

The effect of the different thresholds becomes more pronounced in these charts, where it is quite clear that the higher the threshold value (PG > 5σ > 3σ), the fewer the particles detected. This comes as no surprise, as it is expected that smaller particles (resulting from the extensive AgNP dissolution) may not be detected when applying higher threshold value.

What is worth noticing, is the dramatic decrease the application of 5σ and PG criterion has on the determined particle concentration compared to the 3σ threshold. That is supporting the initial suggestion -, according to which larger particles are identified by any threshold while the nature of lower – intensity signals is unclear. However, the trendline fitting is apparently much better in the 3σ case (higher R^2 value), suggesting a more consistent result over time.

Overall, the trend is more or less clear on all the different thresholds, exhibiting an increase (less of it, the higher the threshold) over time, as one could expect due to the daily addition of particles. It is clear that some of the signals are intense enough to be identified as particles using the 3σ threshold, but are eliminated when higher threshold criteria are applied. That could suggest the removal of portions from bigger particles, that could cause a significant pulse themselves, detectable by the lower 3σ threshold, but eliminated by higher threshold criteria.

4.1.1.3. AgNP mean size for AgNP treated seawater tanks as determined using 10 ms dwell time detection

The following charts (*Fig. 10-12*) are devoted to the study of the detected particle Mean Size. They resulted from the conversion of the corresponding Mean Intensity by using the mass calibration equation. Charts of the Mean Intensity can be found in the supplementary section (*Supplementary Section 1.1.3, Fig.7-9*). They should provide an insight on the Ag nanoparticle - seawater system dynamics. Same as before, the results represent an average value of all three tanks. Similar charts regarding the Most Frequent size can be found in the supplementary (*SS 1.1.2 Fig. 4-6*), as they exhibit similar behavior and they do not include any additional information.

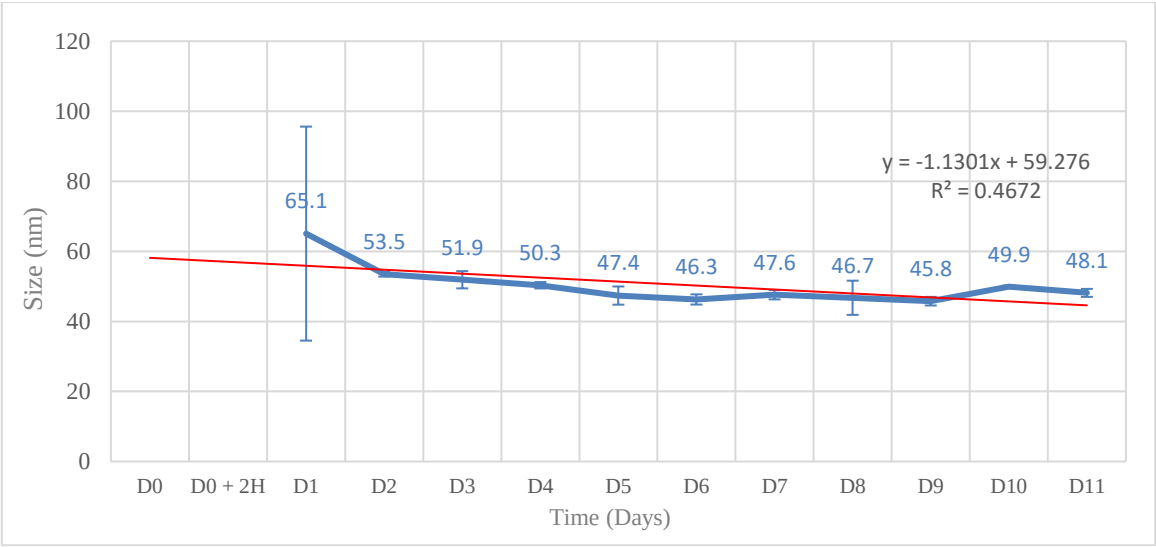

Figure 10. Detected particle mean size for the AgNP treated seawater tanks, 10 ms dwell time, 3σ threshold.

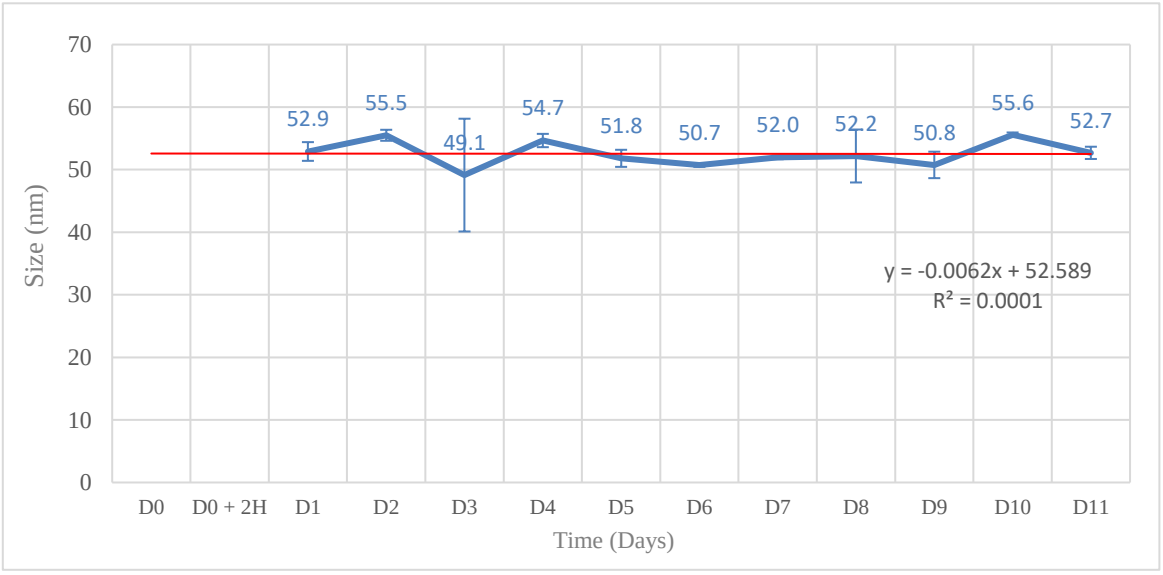

Figure 11. Detected particle mean size for the AgNP treated seawater tanks, 10 ms dwell time, 5σ threshold.

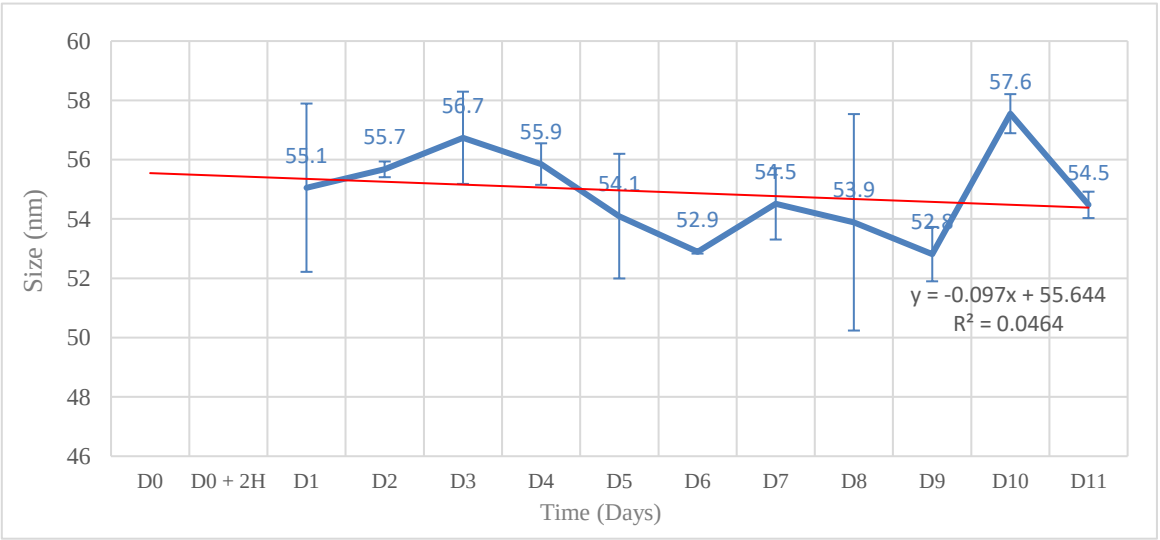

Figure 12. Detected particle mean size for the AgNP treated seawater tanks, 10 ms dwell time, PG threshold.

What is expected for this system (based on the literature[85]), is a decrease of the mean particle size, due to particle dissolution under the effect of the seawater matrix. Both the 5σ and the PG thresholds exhibit a significantly smaller decrease in mean size compared to that observed for the 3σ criterion. These observations further strengthen the validity for why the 3σ criterion has been so widely used for the analysis of nanoparticles, when it comes to ms dwell time detection. It is possible that the spiked nanoparticles indeed do not decrease in size as much as the 3σ threshold criterion chart suggests, but previous studies[85] support the 3σ results over the 5σ or PG results in this case.

Regardless of the threshold criterion applied, the overall trend of the mean size, though slight, is declining, which is, as mentioned before, consistent with the expectations from this specific setting. The seemingly low dissolving rate could be attributed either to the daily addition of more particles of specific dimensions (60 nm), or to the degradation of some particles up to the point that they would no longer be detected by the system. In the first case, the freshly added nanoparticles will not have dissolved as much as the preexisting particles in the tanks. Therefore, they will contribute their higher size (a little less than 60 nm) to the overall mean value, raising it, and therefore somehow ''masking'' the overall dissolving of the preexisting particles. In the second case, preexisting particles might be extremely dissolved, leading them lower than the detection limit. In such a case, they will not contribute their lower size value to the overall mean size value, and the mean size will be raised, since it is only calculated by the sizes of bigger (more recently added) particles. Both of the above-mentioned phenomena are probable, and their effect is supported by the fact that higher threshold criteria exhibit smaller rates of degradation. That means that there are more lower intensity signals (i.e., smaller particles) to be eliminated.

4.1.1.4. Dissolved Ag concentrations for AgNP treated seawater tanks as determined using 10 ms dwell time detection

In order to complete the study of the fate of the Ag particles, the dissolved Ag concentration is required, and it is shown in *Figures 13-15* for the different threshold criteria. As mentioned before, whatever degradation the particles are subjected to it should also be reflected in the dissolved Ag concentration. Same as before, the results represent an average value of all three tanks, and the Ag concentration values have been automatically converted from the dissolved intensity values, also presented in this thesis' supplementary information (*SS 1.1.4, Fig 10-12*).

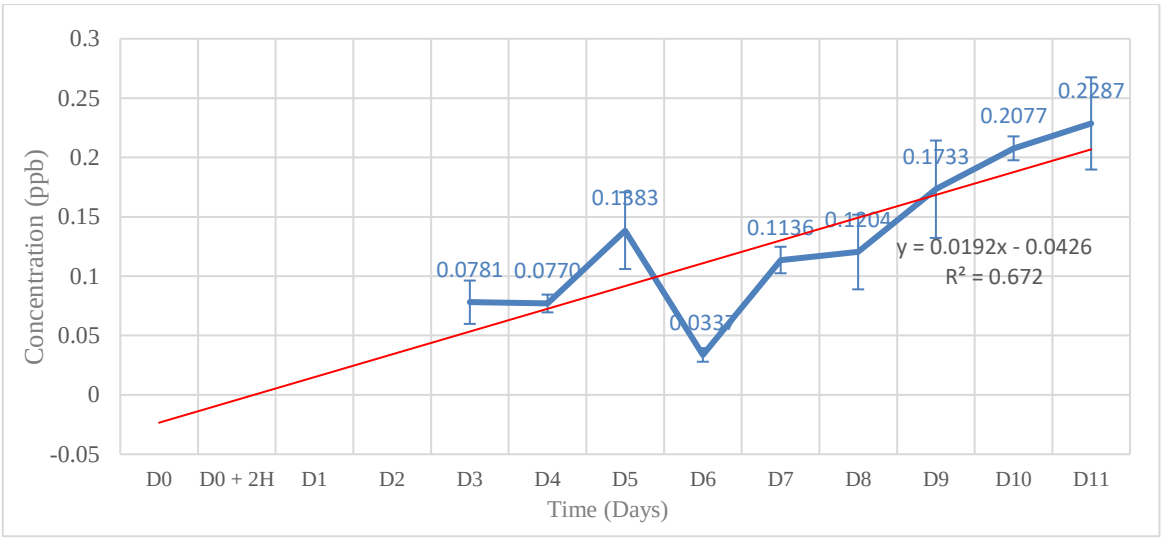

Figure 13. Dissolved Ag Concentration for the AgNP treated seawater tanks, 10 ms dwell time, 3σ threshold.

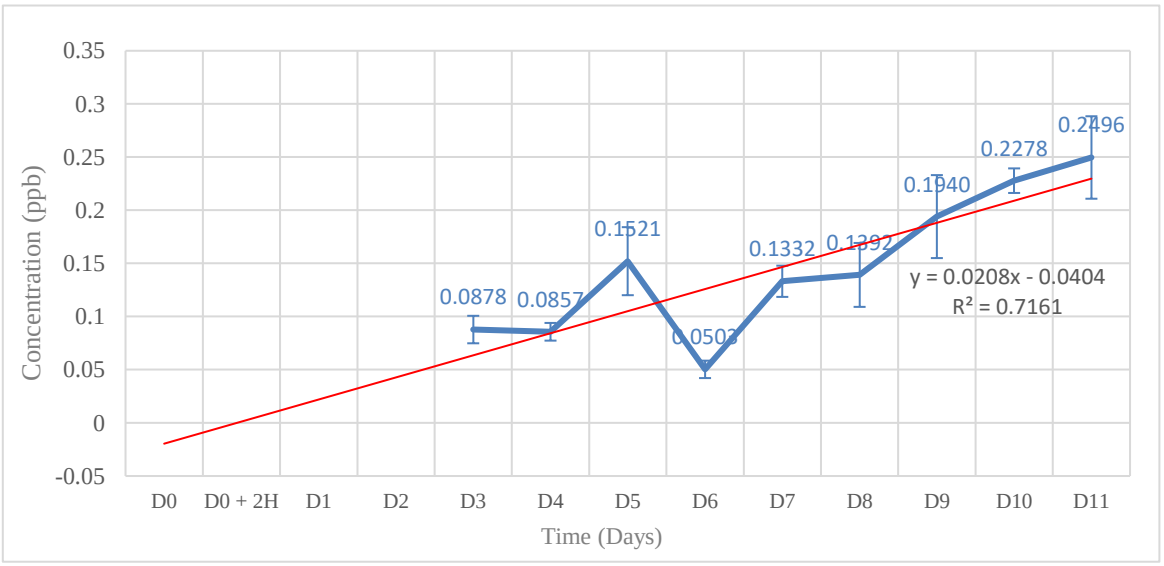

Figure 14. Dissolved Ag Concentration for the AgNP treated seawater tanks, 10 ms dwell time, 5σ threshold.

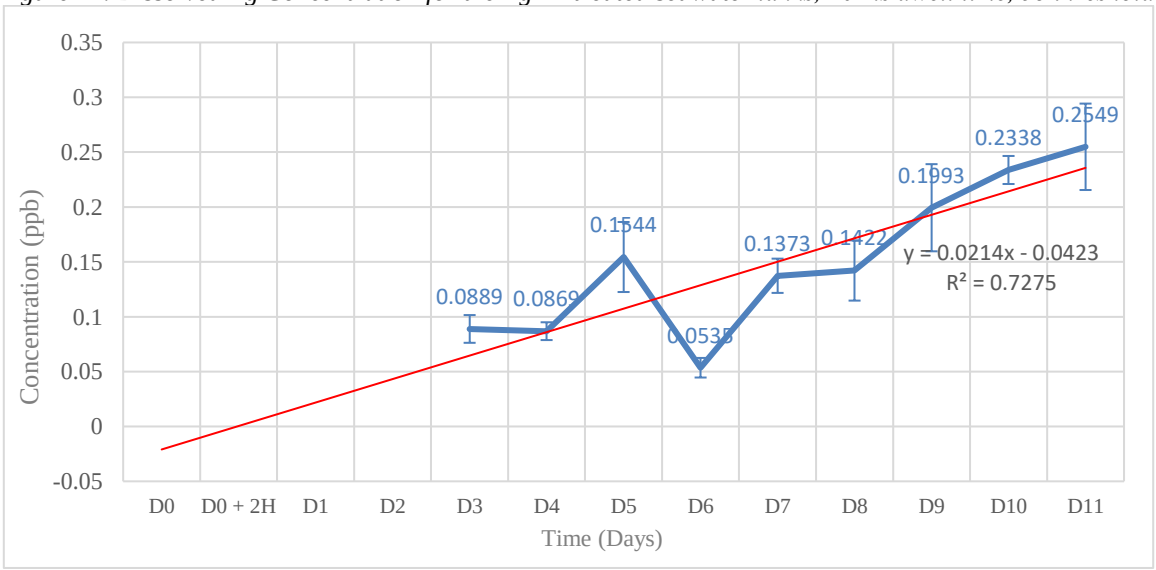

Figure 15. Dissolved Ag Concentration for the AgNP treated seawater tanks, 10 ms dwell time, PG threshold.

Unsurprisingly, the trend is clear no matter the applied threshold criterion, and it shows that the dissolved Ag concentration within the mesocosm system is increasing over time. This clearly shows that AgNP dissolution is occurring over the course of the experiment.
The different threshold values once again result in Ag values very close to one another, while the 3σ is somehow lower. This comes as no surprise, since some lower intensity signals are considered particles, when applying the 3σ threshold, while they are attributed to dissolved after the application of a higher threshold value.

4.1.1.5. Conclusions for the behavior of Ag in AgNP treated seawater tanks as investigated using 10 ms dwell time detection

As far as the 10 ms dwell time is concerned, the system in general yields very high Ag recovery values. What is also very important, is that it remained robust and reliable, meaning that the on – line dilution introduction system sufficiently protected the instrumentation from damage due to the usually detrimental seawater matrix, and its performance was more or less equally sufficient throughout the experiment. While the use of higher thresholds (5s and PG) has provided useful information on the dissolving of the detected particles, the 3σ threshold proved reliable, yielding higher recovery values. It also exhibited higher consistency regarding the study of nanoparticles' size, leading to more reasonable conclusions. Therefore, it is safe to conclude, that for the analysis of suspensions as concentrated as the ones mentioned above ($>10^5$ particles/ml), using 10 ms dwell time detection, the 3σ threshold criterion is better suited, and rightfully used as widely as it currently does. Furthermore, the on – line dilution system proved to be suitable for this kind of analysis of seawater samples, both in terms of results' validity, and protections of the instrumentation.

4.1.2. AgNP treated seawater tanks, analyzed using 75 μs dwell time detection

4.1.2.1. Ag mass balances for AgNP treated seawater tanks as determined using 75 μs dwell time detection

The following charts (*Fig. 16-18*) summarize the quantity of Ag detected, both as dissolved ionic Ag, as well as AgNP, for each of the three thresholds applied. Each data point represents an average value that has resulted from the analysis of the three seawater tanks. The ''spiked'' values (yellow line) refer to the cumulative amount of silver (Ag) added to each tank as AgNPs, i.e., 50 parts per trillion (ppt) Ag daily in the form of AgNP. The trendline (red line) is a fit to the experimental data, whereas each numerical value given in the figures corresponds to an average value from the three tanks.

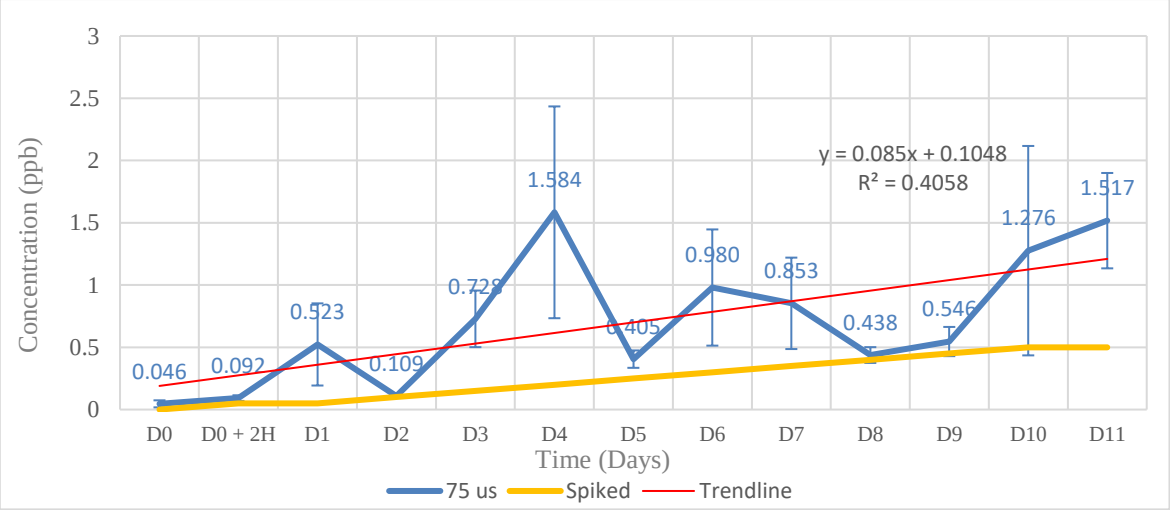

Figure 16. Mass balance for the AgNP treated seawater tanks, 75 μs dwell time, 3σ threshold.

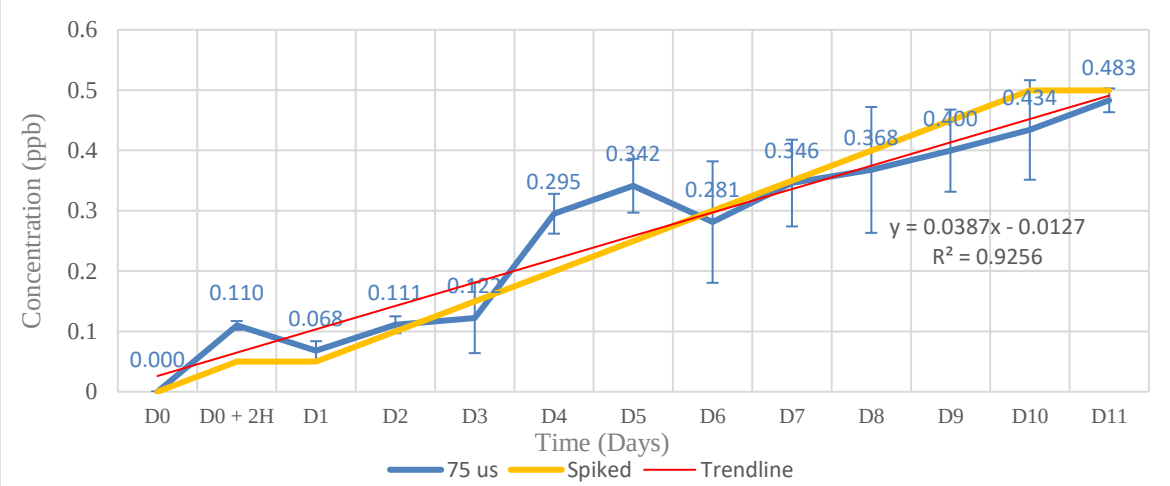

Figure 17. Mass balance for the AgNP treated seawater tanks, 75 μs dwell time, 5σ threshold.

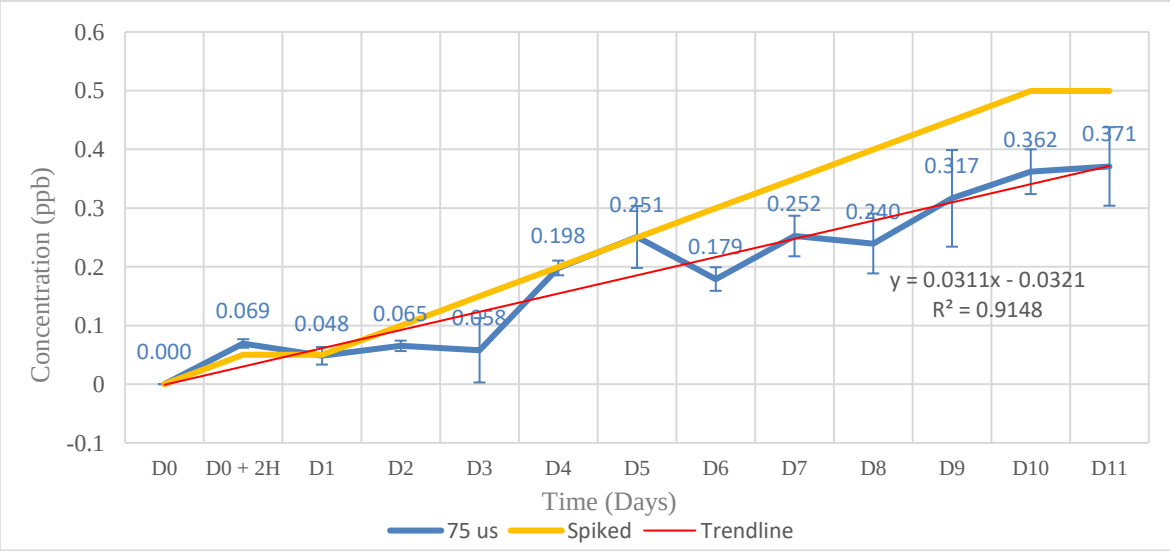

Figure 18. Mass balance for the AgNP treated seawater tanks, 75 μs dwell time, PG threshold.

Right from the very start, it is quite obvious by the presented uncertainties and the unrealistically high and highly inconsistent recovery value (345.2%, ±294.4% standard deviation, while the R^2 value is also very low), that the 3σ threshold is entirely unsuitable for the analysis when using μs dwell time detection. Both of the other thresholds are characterized by reasonable recovery values (5σ = 115.9%, ±39.5% standard deviation, and PG = 79.0%, ±26.1% standard deviation), and clear trends, while their R^2 values indicate an acceptable fitting of the data (>0.9 for the both of them) so the most suitable among them will have to be determined after a more in – depth analysis of the data. Despite the obvious miscalculation, quite possibly due to the detection of false positive pulses (pulses falsely attributed to particles), even the 3σ threshold exhibits an increasing trend of Ag recovery over the days. However, both the 5σ and the PG thresholds exhibit very similar increasing trends, as expected, taking into account the daily addition of the 50 ppt of Ag nanoparticles.

4.1.2.2. AgNP particle concentrations for AgNP treated seawater tanks as determined using 75 μs dwell time detection

Looking deeper into the nature of the Ag species in the seawater samples, the determined Ag particle concentration is shown in *Figures 19-21*, obtained using different threshold criteria. The actual numbers of detected peaks have also been presented in charts and can be found in the supplementary section of the present thesis (*SS 1.2.1, Figures 13-15)*. The results represent an average value that has resulted from the data obtained from all three tanks. The ''spiked'' values refer to the cumulative amount of silver (Ag) added as AgNPs daily at 50 parts per trillion (ppt) corresponding to 42125 particles per mL of seawater sample.

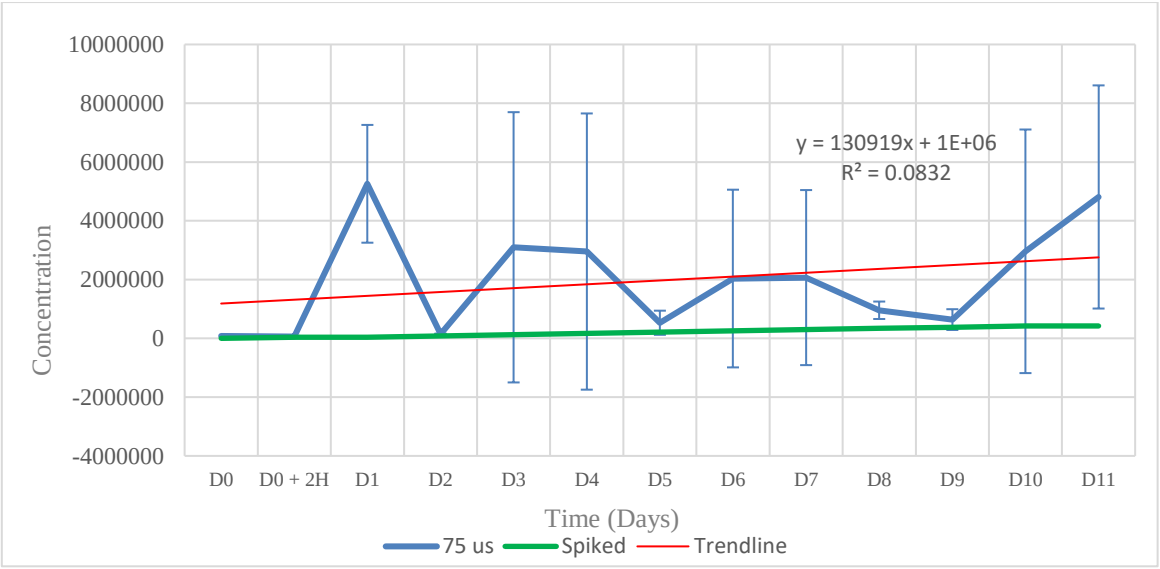

Figure 19. Particle concentration for the AgNP treated seawater tanks, 75 μs dwell time, 3σ threshold.

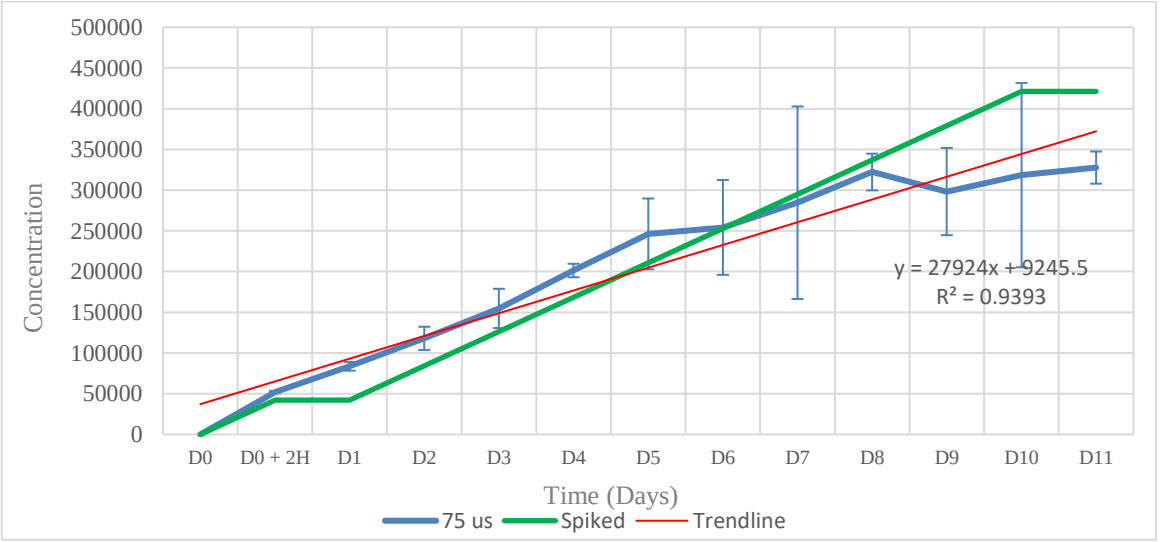

Figure 20. Particle concentration for the AgNP treated seawater tanks, 75 μs dwell time, 5σ threshold.

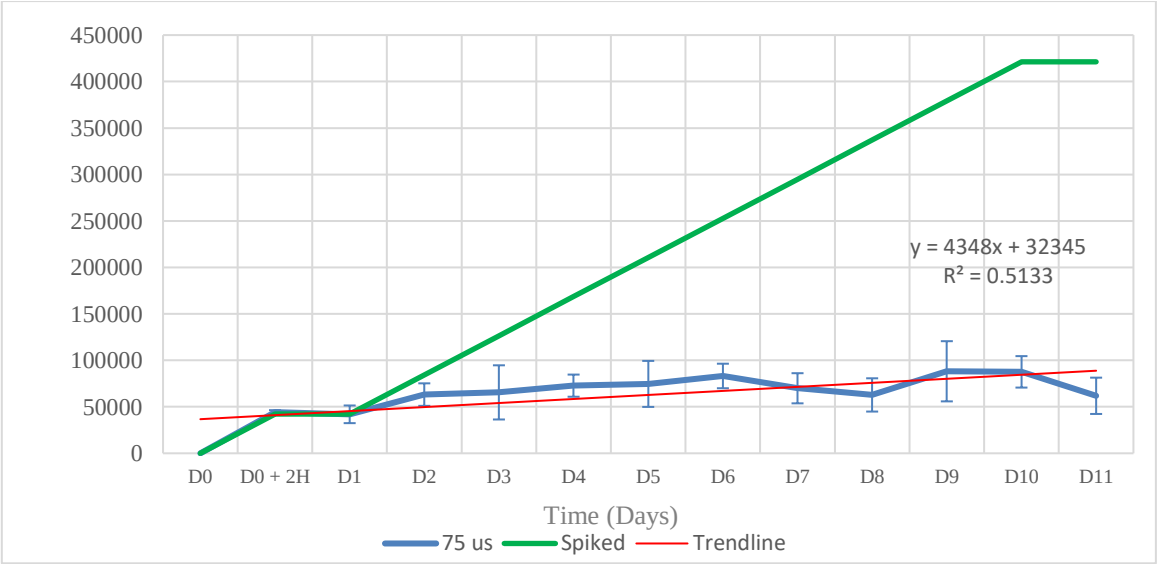

Figure 21. Particle concentration for the AgNP treated seawater tanks, 75 μs dwell time, PG threshold.

As mentioned before, the 3σ threshold is way off when it comes to using a dwell time as low as 75 μs, probably due to the mean value of the dataset significantly approaching zero, following a non - normal background distribution (Poisson – Gaussian[41,117,125,131]). Apparently, the application of a higher threshold that incorporates a higher number of standard deviations (5σ) results in the correction of that miscalculation by a significant factor, leading to much more realistic particle detection numbers. The arising doubt from the observation of these data though stems from the fact that, despite the addition of intact nanoparticles every day, there should be an observed degradation of the nanoparticles already existing in the solution from previous days. On the other hand, the PG thresholds seems to be detecting a not only low, but also more or less fixed number of nanoparticles, while the lower uncertainty suggests that the PG measurements are more reliable. Given the fact that there is a substantial difference in the detected nanoparticles between the two different thresholds (5σ and PG) and taking into account that the particles' degradation is certain, there are two distinct possibilities regarding the system's dynamics: In the first case, the particles have overnight degraded, up to the point that they are small enough to be falsely identified as part of the dissolved analyte by the unnecessarily higher PG threshold. In that case, the 5σ will still be able to detect them. In the second case, the particles have indeed, through the course of a day, dissolved, so the PG threshold detects mainly the newly added particles. As a result, the 5σ threshold also falsely identifies more signals as particles, due to the difference in the background distribution.

Taking into account that the 10ms data clearly show the detection of an increasing number of nanoparticles per mL, it is considered a little more likely that the PG threshold is unnecessarily high, leading to the exclusion of signals that actually correspond to particles. There is also the possibility, due to the detection of every particle over multiple datapoints, that the overall signal of smaller particles would be so stretched (meaning their overall profile peak would be ''flattened''), that no datapoint would be intense enough to overcome the PG threshold. Given the fact though, that both of their recovery values are realistic, despite the fact that the PG threshold is more consistent (lower standard deviation), there are, up to this point, not enough data to decide which one is more suitable for this specific analysis.

Overall, regardless of their differences, all three of the applied thresholds exhibit the same behavior, following an increasing trend over the course of the experiment, as one should expect due to the daily addition of the nanoparticulate analyte.

4.1.2.3. AgNP mean size for AgNP treated seawater tanks as determined using 75 μs dwell time detection

The following charts (*Fig. 22-24*) are devoted to the study of the detected particle Mean Size. They resulted from the conversion of the corresponding Mean Intensity by using the mass calibration equation. Charts of the Mean Intensity can be found in the supplementary section (*SS 1.2.3, Fig. 19-21*). They should provide an insight on the Ag nanoparticle - seawater system dynamics. Same as before, the results represent an average value of all three tanks. Similar charts regarding the Most Frequent size can be found in the supplementary (*SS 1.2.2, Fig. 16-18*), as they exhibit similar behavior and they do not include any additional information.

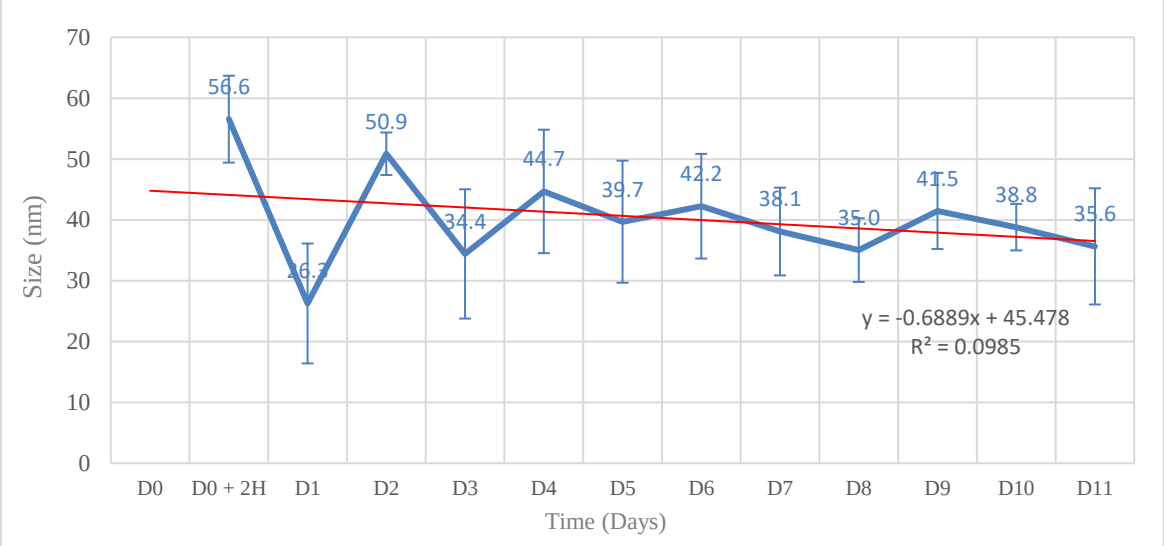

Figure 22. Detected particle mean size for the AgNP treated seawater tanks, 75 μs dwell time, 3σ threshold.

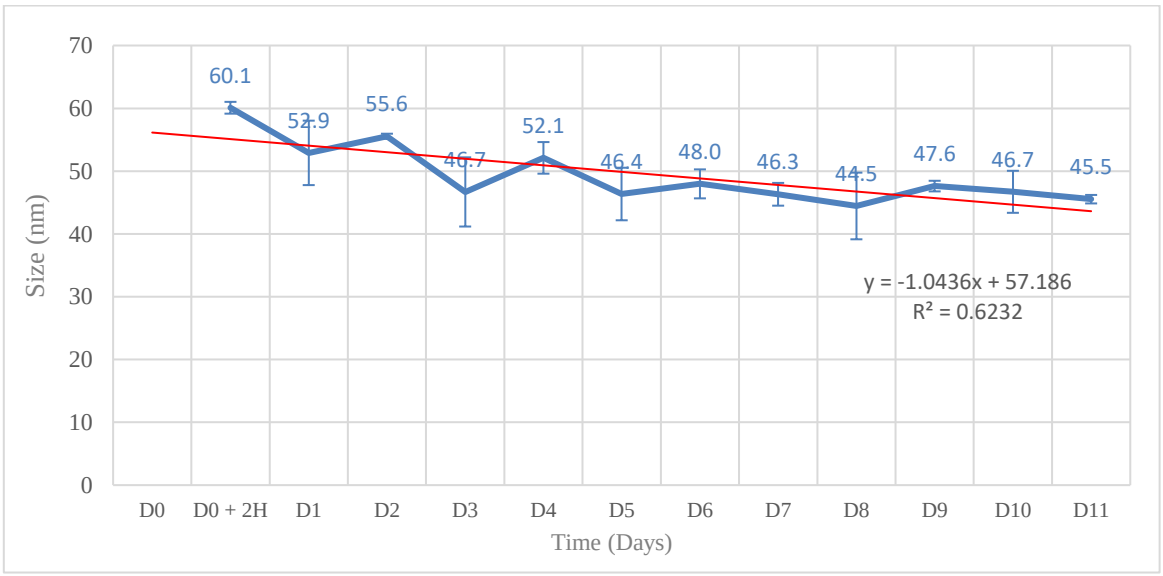

Figure 23. Detected particle mean size for the AgNP treated seawater tanks, 75 μs dwell time, 5σ threshold.

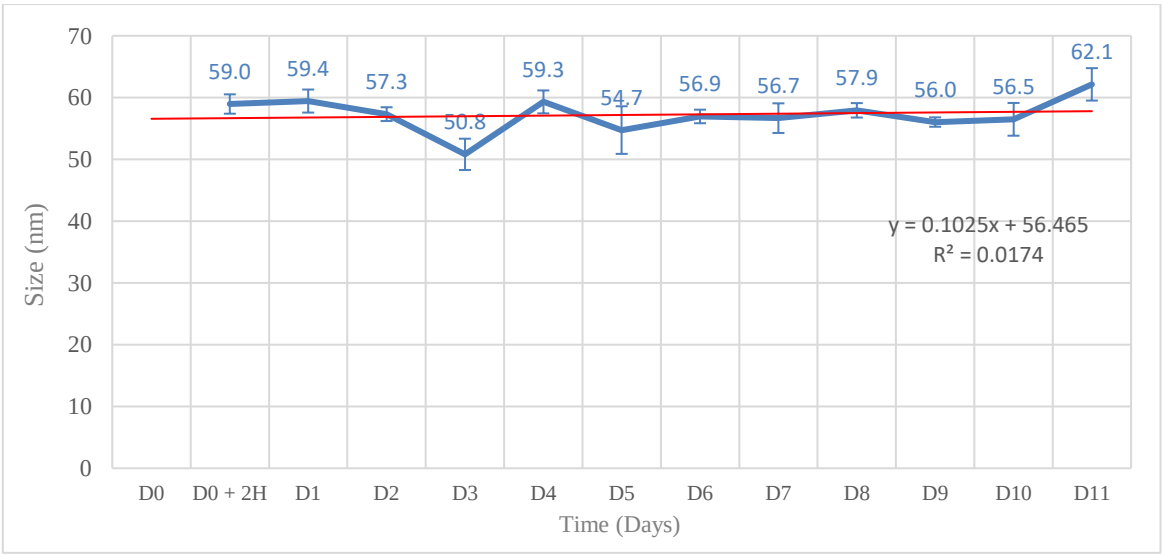

Figure 24. Detected particle mean size for the AgNP treated seawater tanks, 75 μs dwell time, PG threshold.

Observing the uncertainties of all three of the Mean Size charts, it is clear that the 3σ results are quite a bit more inconsistent. It is, no doubt, affected by the sum of the nanoparticles bordering the detection limit, due to slight differences in the conditions every day. The 5σ results exhibit a more consistent and predictable behavior, as the mean size is expected to gradually drop with every passing day, due to the contribution of the smaller -size particles that have resulted because of the observed AgNPs dissolution. The newly added particles should also affect the mean size, but due to their number being lower than the preexisting ones', their cumulative result should probably lead to a decrease of the overall observed mean size. The PG threshold chart though exhibits a constant mean size for the detected nanoparticles as a function of time. That observation, taking into account the almost fixed number of particles detected per day (40000 – 50000 per ml) and the known size of the reference material used (60 nm), would suggest that the PG threshold is mainly detecting the particles that have been added the day prior to the analysis (50 ppt corresponds to around 42000 particles per ml). Whether that means that the particles have indeed dissolved to a size lower than the detection limit, or that the PG threshold is unnecessarily high, cannot be extracted as a conclusion by the data that have been presented so far.

Excluding the PG threshold, the 3σ and 5σ thresholds both suggest a lowering of the particle mean size over the course of the experiment, a conclusion consistent with the expectations of the study. The following comparative figure (*Figure* 25) presents the size distributions of the individual experimental days, for both of the technical replicates (summed up) of the 1st nanoparticle treated tank alone. This in an attempt to look deeper into the PG threshold's results. So far, the results indicate that both the 5σ and the PG thresholds could yield valuable results.

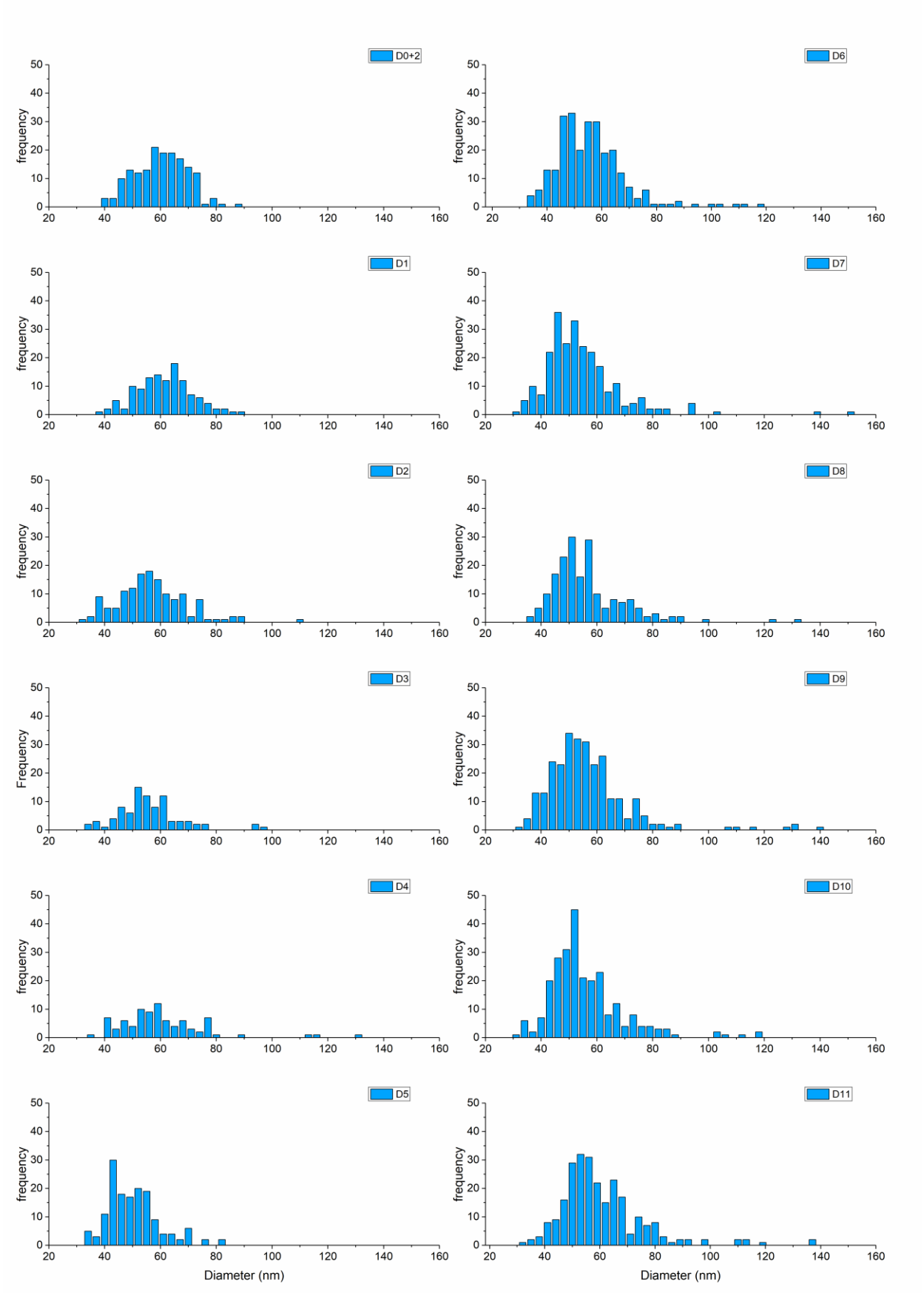

Figure 25. *Size distributions of the sum of the two technical replicates for AgNP1 treated seawater tank, 75 μs dwell time, PG threshold.*

Due to variations of the transport efficiency from day to day, the sum of the detected peaks might differ from day to day (i.e, the sum of the frequencies in each day). It is quite clear though, that the PG threshold accurately depicted the first day's results (AgBPEI reference material: 60 ± 5 nm diameter). Moreover, the distribution expectedly widened over the next few days, and its peak is clearly shifted (up to, maybe, D3). From then on, a second peak appears to be forming at lower size values (Around 45 nm), that becomes quite prominent on D5 and D6, indicating the expected nanoparticles' degradation. Finally, by the end of the experiment (D10 and D11), not only are the two peaks distinct enough to be clearly separated from one another, but the lower sizes peak is more prominent than the, also expected (due to the newly added particles) ~ 60 nm peak. Overall, the results are promising regarding the PG threshold, as the results are quite close to what was expected.

4.1.2.4. Dissolve Ag concentrations for AgNP treated seawater tanks as determined using 75 μs dwell time detection

In order to complete the study of the fate of the Ag particles, the Dissolved Ag Concentration is required, and is shown in *Figures 26-28*. As mentioned before, whatever degradation the particles are subjected to it should also be reflected in the dissolved Ag concentration. Same as before, the results represent an average value of all three tanks, and the Ag concentration values have been automatically converted from the Dissolved Intensity values, also presented in this thesis' supplementary information (*SS 1.2.4, Figures 22-2*).

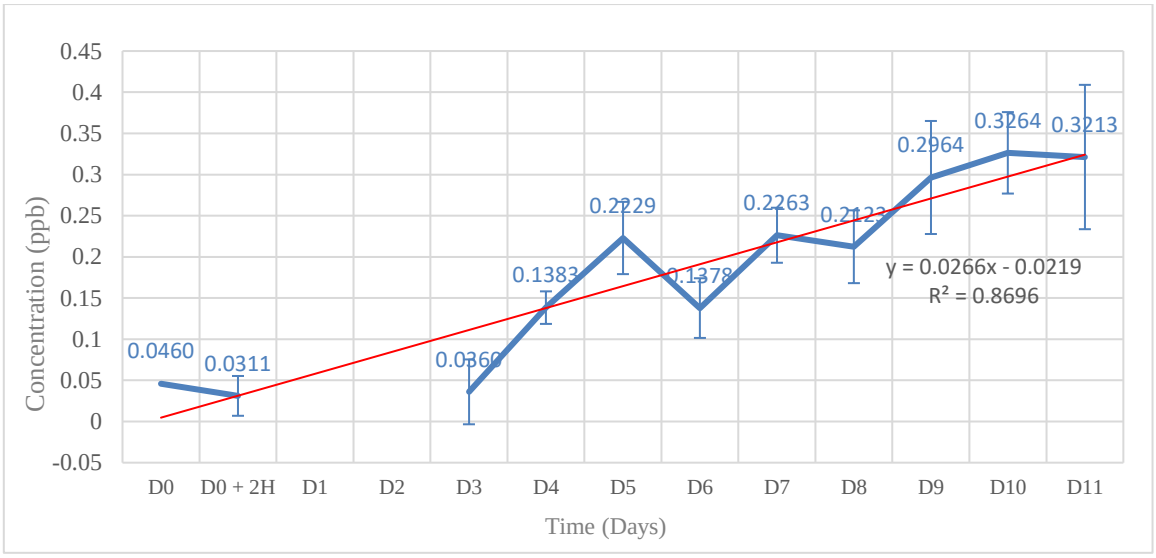

Figure 26. Dissolved Ag Concentration for the AgNP treated seawater tanks, 75 μs dwell time, 3σ threshold.

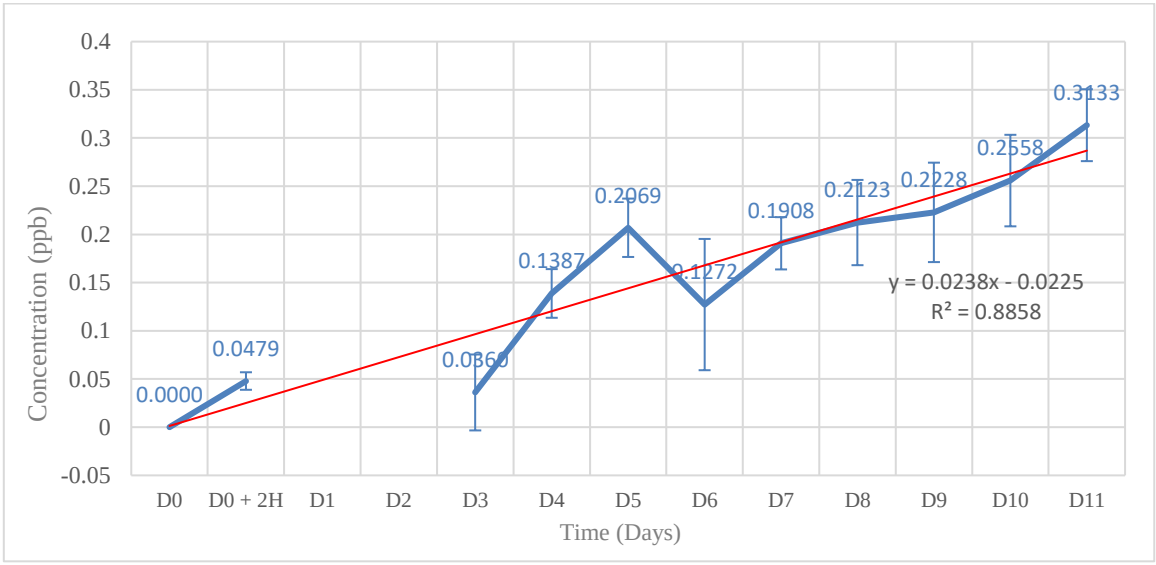

Figure 27. Dissolved Ag Concentration for the AgNP treated seawater tanks, 75 μs dwell time, 5σ threshold.

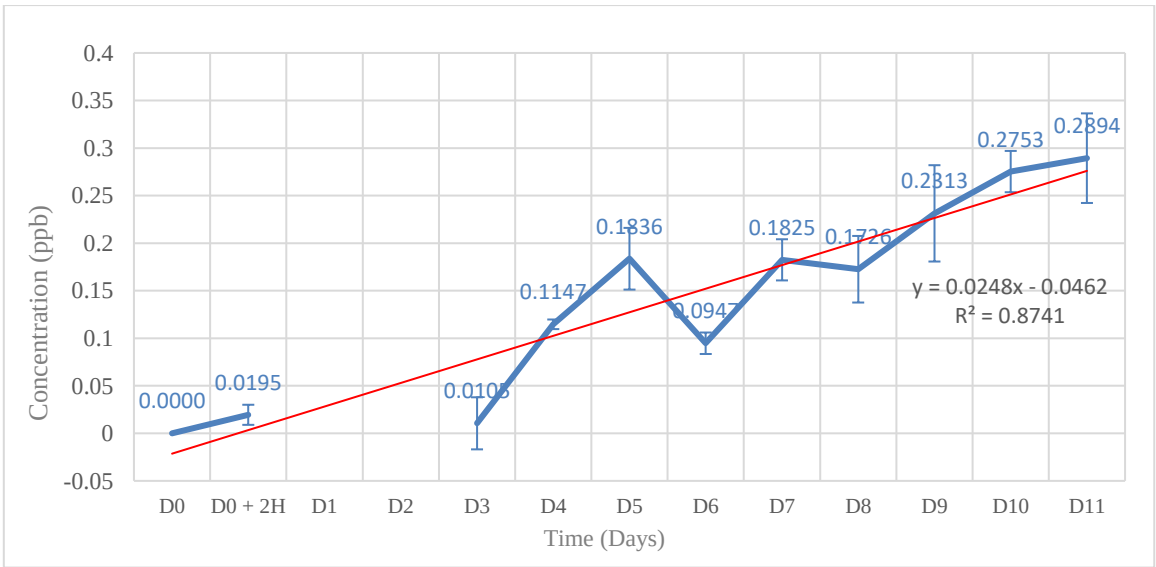

Figure 28. Dissolved Ag Concentration for the AgNP treated seawater tanks, 75 μs dwell time, PG threshold.

Contrary to the expected increase on the detected dissolved Ag after the application of a higher threshold, the concentration of the detected dissolved Ag remains more or less constant, taking into account the associated uncertainties. In addition, not all of the points follow the same behavior, as some of them (D9, D10, etc.) are actually when processed through the PG threshold, while others are lower (D4, D5, etc.). Due to the severe elimination of background (the primary reason for using a lower dwell time), it comes as no surprise that the results on the dissolved analyte, after the 75 μs analysis are somewhat difficult to interpret. Because the vendor's software algorithm for data processing is not entirely understood, it is quite difficult to produce a convincing argument to explain this unexpected behavior. Since the mass calibration procedure does not include the application of any threshold though, it is possible that a significant difference between the threshold of the calibration and the threshold of the sample (or even the ratio of the threshold to the detected dissolved intensity) could cause some unintended miscalculation.

4.1.2.5. Conclusions for the behavior of Ag in AgNP treated seawater tanks as investigated using 75 μs dwell time detection

Taking all the above-mentioned information into consideration, as far as the 75 μs dwell time is concerned, the system in general yields very high Ag recovery values, while remaining robust and reliable, as mentioned before (Section 4.1.1.5.). It is clear that the 3σ threshold is no longer providing reliable results as the Ag mass balance is not maintained. The source of such an error may be the immense contribution of false positives signals to the detected Ag mass due to the non-normal distribution of the background, and therefore the inaccurate normal distribution statistics used to discriminate the nanoparticle signals from the background. There is a high chance that the shape of the background distribution plays a significant role in these miscalculations, but the application of the 5σ threshold overall provided results of similar value to those of the PG threshold. That fact is suggesting that the correction needed could be provided by the study of the gaussian statistics, by adding a case – appropriate number of standard deviations to the determined threshold value[75]. If a single conclusion had to be drawn for all the above-mentioned results, based on the more realistic and more consistent mass balance values of the PG threshold, the slight overestimation of the particle concentration by the 5σ threshold, and the size distributions that exhibited an expected particle dissolution it seems that the PG threshold application might be a better fit for the 75 μs analysis protocol.

4.1.3. Ionic Ag treated seawater tanks, analyzed using 10 ms dwell time detection

4.1.3.1. Ag mass balance for ionic Ag treated seawater tanks as determined using 10 ms dwell time detection

The following charts (*Fig. 29-31*) summarize the quantity of Ag detected, both as dissolved ionic Ag, as well as AgNP, for each of the three thresholds applied. Each data point represents an average value that has resulted from the analysis of the three seawater tanks. The ''spiked'' values (yellow line) refer to the cumulative amount of silver (Ag) added to each tank as ionic Ag, i.e., 50 parts per trillion (ppt) Ag daily in the form of ionic Ag.

The trendline (red line) is a fit to the experimental data, whereas each numerical value given in the figures corresponds to an average value from the three tanks.

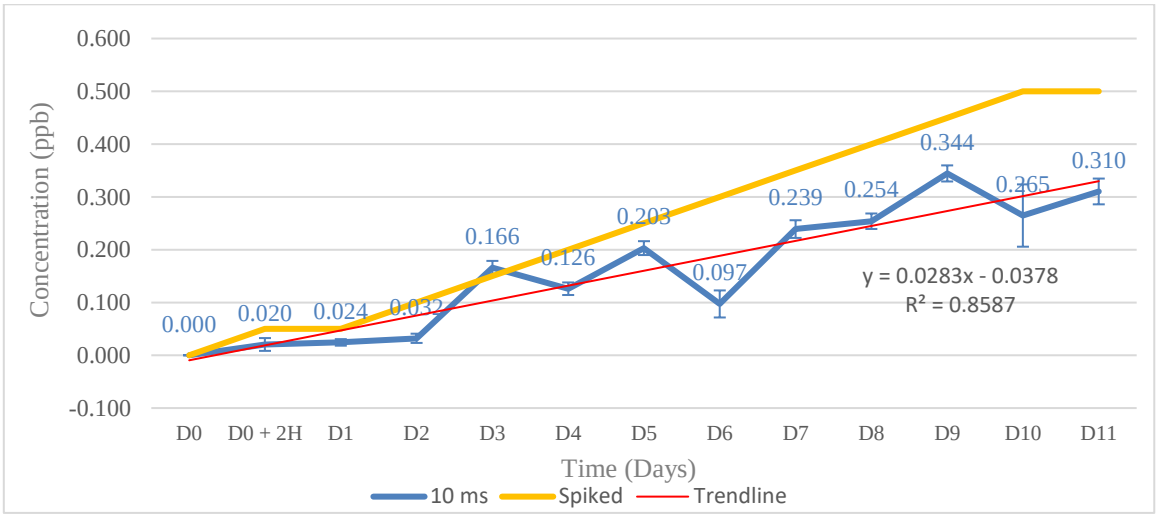

Figure 29. Mass balance for the Ag treated seawater tanks, 10 ms dwell time, 3σ threshold.

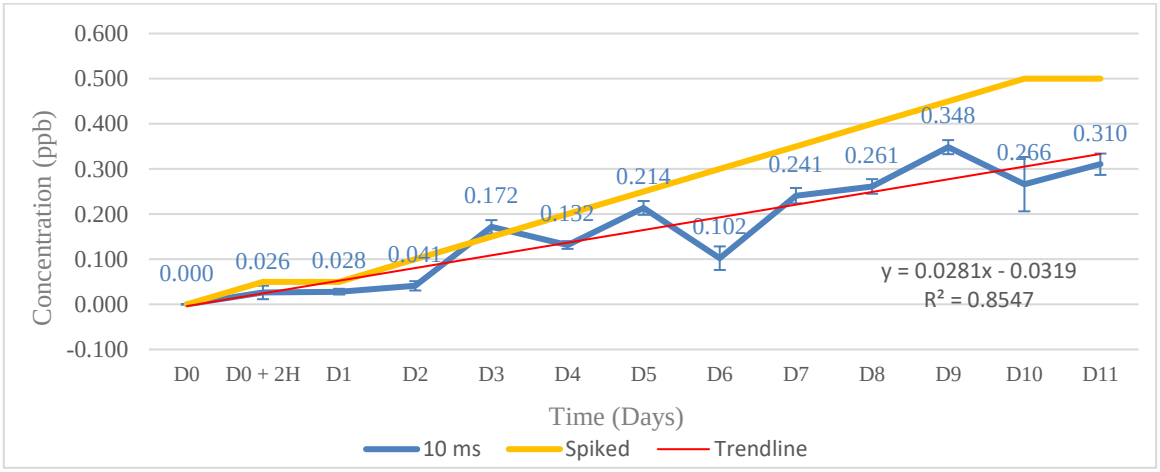

Figure 30. Mass balance for the Ag treated seawater tanks, 10 ms dwell time, 5σ threshold.

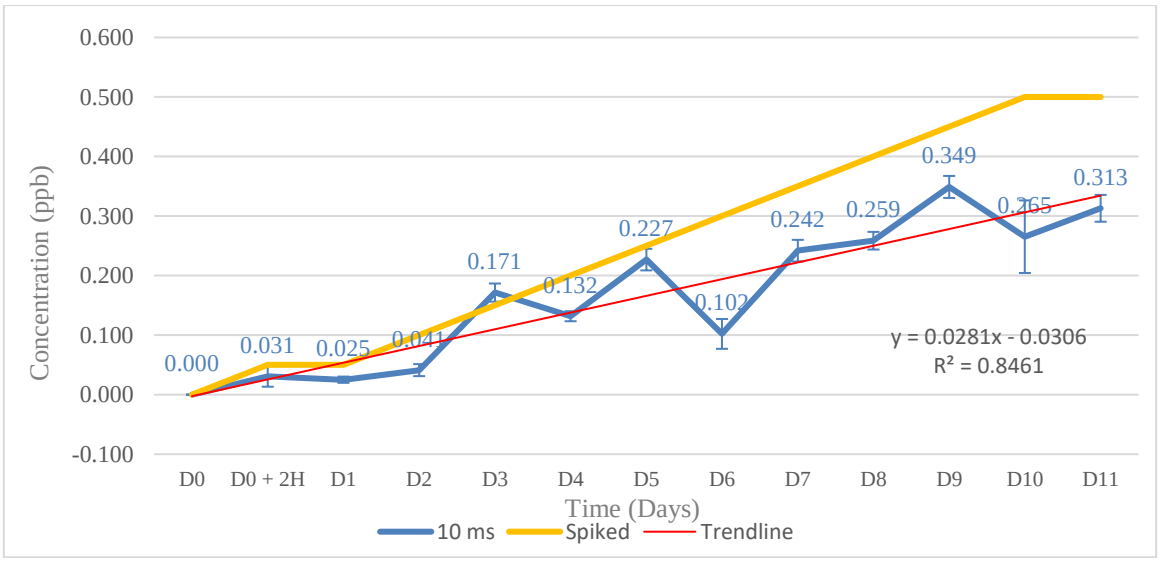

Figure 31. Mass balance for the Ag treated seawater tanks, 10 ms dwell time, PG threshold.

The difference when using a different threshold criterion appears to be nearly insignificant, meaning they are all performing similarly well on this specific setting. All three seem to be in agreement, regarding the expected detected cumulative quantities of dissolved and particulate Ag, as their respective recovery values are 61.1% ±22.3% standard deviation for the 3σ, 64.7% ±21.2% standard deviation for the 5σ, and 65.4% ±21.7% standard deviation. As a first estimation, that high level of agreement could be attributed to the fact that the total Ag quantity in these samples is mostly in ionic form. The dissolved Ag concentration calculation is extracted by averaging the non – particle signals of the whole run, meaning that there are essentially a lot more datapoints, which of course benefits the statistical analysis. So, if the dissolved intensity is well – defined from the beginning, the application of a different threshold will hardly cause any changes, because there are not enough particles detected to severely affect the results. The lower recovery values (even lower on later days) could be an indication of the formation of Ag containing moieties: They could be small enough to not be identified as particles, but would also be ''lost'' in the analysis of the dissolved as well. In that case, they would only appear as slightly more intense pulses, essentially ''diluted'' among all the other lower intensity signals, due to their significantly smaller number.

All three of them exhibit the same behavior over time, being in acceptable agreement with the expected values, as previously discussed, taking into account the daily addition of the 50 ppt of ionic Ag.

4.1.3.2. Dissolved Ag concentrations in ionic Ag treated seawater tanks as determined using 10 ms dwell time detection

The following charts (*Figures 32-34*) represent the detected dissolved intensity, as well as the cumulative quantity of the daily added dissolved Ag. Same as before, the results represent an average value, resulted from the data processing of all three tanks. The values are acquired after automated conversion, through the mass calibration, from the detected Dissolved Intensity. Those charts are available in this thesis' supplementary information (*SS 1.3.4, Figures 34-36*).

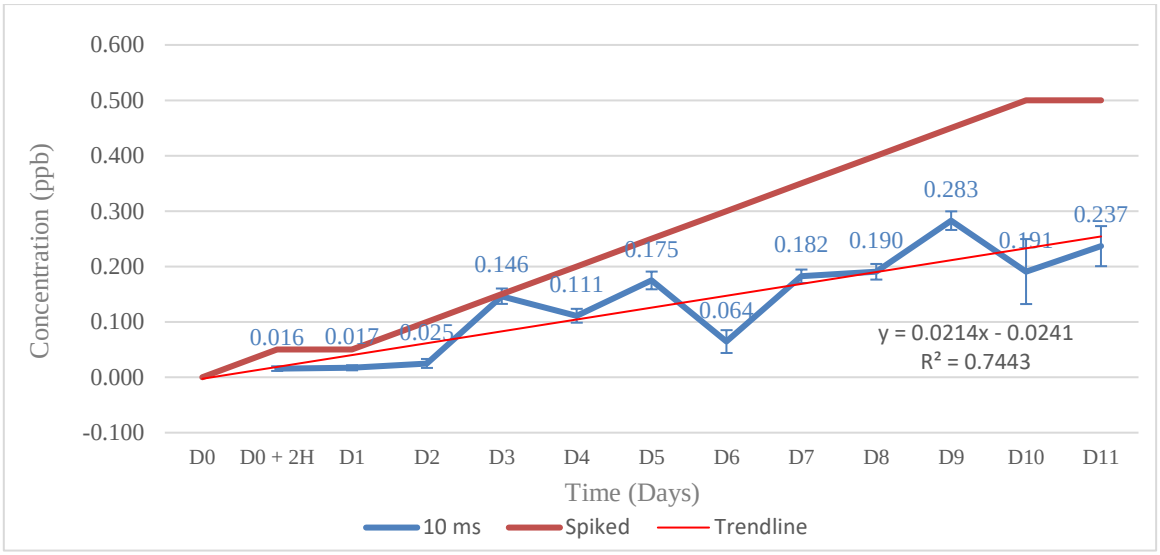

Figure 32. Dissolved Ag Concentration for the Ag treated seawater tanks, 10 ms dwell time, 3σ threshold.

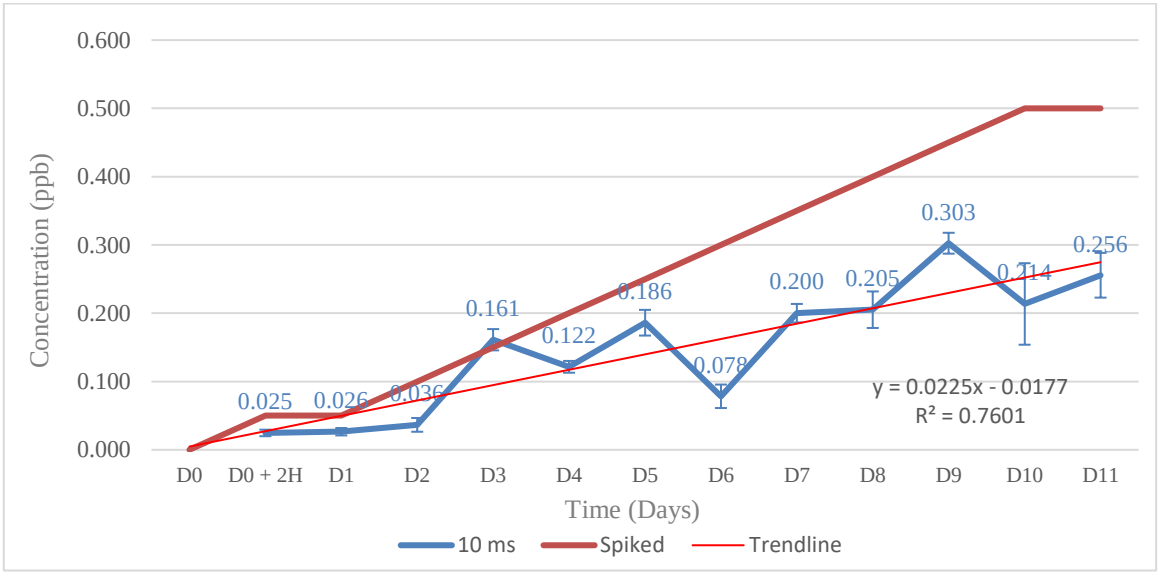

Figure 33. Dissolved Ag Concentration for the Ag treated seawater tanks, 10 ms dwell time, 5σ threshold.

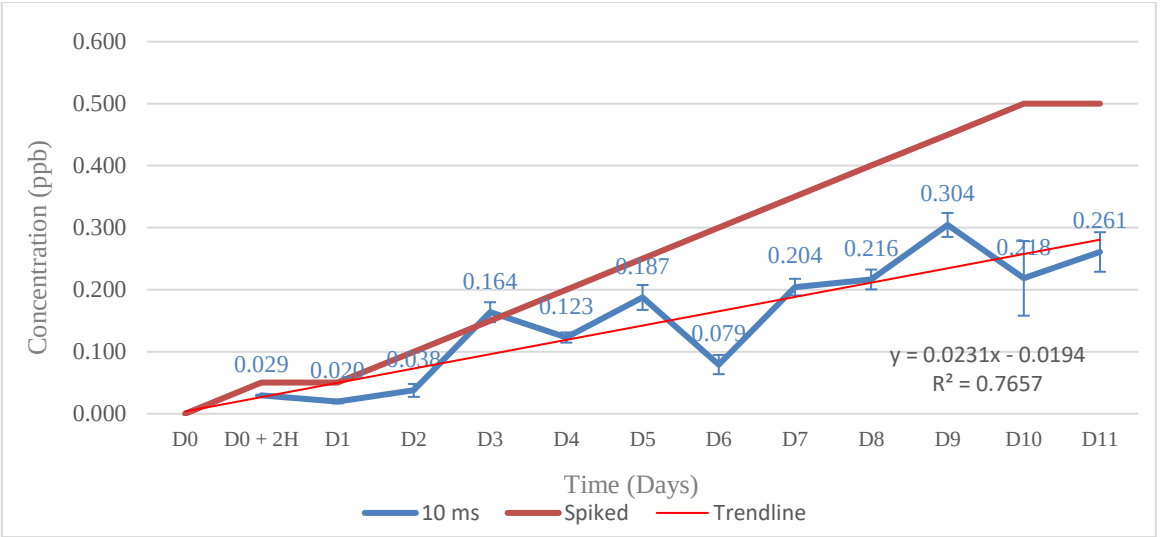

Figure 34. Dissolved Ag Concentration for the Ag treated seawater tanks, 10 ms dwell time, PG threshold.

The application of a higher threshold seems to be leading to the overall rising of the detected dissolved Ag concentrations. Such a change can be expected, taking into account the fact that the higher the threshold is, the less the pulses identified as particles will be, leaving more pulses of higher than the average value to contribute to the dissolved quantity determination.

The trend is clear no matter the applied threshold value, and it shows that the dissolved Ag concentration within the mesocosm system is increasing as a function of time. This observation is in agreement with the expected results, taking into account the daily addition of ionic silver (50 ppt per day). Overall, there is no significant difference when using a different threshold.

4.1.3.3. Particulate Ag in ionic Ag treated seawater tanks as determined using 10 ms dwell time detection

Looking deeper into the nature of the Ag species in the samples, the determined Ag particle concentration is shown in *Figures 35-37*, obtained using different threshold criteria. The actual numbers of detected peaks have also been presented in charts and can be found in the supplementary section of the present thesis (*SS 1.3.1, Figures 25-27*). The results represent an average value that has resulted from the data obtained from all three tanks. It is worth noting, that the detection of pulses that would indicate the formation of any kind of particles, aggregates, or in any way a confinement of high quantities of analyte within defined spatial compartments, was unexpected, since the dynamics of the system are still being documented. Therefore, no assumptions, conclusions or explanations on the nature of the moieties that are responsible for these pulses will be made at this stage of the study, and the ''particle concentration'' titles used in the following charts are used for convenience reasons. Regarding the nature and origin of the detected single moieties, see *Section 4.1.5*.

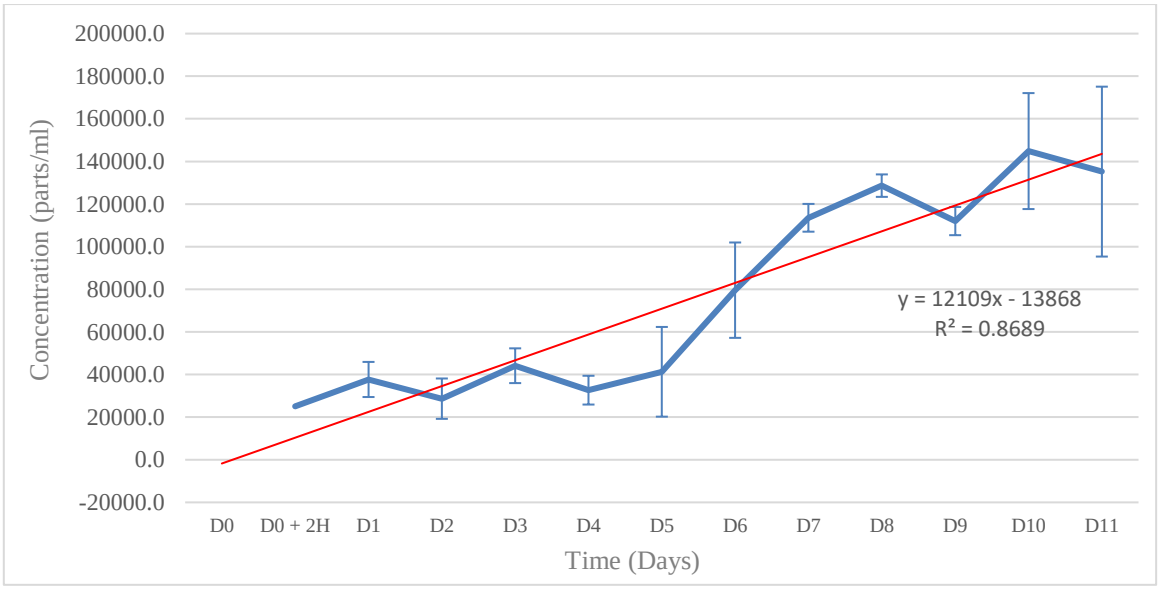

Figure 35. Particle concentration for the Ag treated seawater tanks, 10 ms dwell time, 3σ threshold.

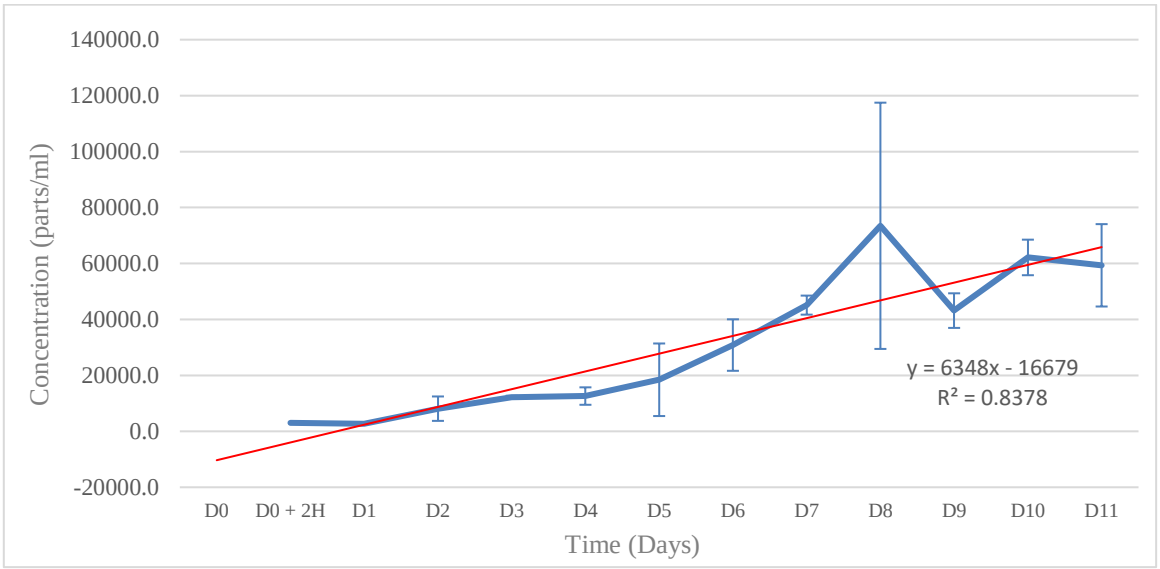

Figure 36. Particle concentration for the Ag treated seawater tanks, 10 ms dwell time, 5σ threshold.

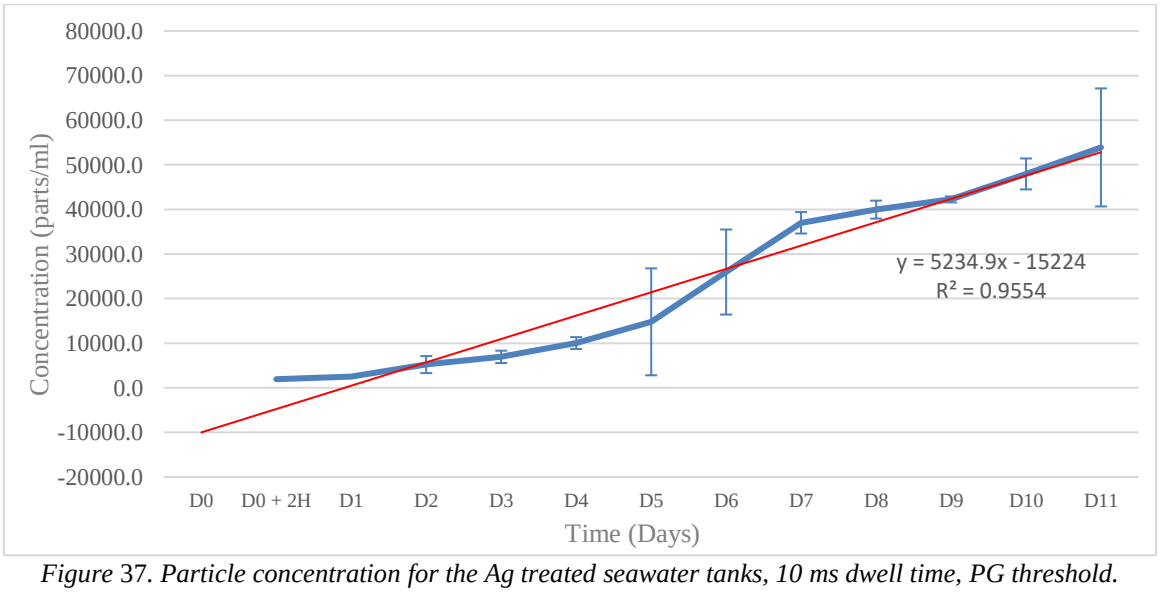

Figure 37. Particle concentration for the Ag treated seawater tanks, 10 ms dwell time, PG threshold.

As expected, the application of higher threshold values leads to the elimination of more spike signals. It is quite interesting, that the difference between the 5σ and the PG threshold is approximately half in comparison to the difference between the 3σ and the 5σ. That is providing an indication that a significant amount of the moieties detected and identified as particles by the 3σ threshold are quite small or are just signal noise.
Overall, all three of the thresholds depict quite clearly the gradually increasing number of some Ag – containing species, regardless of the nature or origin of the detected moieties. That conclusion is suggested by the increasing number of event pulses over the course of the experiment, which means that, regardless of the nature of the detected moieties, there is undeniably a confinement of a significant number of Ag atoms within very small spatial compartments.

4.1.3.4. Ag particle mean size in ionic Ag treated seawater tanks as determined using 10 ms dwell time detection

In an attempt to further investigate the occurrence and nature of the detected moieties, the following charts (*Fig 38-40*) are devoted to the study of their size variations over the course of the experiment. The ''mean size'' titles are used for convenience reasons, in order for the charts to be able to be examined in comparison to the respective charts of the AgNP treated tanks' study. The calculation of the ''size'' values is supposing a spherical shape for nanoparticles, and a composition of pure elemental Ag. Therefore, the equivalent size that is depicted in the following charts corresponds to the size these moieties would have, if they were spherical particles of pure Ag. As previously mentioned, it is resulting from an automated conversion, through the standard mass calibration, of the corresponding Mean Intensity (*SS 1.3.3, Figures 31-33)*. Those charts can also be found in the supplementary section. Same as before, the results represent an average value, resulted from the data processing of all three tanks. Similar charts regarding the Most Frequent size can be found in the supplementary (*1.3.2, Figures 28-30*), as they exhibit the same behavior and they do not include any additional information.

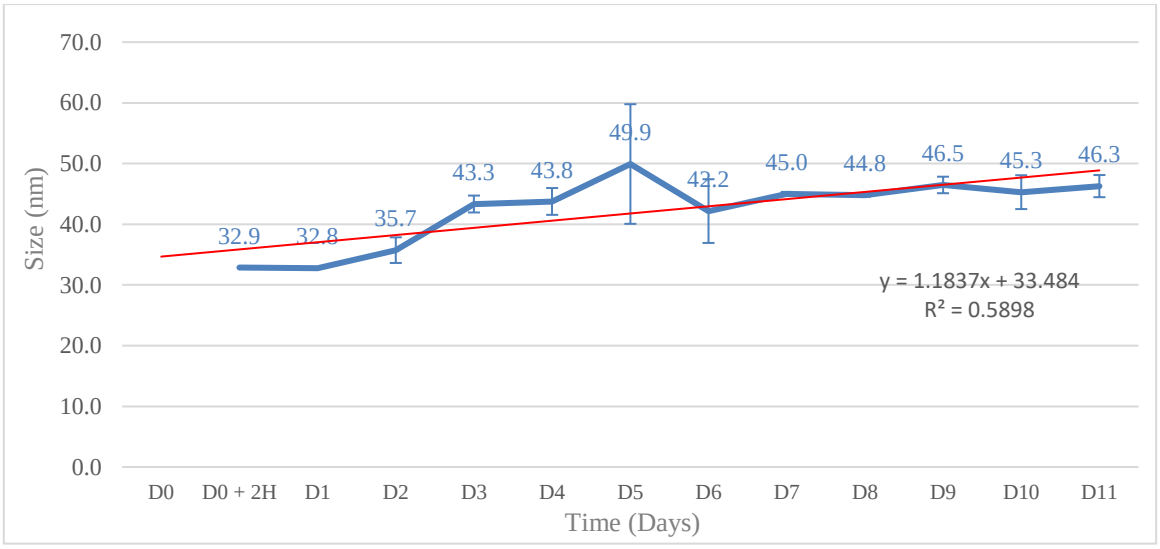

Figure 38. Detected particle mean size for the Ag treated seawater tanks, 10 ms dwell time, 3σ threshold.

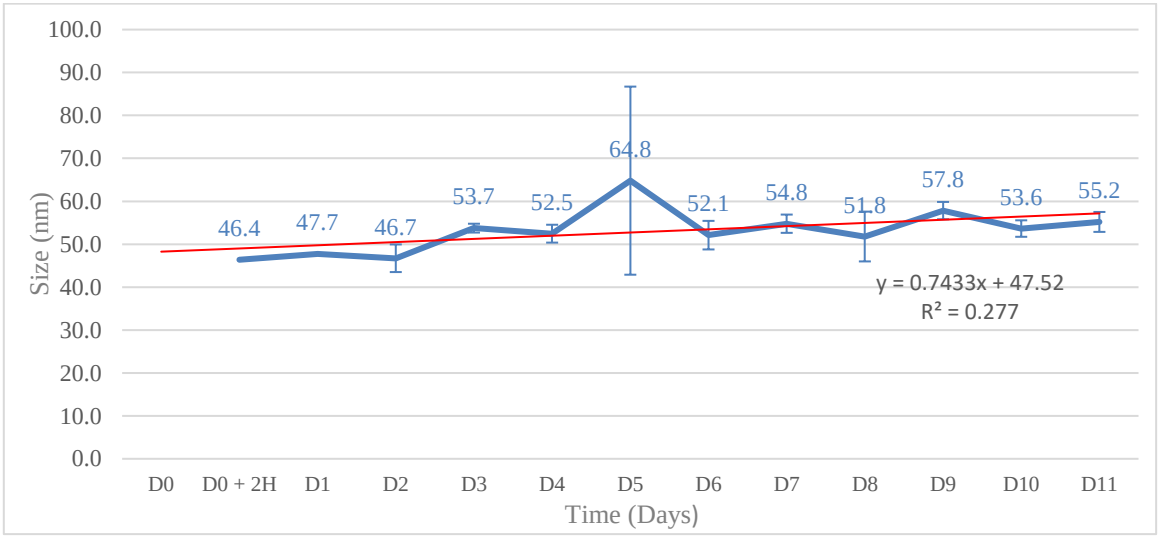

Figure 39. Detected particle mean size for the Ag treated seawater tanks, 10 ms dwell time, 5σ threshold.

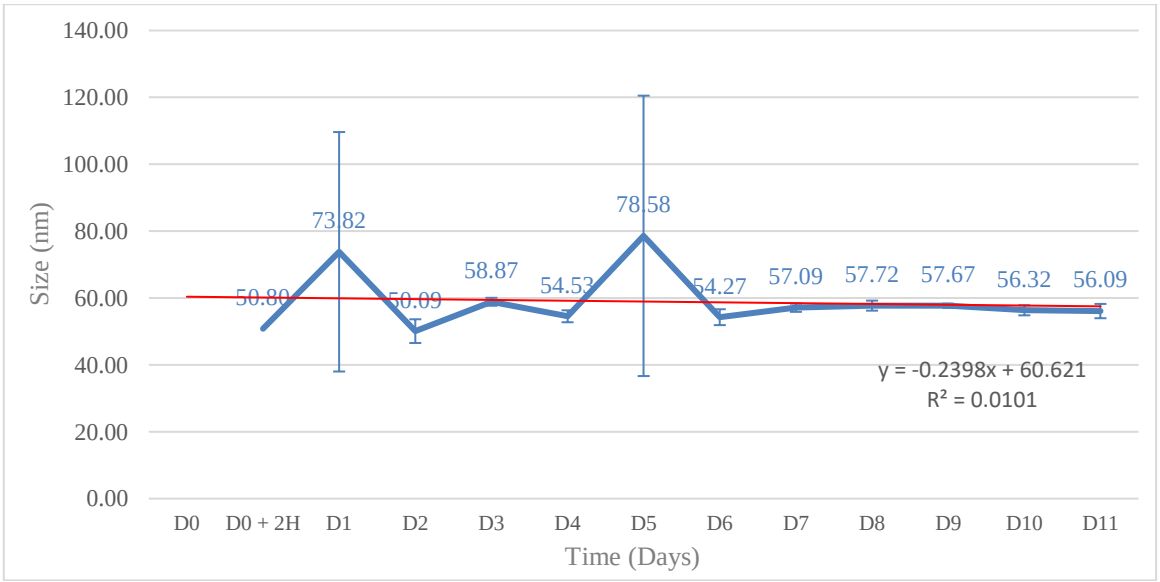

Figure 40. Detected particle mean size for the Ag treated seawater tanks, 10 ms dwell time, PG threshold.

As a first observation, there is a substantial increase across the dataset when swapping from the 5σ threshold application to the PG, and an even bigger one when going from the 3σ to the 5σ. Taking into account the observed similar tendency in the particle concentration data, that is an indication that the eliminated signals correspond to fairly small particles. It is therefore normal, that their elimination would affect the mean size data in such a significant manner. Apart from a couple of points (D1 and D5), all the rest seem to have reasonable uncertainty, indicating consistency and therefore, probably a predictable behavior for the system, not a random occurrence.

The 3σ and 5σ threshold applications suggest an increasing size for the detected ''particles'' over time, while the PG threshold has a slight declining trend. A possible assessment would be that the moieties are indeed formed over time within the solution, which means that they accumulate a greater amount of Ag as the days pass. That would indicate the formation of moieties that have been too small to be detected by the PG threshold during the first days, but have been gradually growing. As a result, they eventually overcome the detection threshold, and are detected during the later days. Within this paradigm, while only the bigger particles contribute to the size determination during the first days, smaller particles would eventually be detected, slightly lowering the overall mean size.

4.1.3.5. Conclusions for the behavior of Ag in ionic Ag treated seawater tanks as investigated using 10 ms dwell time detection

Whether the above – mentioned assessment is correct or not, is appears that the PG threshold is a little less suitable for the analysis of these samples with this dwell time than the 5σ, since either there are ''particles'' that are small enough for it to miss them, or there is a different reason for the miscalculation that leads to the different trend than the other two thresholds. There is always the chance that the PG threshold leads to the correct results while the others don't. However, the slightly higher uncertainty it exhibits, along with the lack (currently) of a plausible explanation on the formation of larger moieties during the first days, that eventually either disappear (dissolve) or they were falsely detected in the first place, do not make for a convincing case.

In any case, the actual detected event peaks are not enough to draw a robust statistical conclusion from their analysis, especially in the early days, and the application of the higher PG threshold only makes things even harder. Both of the other two thresholds appear to have a reasonable behavior, quite possibly due to the addition of the ionic analyte. That causes a raise of the dissolved signal, which would allow for the shape of the background distribution to better approach a Gaussian shape.

4.1.4. Ionic Ag treated seawater tanks, analyzed using 75 μs dwell time detection

4.1.4.1. Ag mass balance for ionic Ag treated seawater tanks as determined using 75 μs dwell time detection

The following charts (*Fig. 41, 42 and 44*) summarize the quantity of Ag detected, both as dissolved ionic Ag, as well as AgNP, for each of the three thresholds applied. Each data point represents an average value that has

resulted from the analysis of the three seawater tanks. The ''spiked'' values (yellow line) refer to the cumulative amount of silver (Ag) added to each tank as ionic Ag, i.e., 50 parts per trillion (ppt) Ag daily in the form of ionic Ag. The trendline (red line) is a fit to the experimental data, whereas each numerical value given in the figures corresponds to an average value from the three tanks. Due to an anomaly detected before D2, *Figures 43*, *45* show the system's mass balance for the 5σ and PG threshold criteria respectively, after D1.

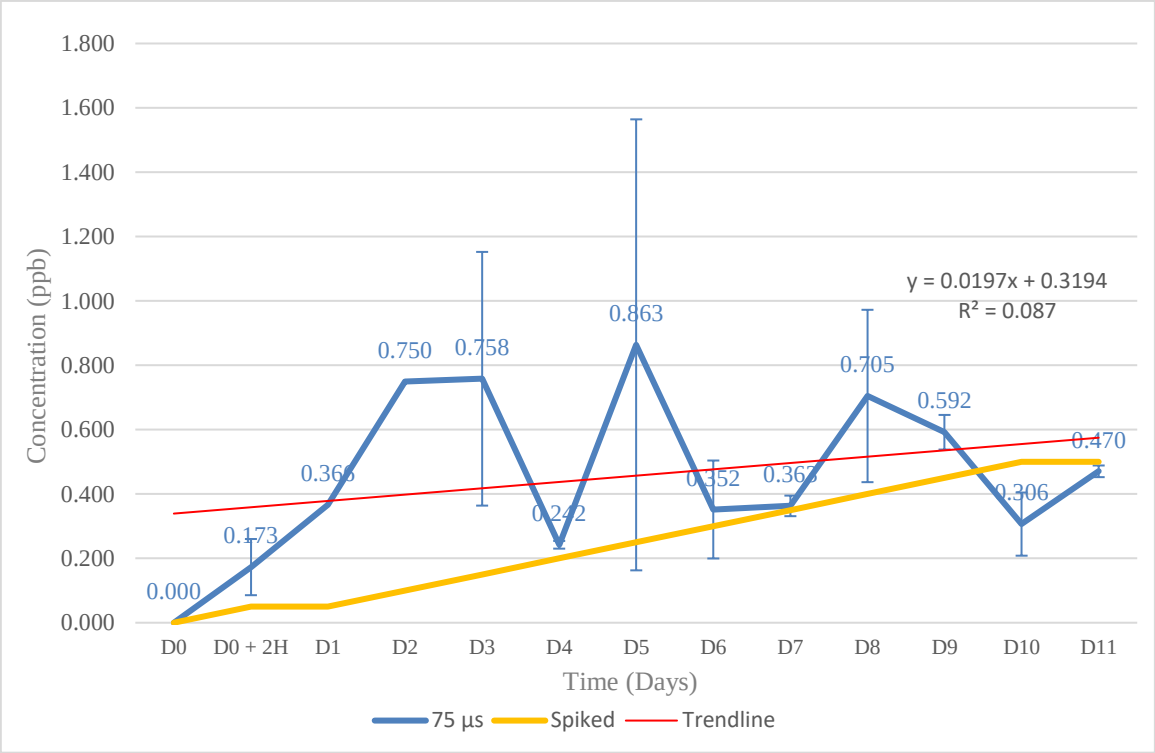

Figure 41. Mass balance for the Ag treated seawater tanks, 75 μs dwell time, 3σ threshold.

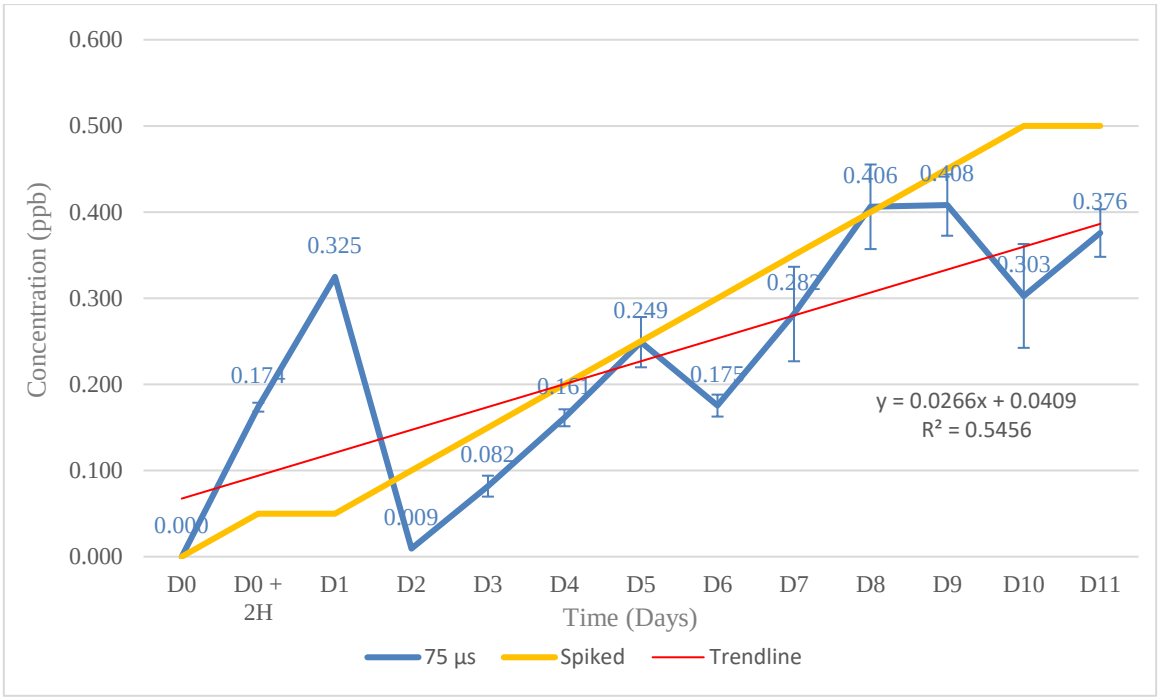

Figure 42. Mass balance for the Ag treated seawater tanks, 75 µs dwell time, 5σ threshold.

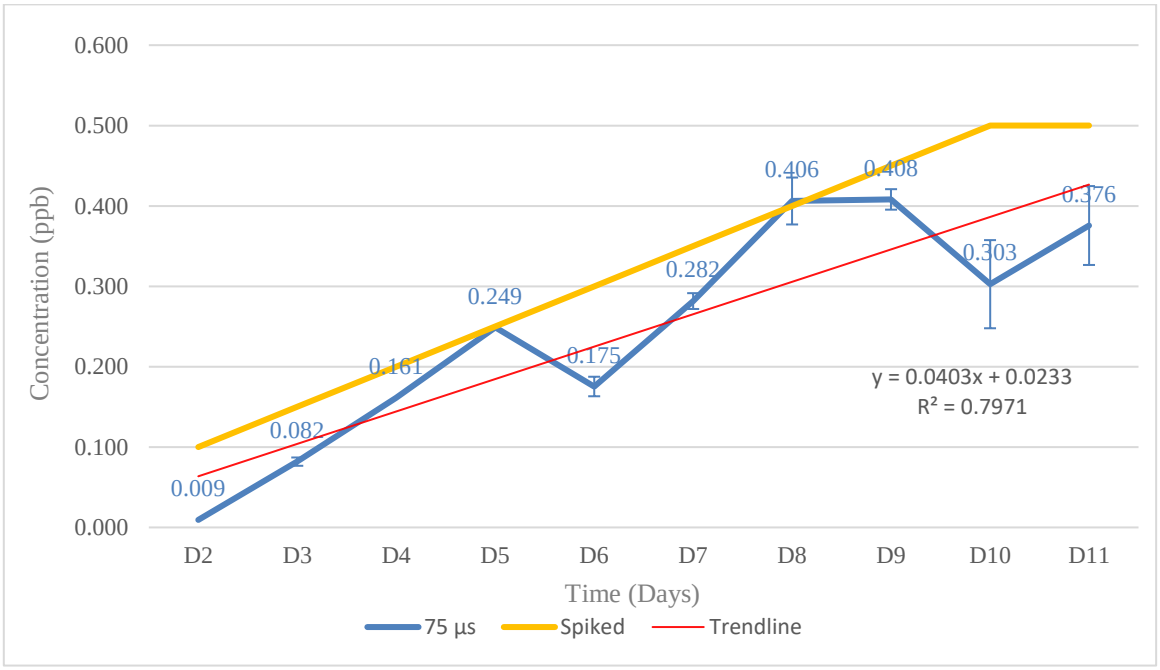

Figure 43. Mass balance for the Ag treated seawater tanks, 75 µs dwell time, 5σ threshold, after D1.

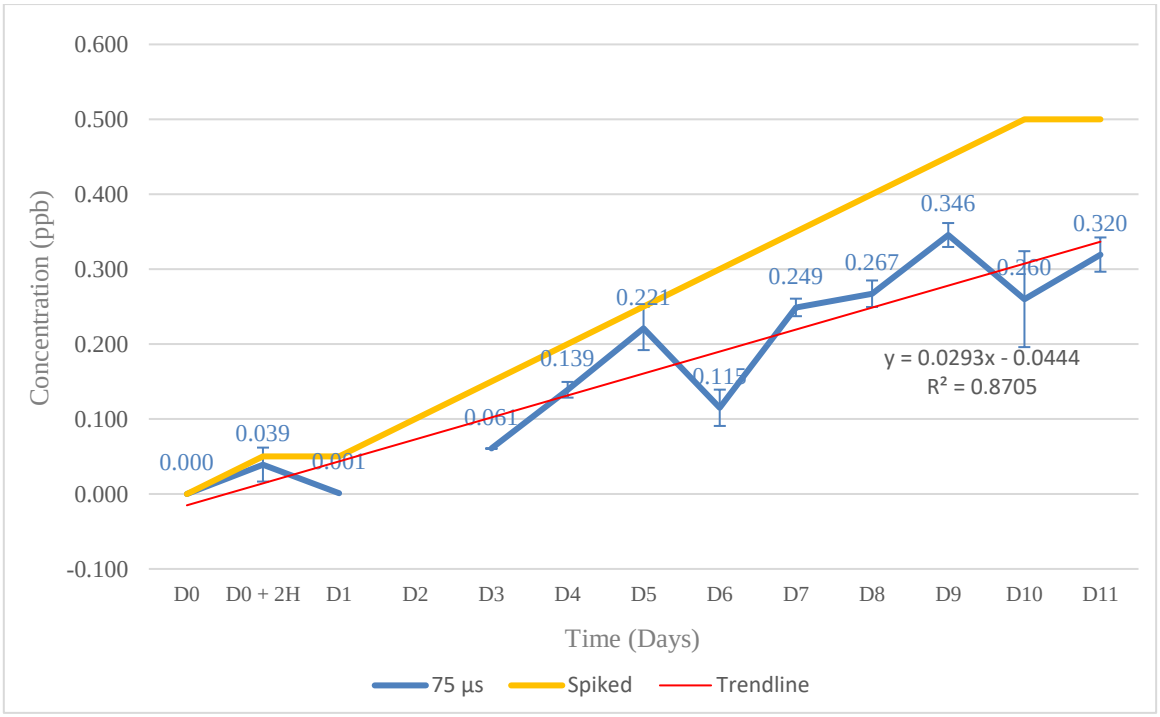

Figure 44. Mass balance for the Ag treated seawater tanks, 75 µs dwell time, PG threshold.

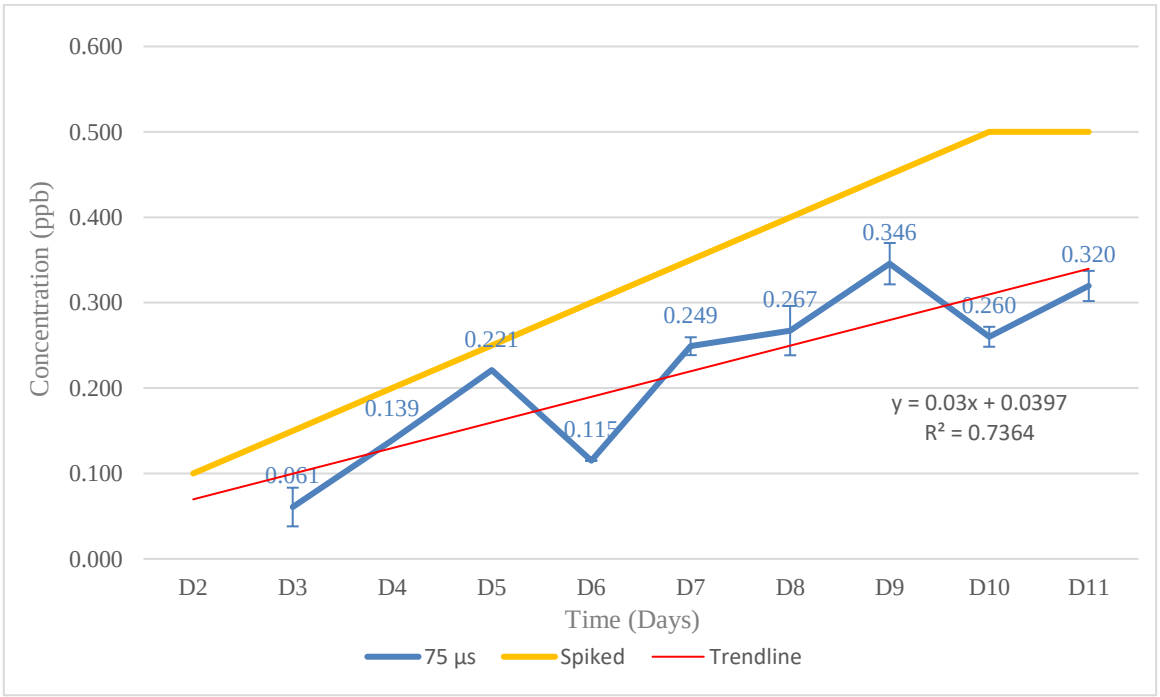

Figure 45. Mass balance for the Ag treated seawater tanks, 75 µs dwell time, PG threshold, after D1.

To start with, it is quite obvious that the 3σ threshold is, once again, not suitable for this kind of analysis, a fact demonstrated by the significant uncertainty and the unrealistic mean recovery value (290.4% ±249.0% standard deviation). It is unclear, despite the similar conclusion drawn by the analysis of the AgNP treated tanks' data, why the 3σ threshold so wildly overestimates the system's mass balance, but the fact that it can't be used for the µs dwell time range analysis cannot be argued.

Both of the other dwell times demonstrate a more or less expected behavior for the system, although the 5σ

exhibits an anomaly in the first two days of the experiment (D0 + 2H and D1). Quite probably due to the very low background, a result of the low dwell time, it is possible that a big part of this signal comes from falsely identified particles, that have been contributing their overestimated mass to the balance. That phenomenon, should this be the case, ceases to affect the results after D1. That probably happens due to the raising of the background level enough, so that the 5σ statistics would suffice to explain the data, as it seems by the plotting of the data after D1. The respective recovery values are 142.3% ±180.1% standard deviation, for the full dataset, and 71.1% ±27.2% standard deviation for the results after D1, further strengthening the conclusion of an unfortunate miscalculation on those two days.

Regarding the PG threshold, no useful information has been obtained for D2, but is seems that, in general, it is exhibiting an acceptable level of agreement with the expected results, with very reasonable uncertainty, and a recovery of 58.9% ±24.4% standard deviation. The chart depicting the data excluding those prior to D2 has been added mainly for the easier comparison between the two thresholds. It is interesting though, that the recovery of the reduced dataset for the PG threshold is higher than that of the full dataset (63.0% ±16.6% standard deviation). It is obvious that the higher threshold value eliminated the falsely identified particles during those days, and due to its inherent incompetence in the analysis of dissolved material, some part of the dissolved Ag has gone undetected. Therefore, the mass balance value dropped. It is a fair assumption, that the exhibited inadequacy in the determination of dissolved analytes (and therefore of the lower recovery values, compared to more particle – rich samples) stems from the lowering of the dwell time. The small detection window would lead to the cumulatively acquired signals per datapoint not being enough to generate a detectable pulse.

4.1.4.2. Dissolved Ag concentrations in ionic Ag treated seawater tanks as determined using 75 μs dwell time detection

The following charts (*Figures 46-48*) represent the detected dissolved intensity, as well as the cumulative quantity of the daily added dissolved Ag. Same as before, the results represent an average value, resulted from the data processing of all three tanks. The values are acquired after automated conversion, through the mass calibration, from the detected Dissolved Intensity. Those charts are available in this thesis' supplementary information (*SS 1.4.4, Figures 50-52*). In service of a better understanding of the overall image composed by all the available data, from this point forward, both the 5σ and the PG thresholds' charts will be presented with and without the data before D2.

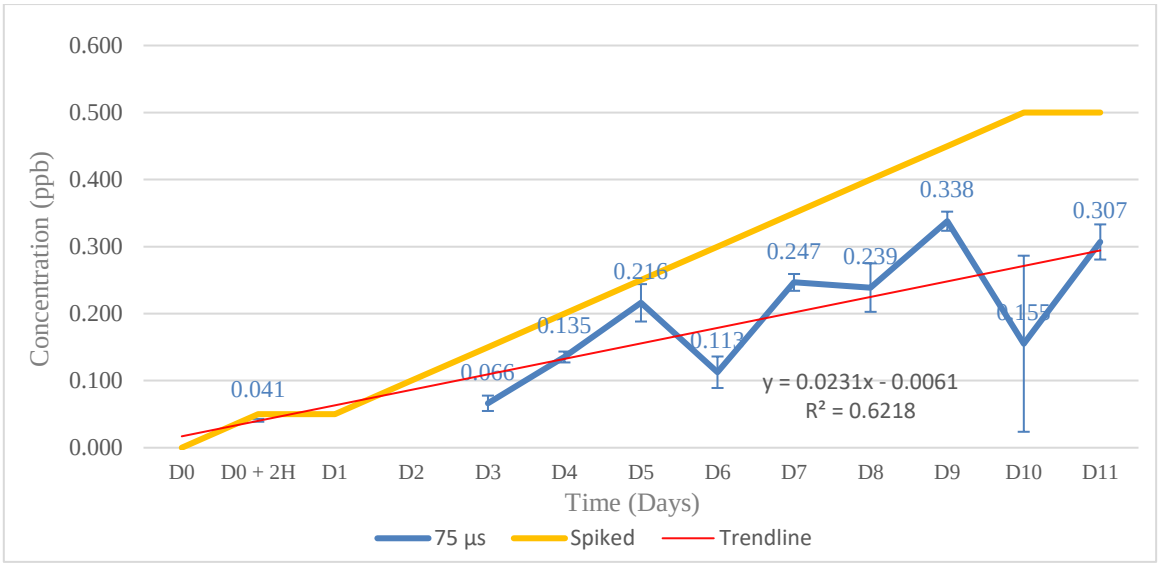

Figure 46. Dissolved Ag Concentration for the Ag treated seawater tanks, 75 µs dwell time, 3σ threshold.

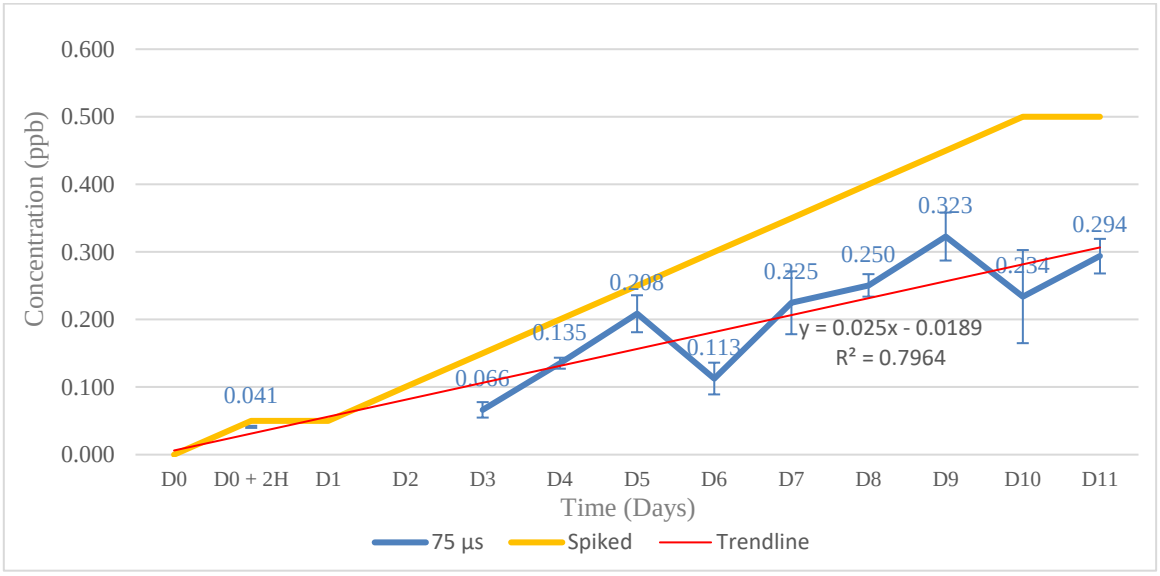

Figure 47. Dissolved Ag Concentration for the Ag treated seawater tanks, 75 µs dwell time, 5σ threshold.

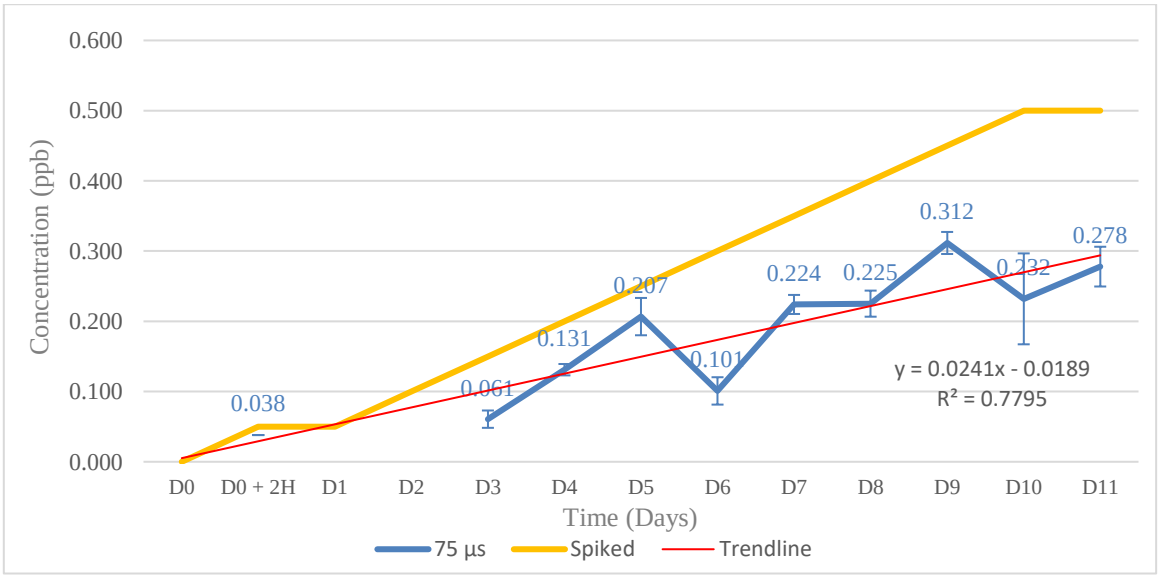

Figure 48. Dissolved Ag Concentration for the Ag treated seawater tanks, 75 µs dwell time, PG threshold.

Contrary to the expected increase on the detected dissolved Ag after the application of a higher threshold, the charts show a decrease overall of the measured dissolved Ag concentration from 3σ to 5σ and then to PG. It might, though, provide an explanation on the lowering of the overall mass balance, as it is apparent that the application of higher thresholds eliminates, for some reason, part of the detected dissolved. This behavior, though troublesome to interpret at this point, is actually in agreement with the previous results of the 75 μs dwell time, used in the analysis of the AgNP treated tanks. That creates a pattern of dissolved Ag concentration being lowered by the application of higher thresholds. As mentioned before, owing to the obscurity of the internal logic with which the software applies the new thresholds, when they are manually inserted, it is quite difficult to produce a convincing argument to explain this unexpected behavior. Since the mass calibration procedure does not include the application of any threshold though, it is possible that a significant difference between the threshold of the calibration and the threshold of the sample (or even the ratio of the threshold to the detected dissolved intensity) could cause some unintended miscalculation.

Interestingly enough, also, there is no significant difference when using each of the three different thresholds, certainly not one of the magnitude their mass balance charts exhibit. The 3σ is characterized by a bit higher uncertainty, but overall, they exhibit the same trend, and they are all in tentative agreement with the expected results of the dissolved Ag quantity being higher with each passing day, due to the daily addition of ionic Ag.

4.1.4.3. Particulate Ag in ionic Ag treated seawater tanks as determined using 75 μs dwell time detection

Looking deeper into the nature of the Ag species in the samples, the determined Ag particle concentration is shown in *Figures 49 - 53*, obtained using different threshold criteria. The actual numbers of detected peaks have also been presented in charts and can be found in the supplementary section of the present thesis (*SS 1.4.1, Figures 37-41*). The results represent an average value that has resulted from the data obtained from all three tanks. It is worth noting, that the detection of pulses that would indicate the formation of any kind of particles, aggregates, or in any way a confinement of high quantities of analyte within defined spatial compartments, was unexpected, since the dynamics of the system are still being documented. Therefore, no assumptions, conclusions or explanations on the nature of the moieties that are responsible for these pulses will be made at this stage of the study, and the ''particle concentration'' titles used in the following charts are used for convenience reasons.

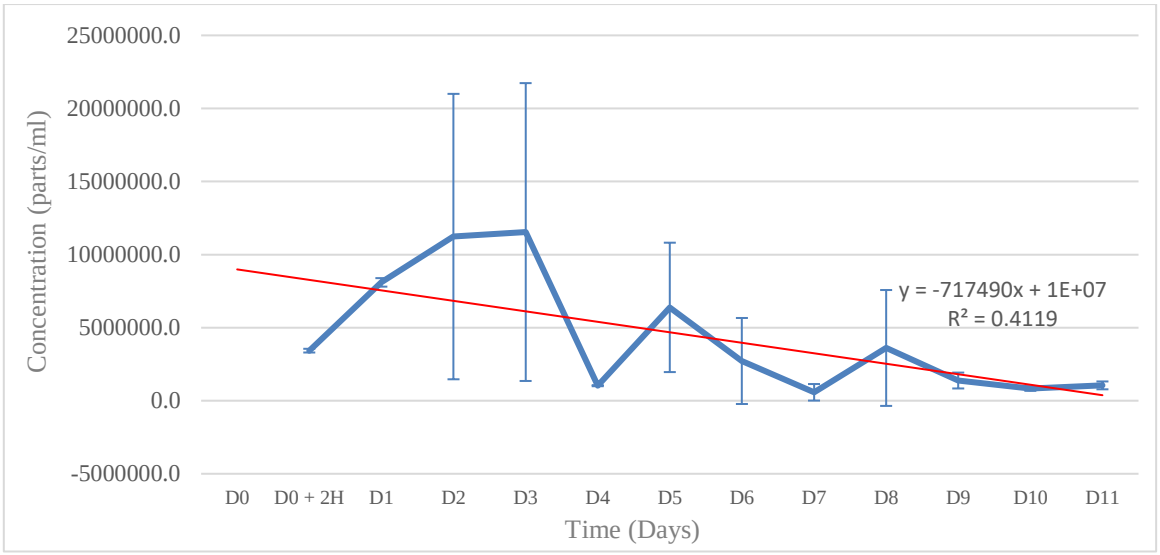

Figure 49. Particle concentration for the Ag treated seawater tanks, 75 μs dwell time, 3σ threshold.

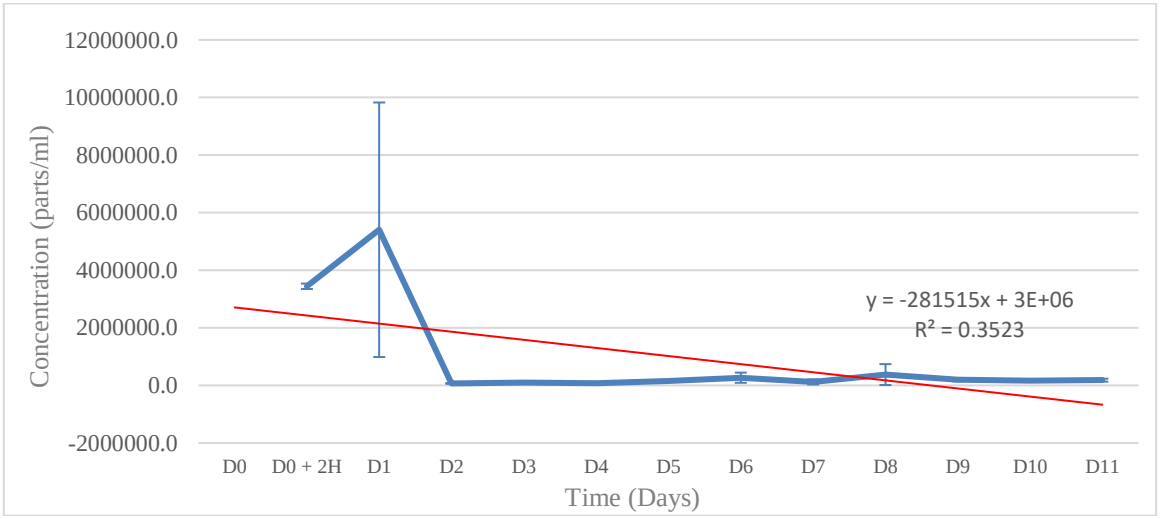

Figure 50. Particle concentration for the Ag treated seawater tanks, 75 μs dwell time, 5σ threshold.

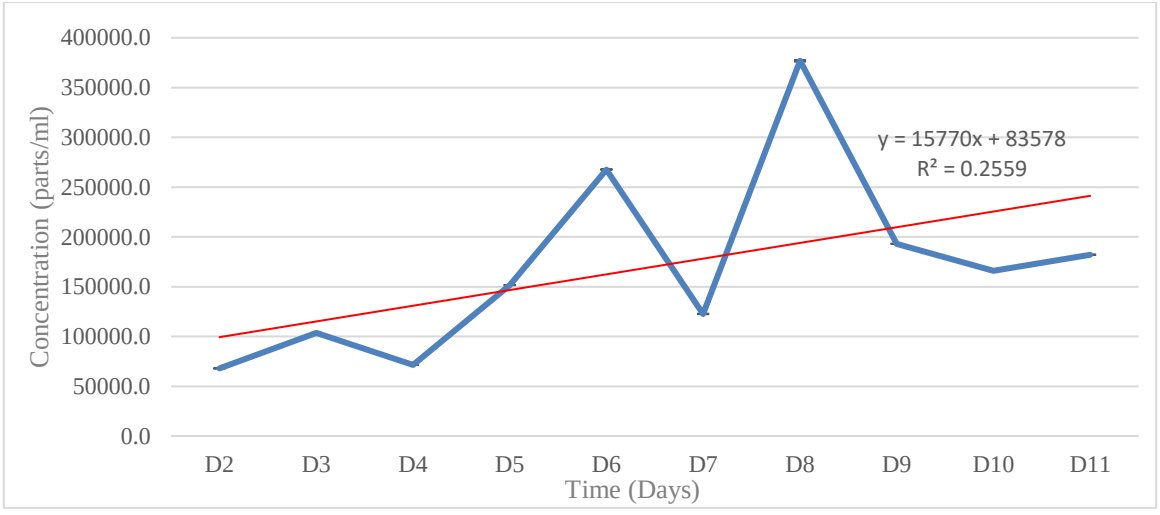

Figure 51. Particle concentration for the Ag treated seawater tanks, 75 μs dwell time, 5σ threshold, after D1.

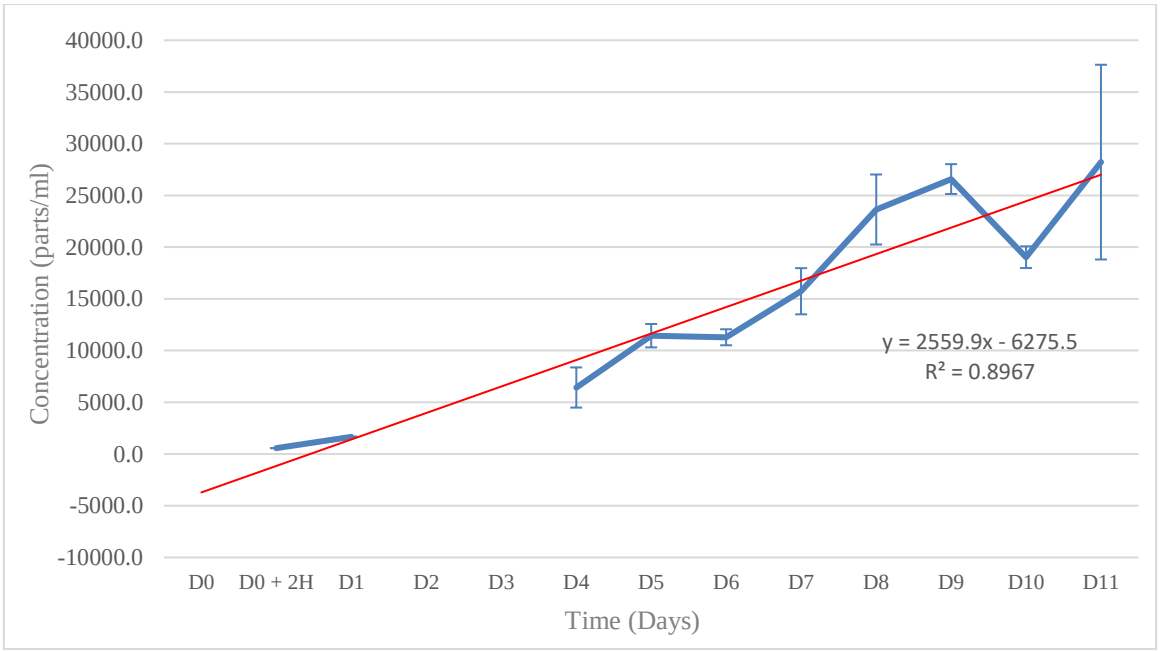

Figure 52. Particle concentration for the Ag treated seawater tanks, 75 μs dwell time, PG threshold.

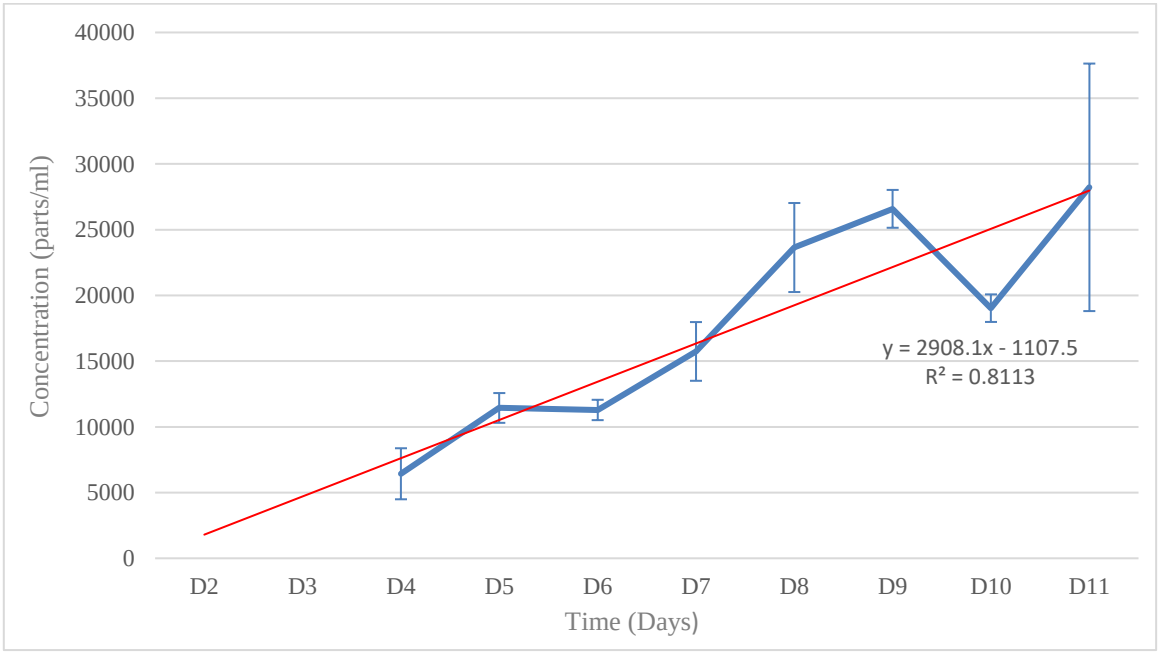

Figure 53. Particle concentration for the Ag treated seawater tanks, 75 μs dwell time, PG threshold, after D1.

Looking at the 3σ chart, there seems to be a trend concerning the inconsistency, as the earlier days seem to have way higher uncertainty than the later ones. Also, the overall trend of the chart shows a decreasing number of particles detected over the course of the experiment. That behavior that can hardly be logically explained by accepting that those signals are indeed formed moieties of any nature, as is would not make much sense for them to be suddenly formed in the early days, and then either shrink or disappear on later days. A much more plausible explanation could be, that by increasing the dissolved Ag quantity within the system, the background was raised high enough to hide part or all of the signals that have been falsely identified as particles. That would also provide an explanation for the ever – shrinking uncertainty, as the number of actual event pulses should be quite a bit more consistent than the number of false positive signals.

The complete 5σ dataset representation obviously suffers from the same problem as the respective mass balance data representation (or is the cause of it). There is an unrealistically high number of particles per ml detected on D0 + 2H and D1, that could be attributed to the very low background during these days, and therefore to the existence of a great number of false positive signals. Closer investigation of the raw data from those days (*Figures 54-56*) indeed indicates that the signals identified as particles are quite close to the dissolved signals, and probably are a part of it. Under the effects of the low dwell time, it is quite clear that the background has moved very close to zero, leading the system to falsely identify as particles, pulses that are no higher than 5 counts (or peak area). On the other hand, after eliminating those two points from the dataset, the trend of the chart indicated a gradual increase in the number of particles detected (despite the poor fitting of the linear approximation), an observation that can be verified by the previous data collected with 10 ms dwell time.

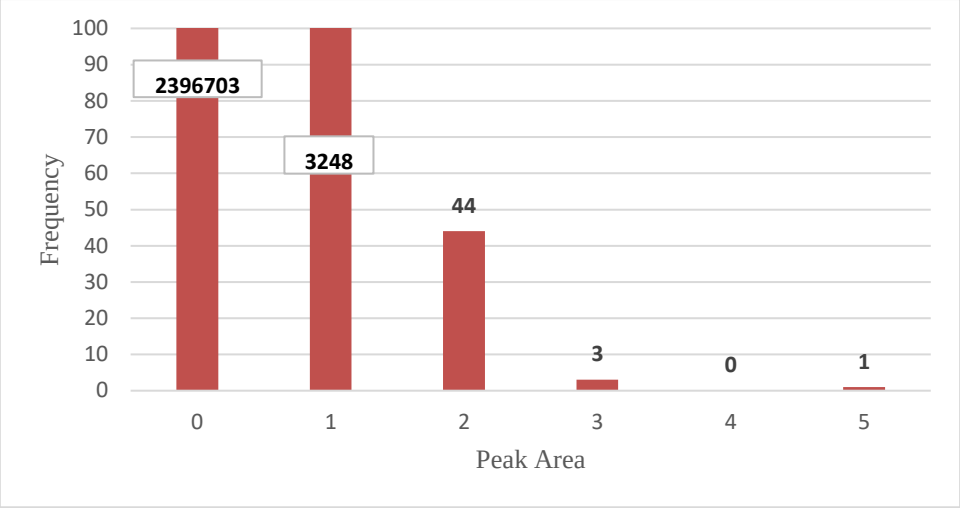

Figure 54. Peak Area Histogram for the first Ag treated seawater tank, 75 μs dwell time, D0.

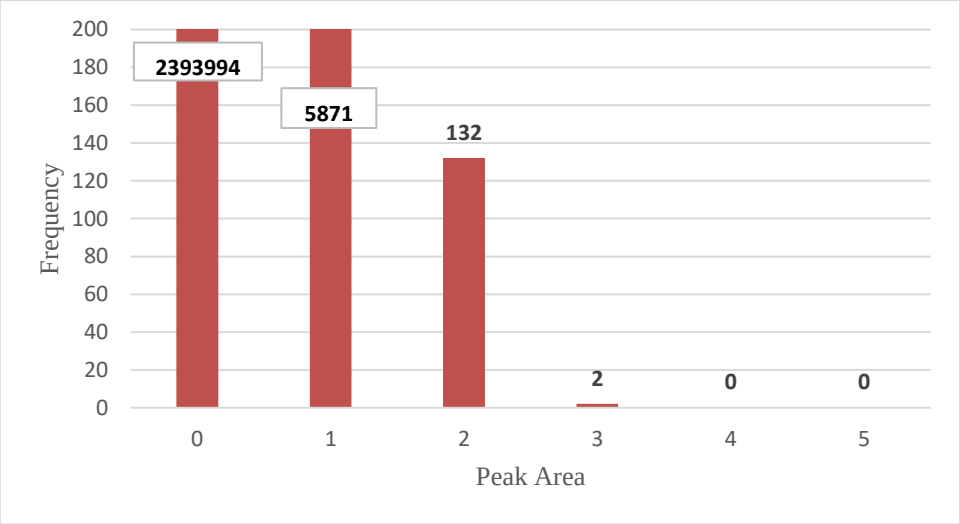

Figure 55. Peak Area Histogram for the first Ag treated seawater tank, 75 μs dwell time, D0+2H.

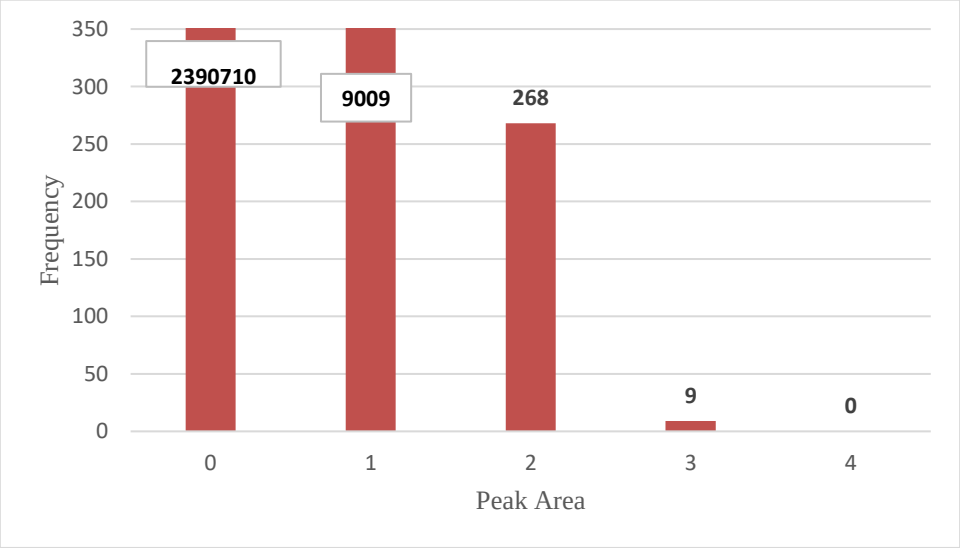

Figure 56. Peak Area Histogram for the first Ag treated seawater tank, 75 μs dwell time, D1.

Regarding the PG threshold, things are more straightforward, as the trend depicted is quite clear with or without the exclusion of the early days (with an acceptable linear fitting). Once again it is suggested that the irregularity in the data is caused by signals of relatively low intensity.

Overall, and by disregarding the 3σ threshold and the data before D2 for the 5σ threshold, after due and thoroughly explained consideration, all remaining data exhibit the same trends. There are clear indications for the formation of growing Ag – containing moieties in the system, an observation in agreement with the assumptions of the 10ms data.

4.1.4.4. Ag particle mean size in ionic Ag treated seawater tanks as determined using 10 ms dwell time detection

In an attempt to further investigate the occurrence and nature of the detected moieties, the following charts (*Fig 57-61*) are devoted to the study of their size variations over the course of the experiment. The ''mean size'' titles are used for convenience reasons, in order for the charts to be able to be examined in comparison to the respective charts of the AgNP treated tanks' study. The calculation of the ''size'' values is supposing a spherical shape for nanoparticles, and a composition of pure elemental Ag. Therefore, the equivalent size that is depicted in the following charts corresponds to the size these moieties would have, if they were spherical particles of pure Ag. As previously mentioned, it is resulting from an automated conversion, through the standard mass calibration, of the corresponding Mean Intensity. Those charts can also be found in the supplementary section (*SS 1.4.3, Figures 47-49*).Same as before, the results represent an average value, resulted from the data processing of all three tanks. Similar charts regarding the Most Frequent size can be found in the supplementary (*SS 1.4.2, Figures 42-46)*, as they exhibit the same behavior and they do not include any additional information.

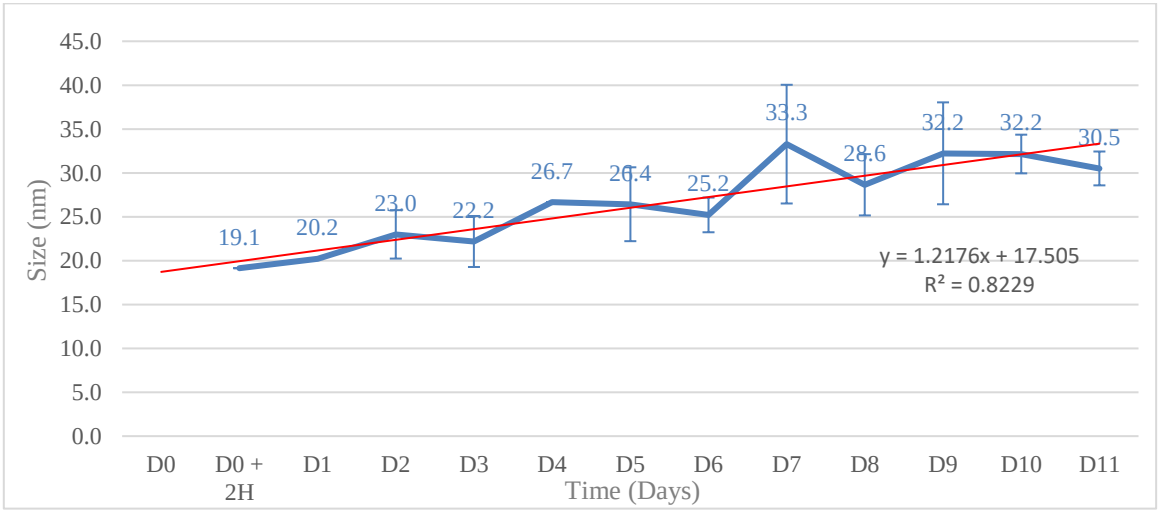

Figure 57: Detected particle mean size for the Ag treated seawater tanks, 75 μs dwell time, 3σ threshold.

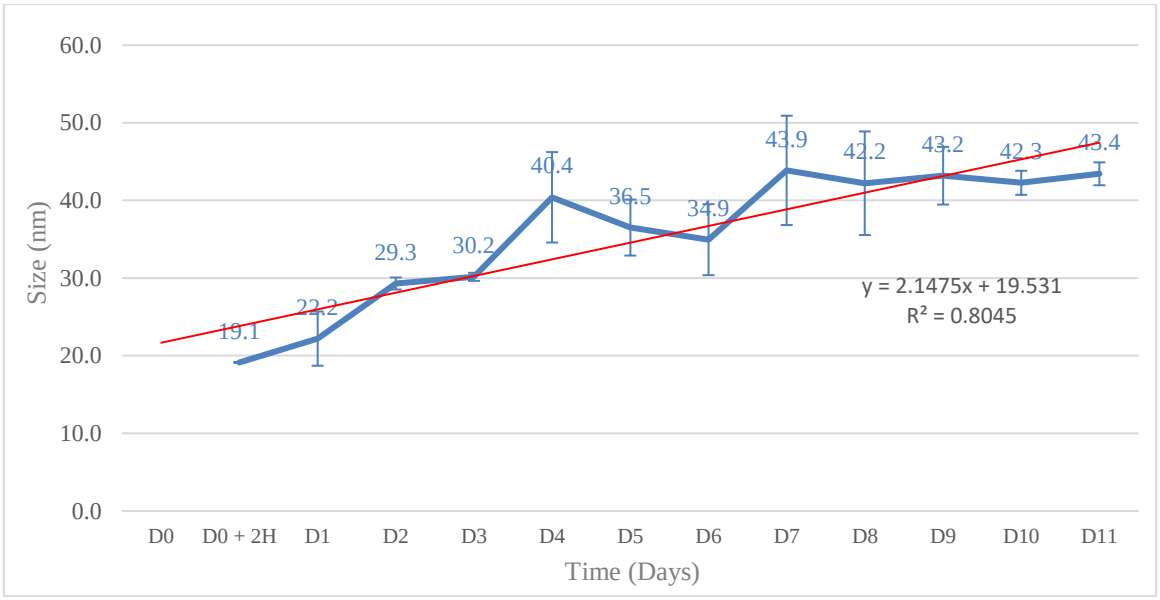

Figure 58: Detected particle mean size for the Ag treated seawater tanks, 75 μs dwell time, 5σ threshold.

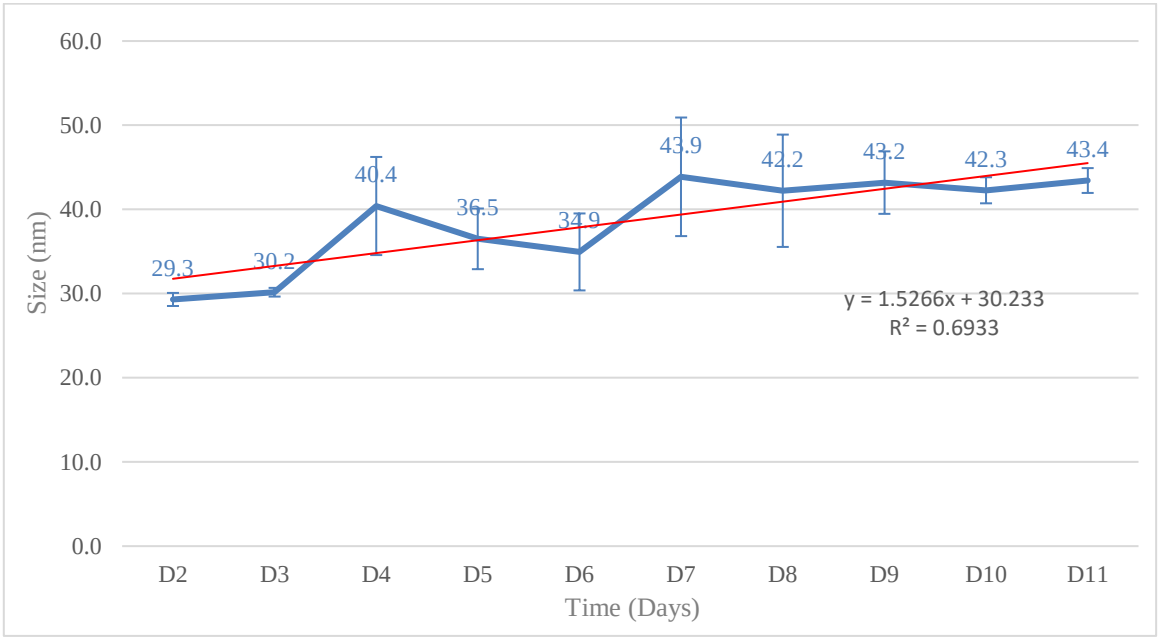

Figure 59: Detected particle mean size for the Ag treated seawater tanks, 75 μs dwell time, 5σ threshold, after D1.

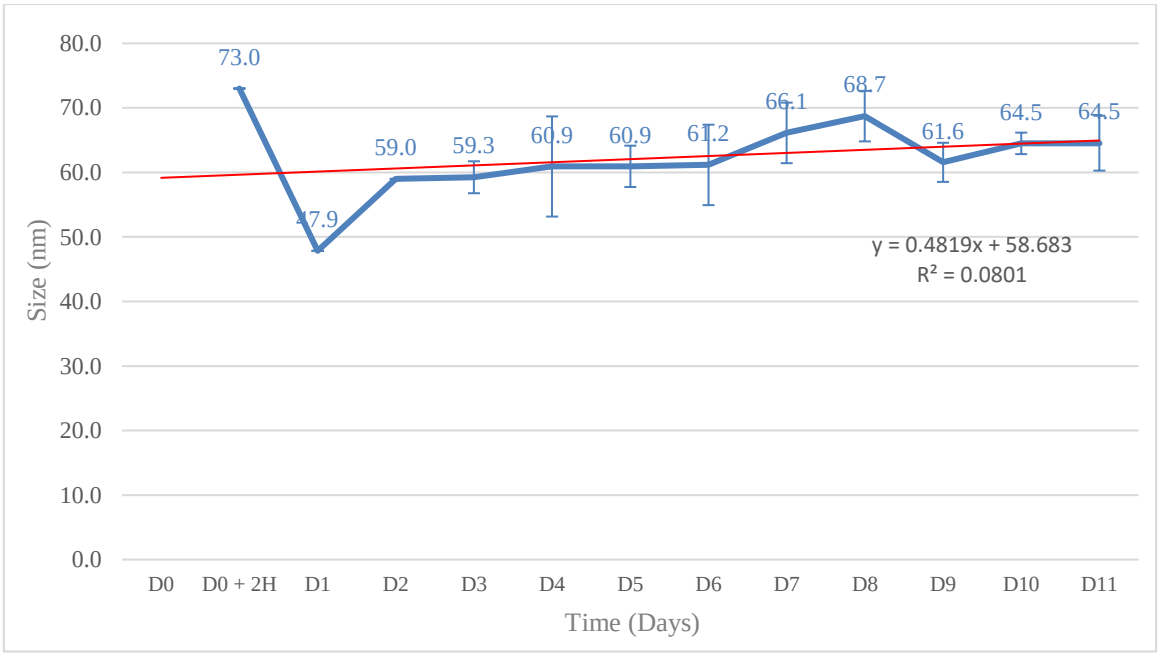

Figure 60: Detected particle mean size for the Ag treated seawater tanks, 75 μs dwell time, PG threshold.

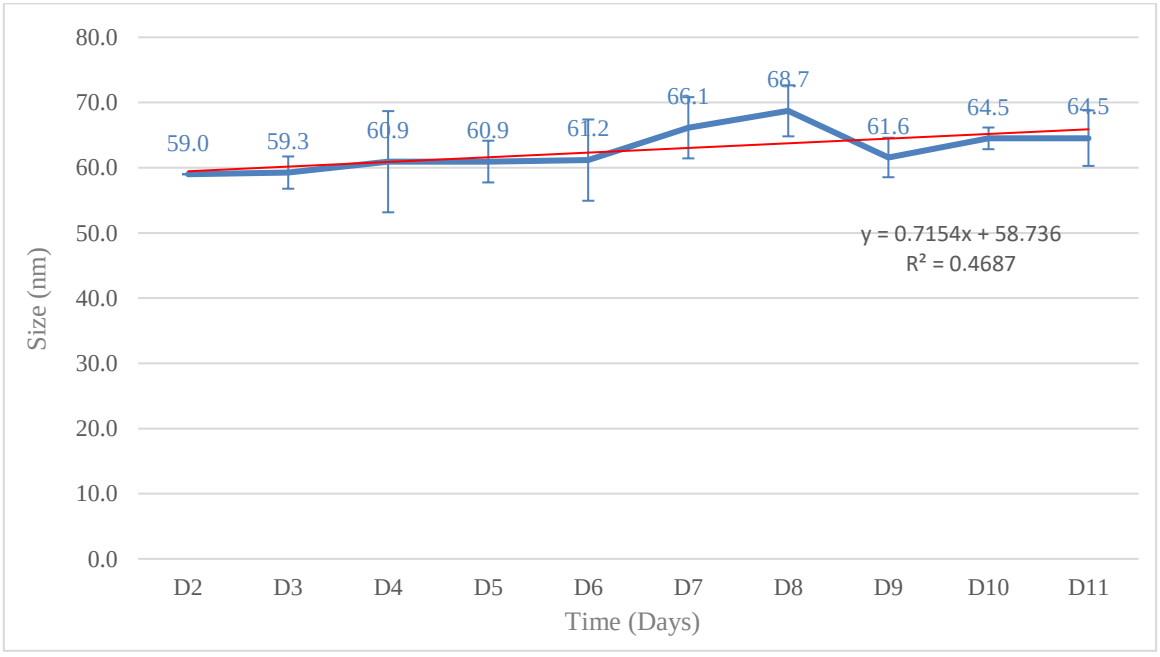

Figure 61: Detected particle mean size for the Ag treated seawater tanks, 75 μs dwell time, PG threshold, after D1.

Studying the difference of the mean size across the different thresholds, it is quite clear that there is an increasing tendency when the threshold gets higher, which of course comes as no surprise, as the higher thresholds eliminate the lower – intensity signals. Of the three, the PG threshold seems to have the biggest outliers (D0 + 2H and D1) and it also exhibits the least increasing trend. The cause of this is probably the fact that it only identifies the higher intensity signals as particles, therefore, from the beginning, the lower intensity signals would not be identified as particles. With or without the exclusion of the earlier days, the 5σ threshold exhibits more or less the same increasing trend, as does the 3σ, despite the fact that the respective mean size value is clearly quite lower.

4.1.4.5. Conclusions for the behavior of Ag in ionic Ag treated seawater tanks as investigated using 10 ms dwell time detection

All the presented data considered, it has become quite clear that the 3σ threshold is not suitable for the analysis of samples using dwell times in the μs range, an observation in agreement with the conclusion reached after the analysis of the AgNP treated tanks data as well. It is also clear, after observing the same occurrence twice out of two experiments, that the 75 μs dwell time is not well suited for the analysis of dissolved analyte, as evidenced by the unexpected behavior it exhibits in dissolved Ag concentration charts, in both Ag and AgNP treated tanks. The possibly undetected dissolved Ag concentration probably accounts for the decrease of the recovery value when swapping from 5σ to PG threshold as well.

As far as the two other thresholds are concerned, if the irregularity of the earlier days of the experiment can be disregarded for the 5σ, it seems like it could be the appropriate threshold for this kind of analysis. Once again, it seems that it can only start functioning the expected way, when the background has risen enough so that its distribution can approach normality. Up until that point, the PG threshold seems to be the suitable one for this kind of analysis, no doubt due to the background distribution being too shifted towards the zeros' side, much more resembling a Poisson – Gaussian distribution.

4.1.5. Nature of Event Pulses Detected in the Ionic Ag Treated Seawater Experiments

It has been observed, that during the ionic silver treated tanks analysis, event pulses have appeared, with increasing frequency and intensity. They have been examined by the above – presented data, using two different dwell times and three different thresholds. However, the nature of those detected moieties is unknown, and can, at this point, only be speculated.

It is highly unlikely that, in a matrix as complex as seawater, and at concentrations as low as 50 to 500 ppt, pure Ag nanoparticles could have formed. There are, however, some possible alternatives. The fact that cannot be denied, after the observations made up until this point, is that there is a confinement of increasing quantity of Ag within small spatial compartments. Moreover, these build-ups are sufficient to generate pulses high enough to be identified as particles even by the higher thresholds. On average the detected pulse intensity corresponds to a mean of ~1.5×10^6 Ag atoms per pulse event.

Single cell organisms that have accumulated increasing amounts of silver during the experiment have been proposed. It is, however, considered unlikely that any single cells could accumulate to the calculated number of silver atoms within the low – concentration solution. Despite the fact that pure Ag particles are unlikely under these conditions, there have been numerous reports about the formation of Ag or Ag – containing particles in similar systems, under the effect of Natural Organic Matter (NOM)[21,132] and/or fulvic acid[132,133]. Other relative conditions include interaction with sunlight[36,134], the presence of precursor Ag compounds, such as Ag_2S[135], while the implication of iron ions is also suggested[132,135]. The important difference with the system in question, however, is that all of these references study systems that contain much higher Ag concentrations (from high

ppb to ppm).

Considering how stable the Ag_2S is, after its formation (K_{sp} = 8 x 10^{-51}), it was investigated for its formation under the existing mesocosm conditions. Since the experiment has already been conducted, the only alternative was a simulated experiment, at least to obtain a general idea of the interaction between silver ions and the sulfide ions. For this purpose, a widely used, simulated chemical speciation program was used (GEOCHEM – EZ)[129], using known constituents of seawater[136], and a reported mean concentration for sulfide ions[137]. *Figure 62* shows the program's interface and the input values for the seawater constituents.

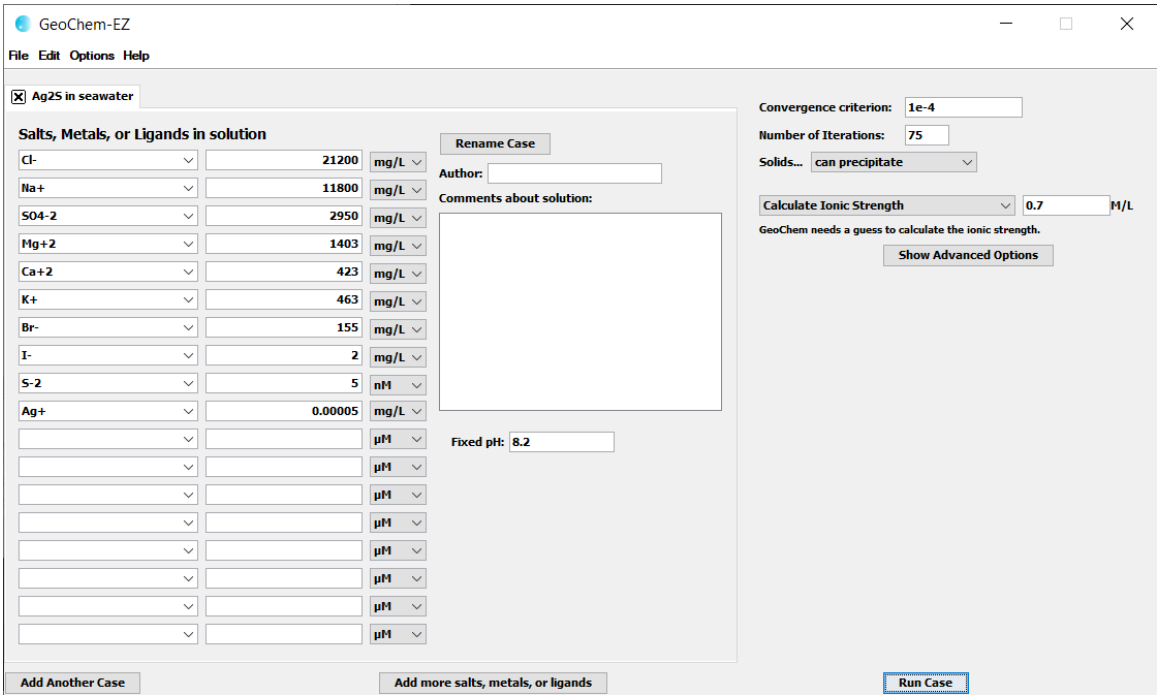

Figure 62. GEOCHEM - EZ interface, showing the input values for the seawater constituents.

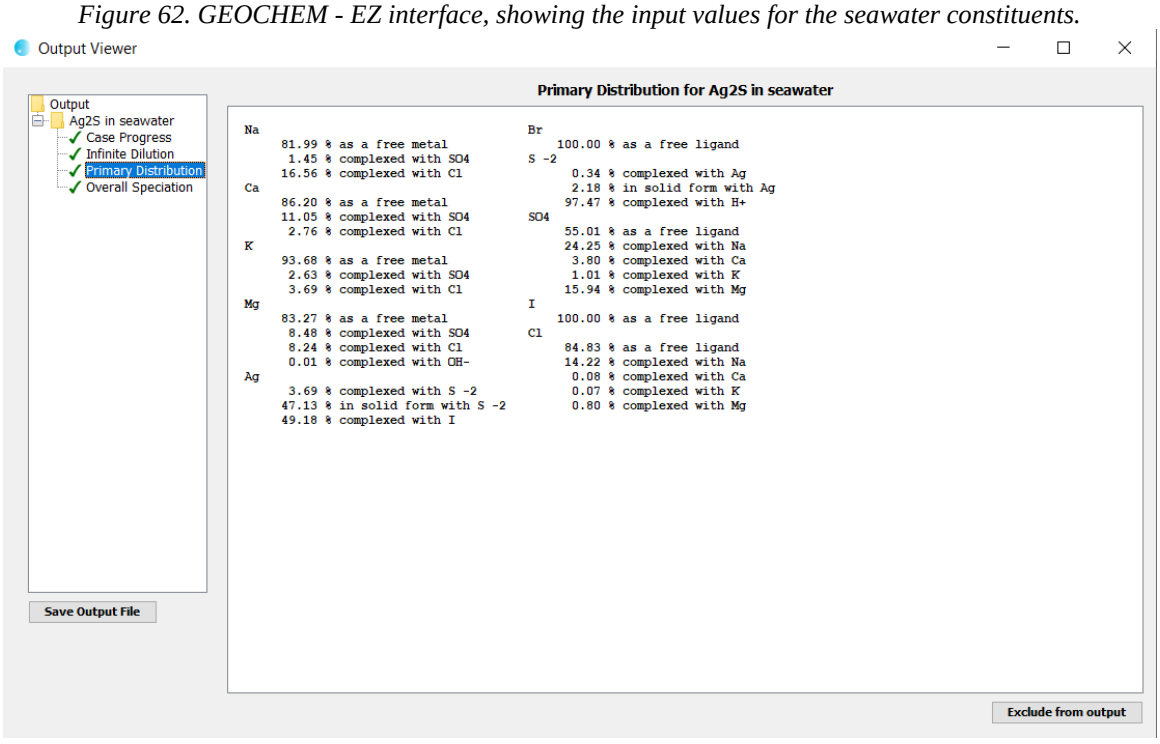

Figure 63. GEOCHEM - EZ output, exhibiting the percentage interactions of every constituent with one another.

Figure 63 shows the percentages for the outcomes of the interactions between each of the constituents with one another. Under the conditions used, the simulation shows that more than 50% of the silver quantity is interacting with sulfide ions, with 47.13% being in solid form (e.g., particles). It is also clear, that there is a substantial interaction with iodide ions, which overtakes the total silver quantity at lower sulfide concentrations.

In order to better understand the dynamics of the silver – sulfide ions interaction, the whole of the mesocosm experiment was essentially simulated. Keeping concentrations of the rest of the known constituents fixed, and removing the iodide factor, the systems behavior was monitored during the dissolved Ag concentration increase, for 5 different sulfide concentrations (*Figure 64*).

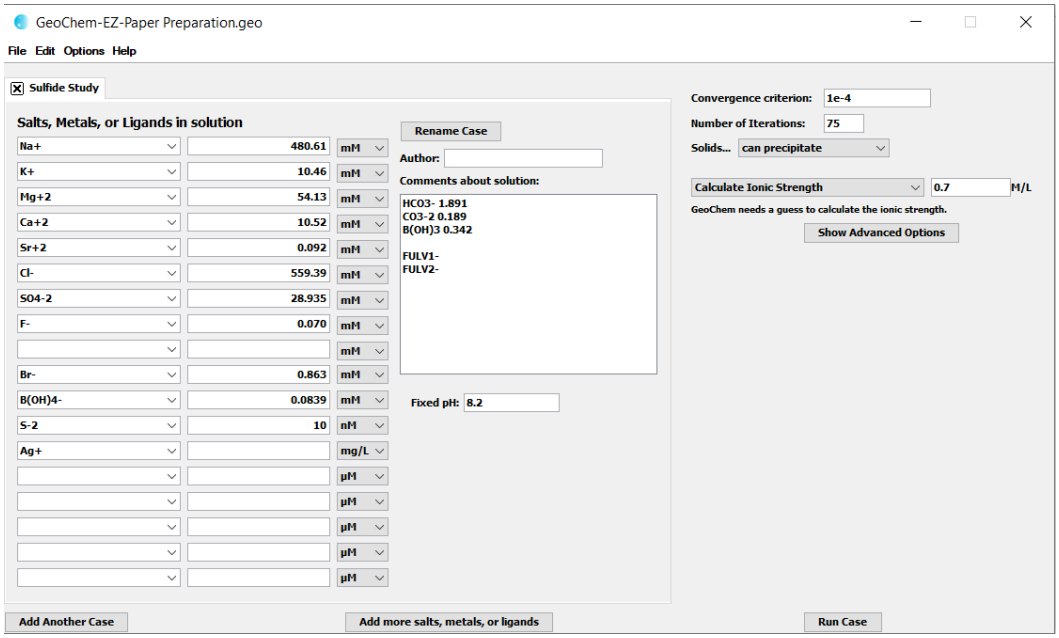

Figure 64. GEOCHEM - EZ interface, showing the input values for the silver sulphide study.

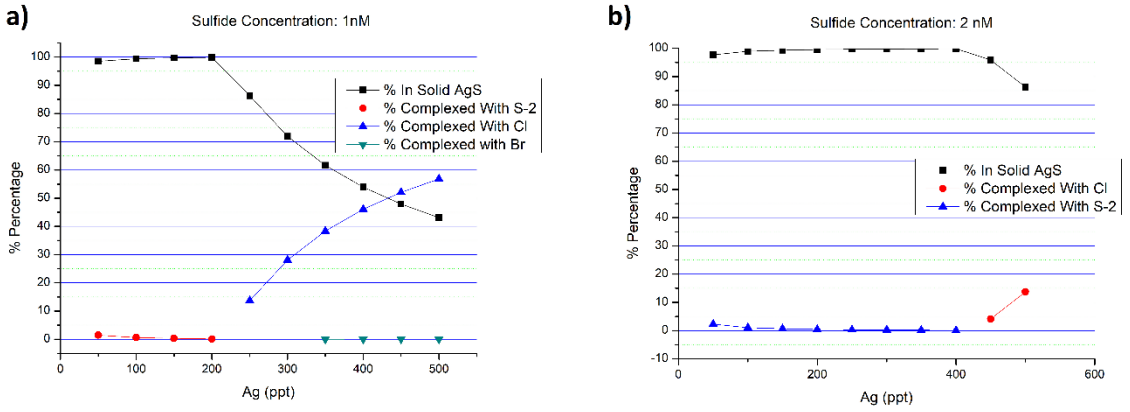

Figure 65. Percentage of the silver interactions in seawater media, in the presence of 1nM and 2 nM sulfides.

As it appears in *Figure 65a*, (1 nM sulfide concentration), the whole of the Ag quantity is bound by the sulfide ions up to 200 ppt of Ag. Similar behavior is observed in *Figure 65b* (2 nM sulfide concentration), for Ag concentrations up to 400 ppt. Keeping in mind that 100 ppt of Ag corresponds to around 1nM (Ar_{Ag} ~ 107.87 Da), the result is consistent with the formation stoichiometry of Ag_2S. So, it seems that Ag only interacts with

the remaining ions after the sulfide supply has been depleted, indicating a very high preference towards the formation of the Ag_2S particles. All three of the following *Figures (66-68)* indicate the same thing: in the presence of sulfide ions, and absence of iodide ions, the whole of the Ag amount will be bound by the sulfide ions, and an extremely high percentage of it will be forming solids. Similar studies regarding interactions with fulvic ligands showed no significant effect on the system.

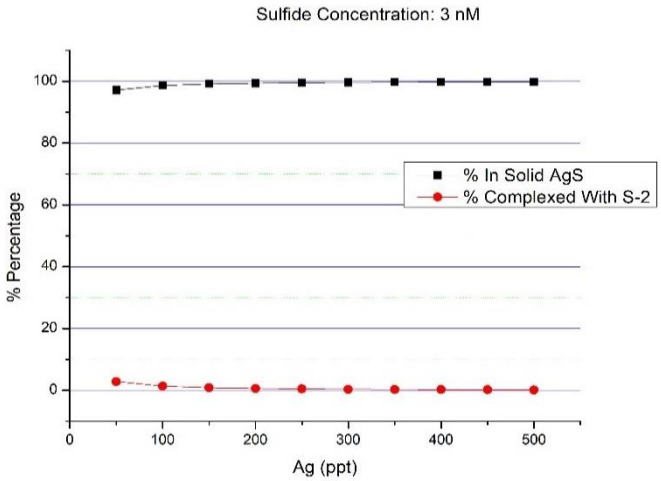

Figure 66.*Percentage of the silver interactions in seawater media, in the presence of 3 nM sulfides.*

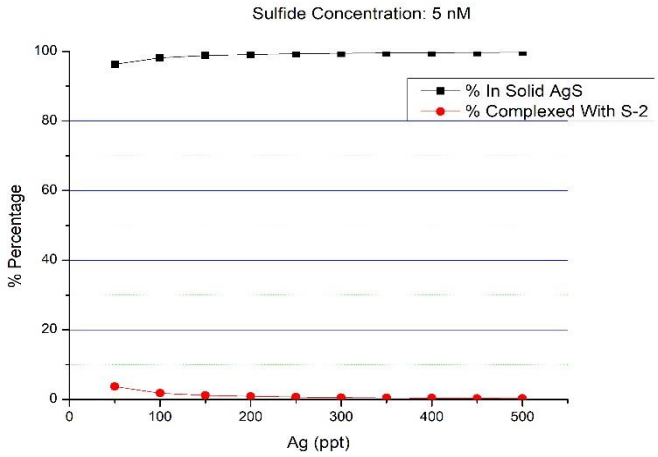

Figure 67. Percentage of the silver interactions in seawater media, in the presence of 5 nM sulfides.

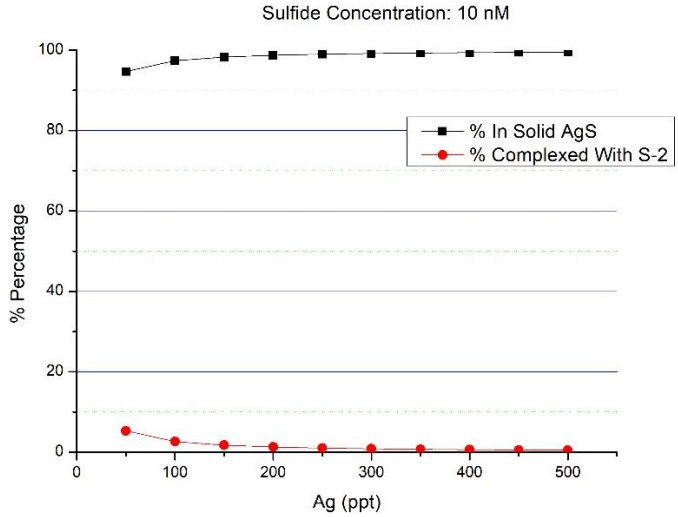

Figure 68. Percentage of the silver interactions in seawater media, in the presence of 10 nM sulfides.

Taking all the above inquiries into consideration, the formation of silver – containing particles from dissolved silver in ppt concentrations is tentatively suggested.

4.2. Results and Discussion for Investigating the Occurrence and Metal Content (Cu) of Copper – containing Particles in Seawater Samples from the Proximity of the Island of Santorini

The on – line dilution introduction system has been proven able to adequately protect the ICP – MS instrumentation, and proved reliable. Therefore, it was incorporated in the analysis of seawater samples acquired from the proximity of Santorini Island, in order to study the occurrence of metal – containing nanomaterials in these waters, under project *NanoIsland* (ELIDEK, Title of Proposal: Detection of engineered, incidental, and natural nanoparticles in marine waters, in the proximity of islands).

During this program, as it was mentioned before, a number of samples have been acquired from several sampling sites, mainly within the volcanic caldera (the remnant of the magma chamber of a volcano, after all the magma has withdrawn). Samples have also been acquired from different depths of the same sampling site, and different time periods. In total, during the program, as many as 17 sampling sites have been evaluated for their importance and relevant differentiations (their tags bring the abbreviations S01 – S17). Samples have been acquired from the water surface, and on occasion, from the depth of 5, 50 and 250 meters (bringing the abbreviations D000 – D250). There have been five different samplings, spread over two years, as evenly as the circumstances allowed for: July 2019 (abbr. JL19), October 2019 (abbr. OC19), January 2020 (abbr. JA20), June 2020 (JN20) and August 2020 (abbr. AU20). The tag for each sample is composed as follows: ((Sampling)_(Sampling site)_(Depth)_F10. F10 stands for ''filtered through 10 μm filters'', and the tag is sometimes followed by an abbreviation of the sampling site, like f.e. NB for ''North Basin''[1]. So, the sample ''OC19_S08_D000_F10 NB'' is the tag of a sample that has been sampled in October 2019, from the surface (D000) of the 8th sampling site, that happens to be North Basin, and has been filtered through 10 μm filters. ''FLT'' stands for ''filtered'' and ''BLK'' stands for ''blank'', while ''P'' samples are acquired from the port of Piraeus (2 is from a neutral area, while 4 is from the trail left by a ship). D1 or D2 stand for ''Day 1'' and ''Day 2'' respectively, indicating that two samples have been acquired on consecutive days.

Samples have been selectively acquired through the experiment, eliminating sampling sites in the process, either due to lack of interest in their produced data, or due to proven similarity with other sampling sites. Some might have also been added. The samples' list can be found in Table 2.

[1] See Supplementary Section 4.1 for a map of the locations and their abbreviations.

Table 2. Samples acquired through the NanoIsland Project				
July 2019	October 2019	*January 2020*	*June 2020*	*August 2020*
JL19_S01_D000_F10	*OC19 FLT BLK 2*	*JA20_FLT2_BLK*	*JN20_FLT_BLK1 MQ*	*AU20_FLT_BLK2_F10*
JL19_S01_D005_F10	*OC19 P2*	*JA20_S03_D000_F10 Pag*	*JN20_FLT_BLK2 NISK*	*AU20_S03_D000_F10 D1*
JL19_S02_D000_F10	*OC19 P4*	*JA20_S03_D005_F10 Pag*	*JN20_S03_D000_F10 Pagos D1*	*AU20_S03_D005_F10 D1*
JL19_S02_D005_F10	*OC19_S02_D000_F10 SeaD*	*JA20_S03_D050_F10 Pag*	*JN20_S03_D000_F10 Pag D2*	*AU20_S03_D050_F10 D1*
JL19_S02_D050_F10	*OC19_S02_D005_F10 SeaD*	*JA20_S10_D000_F10 NPK*	*JN20_S03_D005_F10 Pagos D1*	*AU20_S03_D005_F10 D2*
JL19_S03_D000_F10	*OC19_S02_D050_F10 SeaD*	*JA20_S10_D005_F10 NPK*	*JN20_S03_D005_F10 Pag D2*	*AU20_S03_D050_F10 D2*
JL19_S03_D005_F10	*OC19_S03_D000_F10 Pag*	*JA20_S13_D005_F10 SB*	*JN20_S03_D050_F10 Pagos D1*	*AU20_S10_D000_F10*
JL19_S03_D050_F10	*OC19_S03_D005_F10 Pag*	*JA20_S13_D050_F10 SB*	*JN20_S03_D050_F10 Pag D2*	*AU20_S10_D005_F10*
JL19_S08_D000_F10	*OC19_S03_D050_F10 Pag*	*JA20_S13_D250_F10 SB*	*JN20_S10_D000_F10 NPK D1*	*AU20_S13_D000_F10*
JL19_S08_D005_F10	*OC19_S08_D000_F10 NB*	*JA20_S14_D000_F10 Vly*	*JN20_S10_D005_F10 NPK D1*	*AU20_S13_D005_F10*
JL19_S08_D050_F10	*OC19_S08_D005_F10 NB*	*JA20_S14_D005_F10 Vly*	*JN20_S13_D000_F10 SB*	*AU20_S13_D050_F10*
JL19_S08_D250_F10	*OC19_S08_D050_F10 NB*	*JA20_S17_D000_F10 AgRef*	*JN20_S13_D005_F10 SB*	*AU20_S13_D250_F10*
JL19_S09_D000_F10	*OC19_S08_D250_F10 NB*	*JA20_S17_D005_F10 AgRef*	*JN20_S13_D050_F10 SB*	*AU20_S14_D000_F10 D1*
JL19_S09_D005_F10	*OC19_S09_D000_F10 WB*		*JN20_S13_D250_F10 SB*	*AU20_S14_D000_F10 D2*
JL19_S09_D050_F10	*OC19_S09_D005_F10 WB*		*JN20_S14_D000_F10 Vly*	*AU20_S17_D000_F10*
JL19_S09_D250_F10	*OC19_S09_D050_F10 WB*		*JN20_S14_D005_F10 Vly*	*AU20_S17_D005_F10*
JL19_S10_D005_F10	*OC19_S09_D250_F10 WB*		*JN20_S16_D000_F10 AgRef*	*AU20_S17_D050_F10*
JL19_S12_D000_F10	*OC19_S10_D005_F10 NPK*		*JN20_S16_D005_F10 AgRef*	
JL19_S12_D005_F10	*OC19_S12_D000_F10 Akrotiri*		*JN20_S16_D050_F10 AgRef*	
JL19_S12_D050_F10	*OC19_S12_D005_F10 Akro*			
JL19_S13_D000_F10	*OC19_S12_D050_F10 Akro*			
JL19_S13_D005_F10	*OC19_S13_D000_F10 SB*			
JL19_S13_D050_F10	*OC19_S13_D005_F10 SB*			
JL19_S13_D250_F10	*OC19_S13_D050_F10 SB*			
JL19_S14_D000_F10	*OC19_S13_D250_F10 SB*			
JL19_S14_D005_F10	*OC19_S14_D000_F10*			
JL19_S15_D005_F10				
FLT_BLK_1				
FLT_BLK_2				

The sampling sites can be grouped, based on the aspect of their interest:
S08, S09, S13 – Deep water group, sites with relatively deeper waters.
S10 – Hydrothermal Vent.
S12 – Hotels or waste, sites where higher anthropogenic contribution is expected.
S01, S02, S03, S14, P4 – Boats' impact group, sites where higher contribution from the frequency of ships and boats is expected.
P2, S16, S17 – Reference, samples taken in relatively open waters.

Samples have already been analyzed for five different elements (Pb, V, Ni, Cu, Fe) and they are expected to be analyzed for five more (Ti, As, Ce, Zn, Zr). Each of these elements has been chosen after consideration of their environmental impact, the extent of their use from the human industry, and the possibility of their detection (based on literature, or the SEM analysis of the 10 μm filters). In this study, the data from the analysis of Cu are to be presented, a choice justified by all the aforementioned perspectives. Cu has been incorporated in various aspects of modern industry with increasing rate, with Cu nanoparticles finding applications in pesticides[22], or antifouling paints[22,138] and other major parts of human activities, like electrical equipment, construction materials, antimicrobial agents etc.[139] It has been reported, that engineered Cu based nanoparticles can rapidly aggregate up to diameters more than 1 μm wide in natural waters, without necessarily precipitate afterwards.[44] Also, there have been reports for the formation of Cu containing nanoparticles under the effect of hydrothermal

vents, which is a strong motivation for the study of Cu in this specific setting.[58,88,90]Moreover, the toxicity of Cu and Cu containing nanoparticles has been reported, in fish[139] and invertebrate organisms[140], while is has been proposed that it can cause DNA damage in plasmids and affect enzymes relevant to embryos hatching for aquatic and terrestrial organisms[22].

In natural samples, it is reported quite often complexed with natural organic ligands[141], various types of colloidal species[142], or other inorganic material[58,90], which is the reason that the composition of the detected Cu containing nanoparticles is not speculated in this study. Instead, the equivalent Cu mass is investigated.

4.2.1. Cu containing particles' concentration in seawater samples in the proximity of Santorini

Tables 3-6 contain information and the results acquired through the use of the JupyterLab Python Notebook, regarding the particle concentration of the samples analyzed for Cu, for 4 different samplings. For the identification of particle pulses, the 5σ threshold criterion has been applied in most case. Following the process described by Tuoriniemi et al[75], in samples that exhibited, after visual evaluation, significantly low pulses, higher thresholds have occasionally been applied (higher number of standard deviations added). As mentioned before, each sample was analyzed 3 times, for five minutes each, leading to 3 technical replicates. In cases that it seemed obvious that the sample didn't contain enough particles to be detected by the system (after visual evaluation of the real time data acquisition), less than three acquisitions have been obtained. In such cases, the corresponding cell in the table appears empty, which it not the same with the cells containing dashes (''-''), in which case the acquisition has been obtained, but the data process did not reveal any event pulses.

Table 3. Cu containing particles' concentration of samples analyzed for Cu from October 2019 Sampling								
Sample Tag	**Sam. Site**	**Depth (m)**	**Group**	**Replicate 1**	**Replicate 2**	**Replicate 3**	**Average**	**Std**
Cu OC19 FLT BLK 2	-	-	Blank	0	0	0	0	0
Cu OC19 P2	Piraeus	Surf	Reference	0			0	
Cu OC19 P4	Piraeus	Surf	Boats	8266	6199	6199	6888	1193
Cu OC19_S02_D000_F10 SeaD	Sea Diamond	Surf	Boats	517	517	517	517	0
Cu OC19_S02_D005_F10 SeaD	Sea Diamond	5	Boats	517	1550	517	861	596
Cu OC19_S02_D050_F10 SeaD	Sea Diamond	50	Boats	0	0	0	0	0
Cu OC19_S03_D000_F10 Pag	Pagos	Surf	Boats	0	2066	517	861	1075
Cu OC19_S03_D005_F10 Pag	Pagos	5	Boats	3616	517	517	1550	1789
Cu OC19_S03_D050_F10 Pag	Pagos	50	Boats	2583	2066	517	1722	1075
Cu OC19_S08_D000_F10 NB	North Basin	Surf	Deep Water	11365	9815	9815	10332	895
Cu OC19_S08_D005_F10 NB	North Basin	5	Deep Water	4649	3100	1550	3100	1550
Cu OC19_S08_D050_F10 NB	North Basin	50	Deep Water	2583	1550		2067	730
Cu OC19_S08_D250_F10 NB	North Basin	250	Deep Water	517	3100		1809	1826
Cu OC19_S09_D000_F10 WB	West Basin	Surf	Deep Water	1033	2066		1550	730
Cu OC19_S09_D005_F10 WB	West Basin	5	Deep Water	1033			1033	
Cu OC19_S09_D050_F10 WB	West Basin	50	Deep Water	3100	2583	0	1894	1661
Cu OC19_S09_D250_F10 WB	West Basin	250	Deep Water	3616	0	517	1378	1956
Cu OC19_S10_D005_F10 NPK	NPK	5	H. Vent	1033	1550	2066	1550	517
Cu OC19_S12_D000_F10 Akrotiri	Akrotiri	Surf	Hotels' Waste	1550	1033	2066	1550	517
Cu OC19_S12_D005_F10 Akro	Akrotiri	5	Hotels' Waste	4649	2066	3100	3272	1300
Cu OC19_S12_D050_F10 Akro	Akrotiri	50	Hotels' Waste	0			0	
Cu OC19_S13_D000_F10 SB	South Basin	Surf	Deep Water	1033	2066	1550	1550	517
Cu OC19_S13_D005_F10 SB	South Basin	5	Deep Water	1033	2066	2066	1722	596
Cu OC19_S13_D050_F10 SB	South Basin	50	Deep Water	1033	517	0	517	517
Cu OC19_S13_D250_F10 SB	South Basin	250	Deep Water	0			0	
Cu OC19_S14_D000_F10	Vlychada	Surf	Boats	0			0	

Table 4. Cu containing particles' concentration of samples analyzed for Cu from January 2020 Sampling								
Sample	**Sam. Site**	**Depth (m)**	**Group**	**Replicate 1**	**Replicate 2**	**Replicate 3**	**Average**	**Std**
Cu JA20_FLT2_BLK	-	-	Blank	962	481		722	340
Cu JA20_S03_D000_F10 Pag	Pagos	0	Boats	0			0	
Cu JA20_S03_D005_F10 Pag	Pagos	5	Boats	4330	962	1443	2245	1822
Cu JA20_S03_D050_F10 Pag	Pagos	50	Boats	3368	3849	1924	3047	1002
Cu JA20_S10_D000_F10 NPK	NPK	0	H.Vent	481	481	1443	802	555
Cu JA20_S10_D005_F10 NPK	NPK	5	H.Vent	962	481	0	481	481
Cu JA20_S13_D005_F10 SB	South Basin	5	Deep Water	3368	1924	2887	2726	735
Cu JA20_S13_D050_F10 SB	South Basin	50	Deep Water	962	3368	2405	2245	1211
Cu JA20_S13_D250_F10 SB	South Basin	250	Deep Water	1443	481	0	641	735
Cu JA20_S14_D000_F10 Vly	Vlychada	0	Boats	962	1443	1924	1443	481
Cu JA20_S14_D005_F10 Vly	Vlychada	5	Boats	1443	481	481	802	555
Cu JA20_S17_D000_F10 AgRef	Aegean	0	Reference	481	0		241	340
Cu JA20_S17_D005_F10 AgRef	Aegean	5	Reference	962	962	481	802	278

Table 5. Cu containing particles' concentration of samples analyzed for Cu from June 2020 Sampling								
Sample	**Sam. Site**	**Depth (m)**	**Group**	**Replicate 1**	**Replicate 2**	**Replicate 3**	**Average**	**Std**
Cu JN20_FLT_BLK1 MQ	-	-	Blank	0			0	
Cu JN20_FLT_BLK2 NISK	-	-	Blank	1533	1533		1533	0
Cu JN20_S03_D000_F10 Pagos D1	Pagos	0	Boats	1022	0	511	511	511
Cu JN20_S03_D000_F10 Pag D2	Pagos	0	Boats	1022	0		511	723
Cu JN20_S03_D005_F10 Pagos D1	Pagos	5	Boats	0	0		0	0
Cu JN20_S03_D005_F10 Pag D2	Pagos	5	Boats	0	0		0	0
Cu JN20_S03_D050_F10 Pagos D1	Pagos	50	Boats	0	2044	1022	1022	1022
Cu JN20_S03_D050_F10 Pag D2	Pagos	50	Boats	0	0	0	0	0
Cu JN20_S10_D000_F10 NPK D1	NPK	0	H.Vent	2044	3577	0	1874	1795
Cu JN20_S10_D005_F10 NPK D1	NPK	5	H.Vent	3577	1533	1022	2044	1352
Cu JN20_S13_D000_F10 SB	South Basin	0	Deep Water	511			511	
Cu JN20_S13_D005_F10 SB	South Basin	5	Deep Water	1022	511		767	361
Cu JN20_S13_D050_F10 SB	South Basin	50	Deep Water	0			0	
Cu JN20_S13_D250_F10 SB	South Basin	250	Deep Water	511	2555	511	1192	1180
Cu JN20_S14_D000_F10 Vly	Vlychada	0	Boats	2044	0	1022	1022	1022
Cu JN20_S14_D005_F10 Vly	Vlychada	~2	Boats	0	511	511	341	295
Cu JN20_S16_D000_F10 AgRef	Aegean	0	Reference	0			0	
Cu JN20_S16_D005_F10 AgRef	Aegean	5	Reference	511	0		256	361
Cu JN20_S16_D050_F10 AgRef	Aegean	50	Reference	511	511		511	0

Table 6. Cu containing particles' concentration of samples analyzed for Cu from August 2020 Sampling								
Sample	**Sam. Site**	**Depth (m)**	**Group**	**Replicate 1**	**Replicate 2**	**Replicate 3**	**Average**	**Std**
Cu AU20_FLT_BLK2_F10	-	-	Blank	1094	0	0	365	632
Cu AU20_S03_D000_F10 D1	Pagos	Surf	Boats	3281	1641	1641	2188	947
Cu AU20_S03_D005_F10 D1	Pagos	5	Boats	1094			1094	
Cu AU20_S03_D050_F10 D1	Pagos	50	Boats	1094	547	1641	1094	547
Cu AU20_S03_D005_F10 D2	Pagos	5	Boats	547	2188	1641	1459	836
Cu AU20_S03_D050_F10 D2	Pagos	50	Boats	3828	2188	2188	2735	947
Cu AU20_S10_D000_F10	N.P.K.	Surf	H. Vent	0	2734	1094	1276	1376
Cu AU20_S10_D005_F10	N.P.K.	Surf	H. Vent	547	547	1094	729	316
Cu AU20_S13_D000_F10	SB	Surf	Deep Water	547	547	1641	912	632
Cu AU20_S13_D005_F10	SB	5	Deep Water	8750	4922	1641	5104	3558
Cu AU20_S13_D050_F10	SB	50	Deep Water	0	547	547	365	316
Cu AU20_S13_D250_F10	SB	250	Deep Water	1094	0		547	774
Cu AU20_S14_D000_F10 D1	Vly	0	Boats	0			0	
Cu AU20_S14_D000_F10 D2	Vly	0	Boats	1094	0		547	774
Cu AU20_S17_D000_F10	AgRef	0	Reference	2188	1641	1641	1823	316
Cu AU20_S17_D005_F10	AgRef	5	Reference	547	2734		1641	1546
Cu AU20_S17_D050_F10	AgRef	50	Reference	5469	547	0	2005	3012

4.2.1.1. General trends concerning Cu containing particles' concentration

Operating under the assumption, that the study of any sample belonging to one of the aforementioned groups can provide information concerning the group in its whole, and taking into account the limited number of samples analyzed from the January 2020 sampling, a choice of samples has been made to depict the trends concerning the particle concentration (*Figure 69*). ''Reference'' refers to samples not acquired within the caldera:

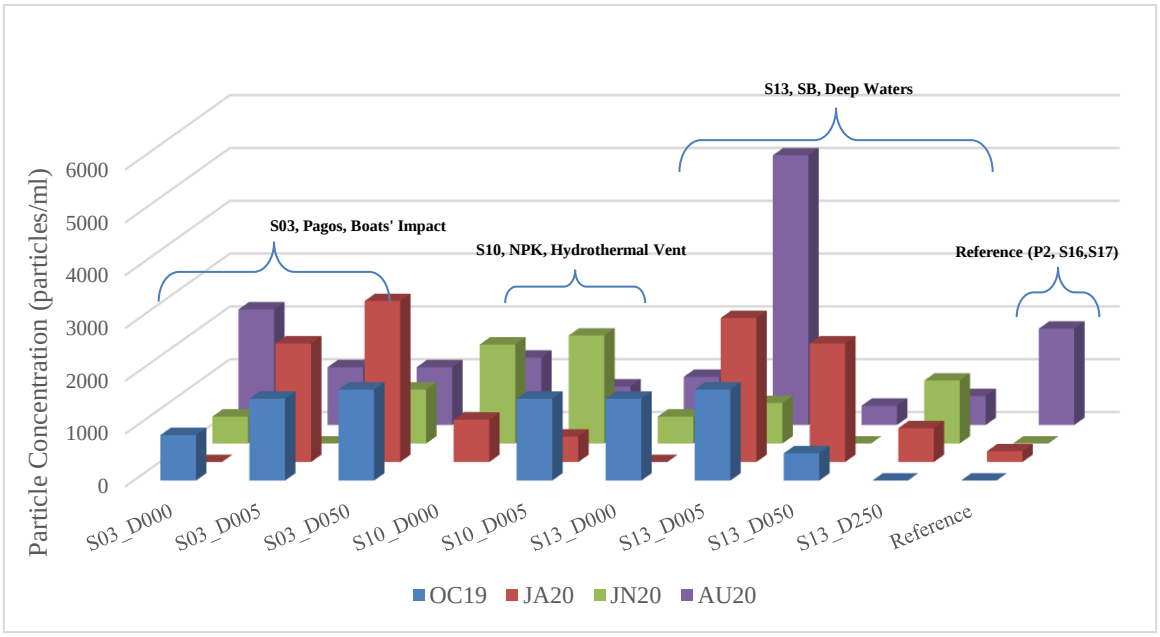

Figure 69. Cu particle Concentration for the different sample groups, from different samplings.

To begin with, August and January are characterized by significantly higher particle concentration values overall, apparently due to S03 and S13 (also a region frequently used by ships, as it leads to the main touristic port of the island).

Interestingly, the sampling site exhibiting the maximum particle concentration in each different time of the year is not the same for all of them. It would appear, that the hydrothermal vent site (S10) exhibits the highest particle concentration among the three different sites in June, while it is actually lower, overall, than both of the other sites in January and August. June appears to be the period of minimum particle concentration, for both the Boats' Impact and the Deep Waters group. That could be attributed to some random environmental factors (like currents) that lead the particles to be gathered in the NPK sampling site during that period. Another scenario would include a combination of lower anthropogenic contribution impact during June, and a hydrothermal vent related release event. Moreover, the available data from October show a more or less homogeneous distribution of nanoparticles across the different sites, indicating that the detected nanoparticles might have been released in the environment before that sampling, long enough, so that they have actually dispersed within the caldera.

Regarding the Boats' Impact group, represented by the S03 (Pagos, a busy crossing for ships and boats) sample, different depths exhibit similar behavior regardless the time period of the sampling. With the exception of D000, it appears that the particle concentration increases from October to January, when it has the maximum value, then decreases in June, and is once again increased In August. On the other hand, the D000 sample reaches its maximum value in August, instead of January, and exhibits zero detected particle concentration in January. That is an indication, that particles released in that site (quite possibly due to boats), do not remain in the surface, rather disperse to lower depths. Supposing this hypothesis is correct, according to the data, and assuming the observed behavior is representative for this site, particles would be released during August (higher particle concentration in D000). Over October and January disperse to lower depths (D005 higher that D000, and D050 higher than D005 in both cases), and would finally be found mainly in lower depths during June (D050 is higher than D000 and D005). The fact that the total particle concentration is lower in June than any other sampling for the S03 is also supporting this hypothesis, as it is highly likely that the particles would have dispersed lower than this depth by that time, or have precipitated. An additional observation that supports the hypothesis, is that October, January and August exhibit an increase in particle concentration as a function of depth, while the exact opposite trend is observed in August. In addition, the assumption that the release of particles in the sites heavily affected by boats' presence mainly happens in a period like August is very reasonable, taking into account that it is the peak of the tourist season.

Turning to the Hydrothermal Vent group, represented by the S10 (NPK) sample, it is worth noting, that not only is June the only time period that this site exhibits higher particle concentration than the other sites, it is also the period that it exhibits the highest concentration among other time periods, in the same site. This observation supports the aforementioned assumptions of some natural release of particles from the hydrothermal vent during that time, or that environmental factors caused the available particles to be gathered in this specific site. Taking into account that this sampling site is actually within a small bay, where particles could be ''trapped'', under certain circumstances.

Finally, the Deep Waters group is represented by the S13 (South Basin, SB) sample. As it was mentioned before, it is also a very busy crossing for boats, compared to the other sites, due to the fact that is leads from the south ''entrance'' of the caldera to the touristic port of the Santorini (Fira). Like the Boats' Impact group, this site too

exhibits higher concentrations of particles in January and August, and lower in June. In this case the additional sample from the lower depth allows for a better understanding of the downward dispersion of the particles. The maximum particle concentration is observed in D005 in October, January and August, and in 250 in June. October and January exhibit the same trend, with the particle concentration increasing from D000 to D005, and decreasing from D005 to D050, and then to D250. June and August also exhibit the same trend between them, as the concentration is increased from D000 to D005, then decreases from D005 to D050, and finally increases again from D050 to D250. Despite these regions being affected by ships, like the Boats' Impact group, the ratio of larger to smaller boats crossing it is much higher. Due to these regions' lower depth, bigger ships prefer to sail through them, whose draft (part of the ship that is underwater while sailing) can be bigger 10m. As a result, during touristic high season, it is expected that the D000 and D005 will be heavily affected, which could be cause of the much higher particle concentration in D005 than D000 in August. Taking that into account, the particles seem to be gathered close to the surface in August and October, while the maximum particle concentration is moved towards D005 and D050 in January, and finally towards D250 in June. This observation is in agreement with the aforementioned hypothesis, that the detected particles are being released sometime close (prior) to August, as the Deep Waters group exhibits the same trend in the relation between their downwards dispersion and time period as the Boats' Impact group.

The comparison of the different sample groups versus the time period of their acquisition, was aiming at observing the temporal variations of the samples. A more in-depth study of each individual sample group should provide some insight on the effect of the different depths on the same site, as well as justify the grouping of the samples. In order to eliminate the time parameter, and given the larger number of samples acquired, October 2020 sampling was chosen. An exception was made for the hydrothermal vent group, because the D000 sample from the October 2020 was not available. The June 2020 data are presented instead.

4.2.1.2. Cu particle concentration trends concerning the Boats' Impact Group, in October 2019

Figure 70 is a representation of the Cu – containing particles' concentration for the Boats Impact sample group, acquired during October 2019.

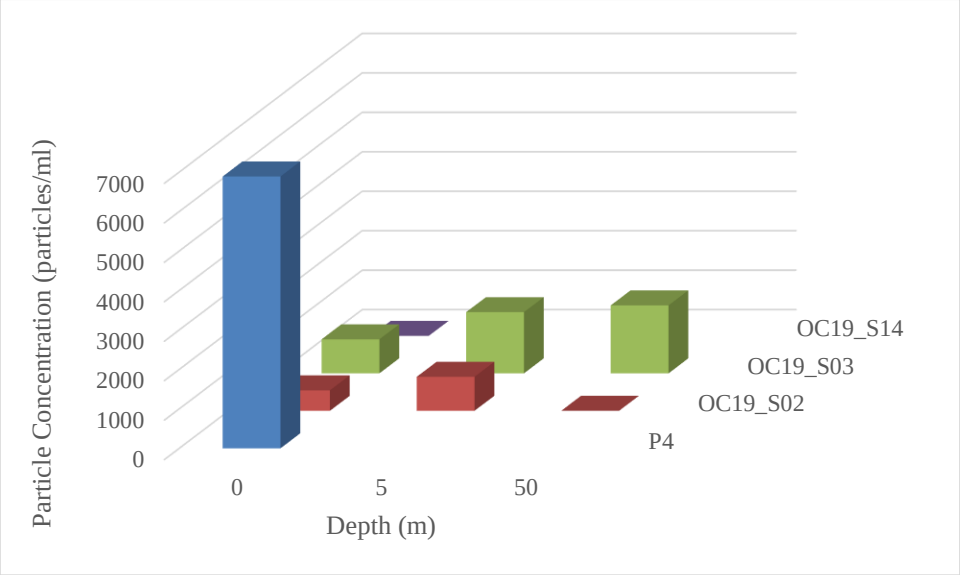

Figure 70. Cu particle Concentration of the Boats' Impact group samples, from OC19.

The P4 (0 depth) sample was only acquired once, from the trail of a ship in the port of Piraeus, so despite the fact that it can be compared to the other samples, the significantly higher particle concentration was not unexpected. S02 and S03 are relatively close to each other (see *Supplementary Section 2.1*), while S14 is in the opposite side of the island, which probably explains the significant difference in their results. S14 was acquired from the surface of the site (a docking site for smaller boats, mainly fishing boats), in order to be evaluated as a sampling site for the future (and is was indeed included in later samplings), but did not show any signs of Cu-containing particles. The S02 sampling site is in the proximity of the *Sea Diamond* shipwreck, while the S03 sample site is a busy crossing for ships that approach the island's port from the north. S02 and S03 behavior regarding the depth changes is similar, as the particle concentration increases from D000 to D005. For some reason, the S03 concentration is increased from D005 to D050, while the respective value for the D050 of the S02 sampling site is zero. The discriminating factor in this case could be one of many, including higher boats activity on S03 than on S02, that also includes higher number of larger ships. Also, S02 is closer to the shore, and a little less deep, which could affect the way the existing particles are distributed between the two sites, and among all others within the caldera of course. Although the particle concentrations of the samples S02 and S03 (essentially, the two samples that are to be monitored) is not identical, their results exhibit similar behavior, and in the same order of magnitude, so the representation of the Boats' Impact group by the S03 sampling site seems to be reasonable.

4.2.1.3. Cu particle concentration trends concerning the Deep Waters Group, in October 2019

Figure 71 is a representation of the Cu – containing particles' concentration for the Deep Waters sample group, acquired during October 2019.

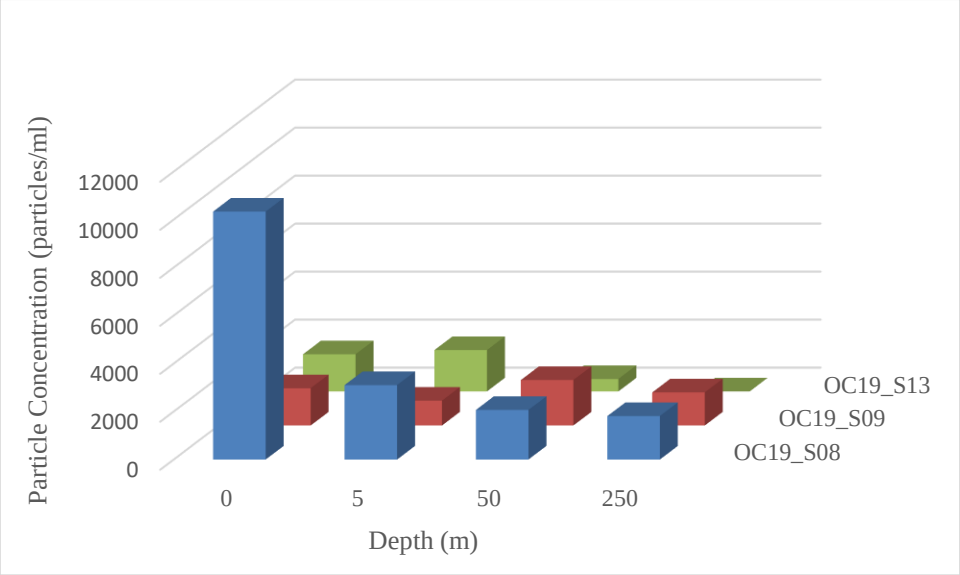

Figure 71. Cu particle Concentration of the Deep Waters group samples, from OC19.

The S09 (West Basin), S08 (North Basin) and S13 (South Basin) sites are the deepest parts of the seabed within Santorini. For this reason, they are usually proffered when picking a route for a larger ship, for safer travelling. S13 and S09 do not appear to have any clear trend, as they exhibit their maximum particle concentration in 5 and 50 meters respectively. The S08 sampling site though exhibits a clear trend regarding its particle concentration, decreasing as a function of depth. It is unclear whether the significantly higher concentration for the D000 of the S08 is a result of a one-time event (the presence or passing of a ship) or it should be expected to form a pattern over time. The choice of the S13 sampling site as representative of the group does not seem ideal, it was though the only one that was acquired in all following samplings. The difference between them can always be attributed to the vastness of the region they all represent, as the three basins combined cover more than 80% of the total seabed within the caldera.

4.2.1.4. Cu particle concentration trends concerning the Hotels and Waste Group, in October 2019

Figure 72 is a representation of the Cu – containing particles' concentration for the Hotels and Wastes sample group, acquired during October 2019.

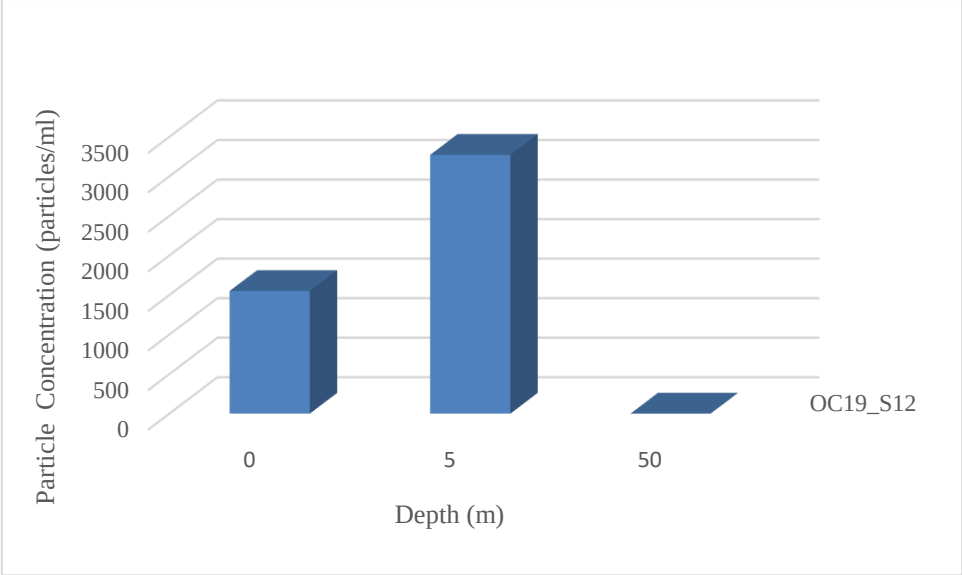

Figure 72. Cu particle Concentration of the Hotels and Wastes group samples, from OC19.

The S12 (Akrotiri) is the last remaining sampling site from the Hotels and Wastes group, after the evaluation of the preliminary data. The particle concentration of D005 is double the concentration of the D000, while the D050 did not yield any particles during the analysis. This behavior might be suggesting the release of Cu nanoparticles around August, as mentioned before, meaning they would be dispersing downwards, but not as far as 50 meters, duo to the limited time frame. However, the data of this chart are not sufficient on their own to support that hypothesis.

4.2.1.5. Cu particle concentration trends concerning the Hydrothermal Vent Group, in October 2019

Figure 73 is a representation of the Cu – containing particles' concentration for the hydrothermal vent sample group, acquired during October 2019.

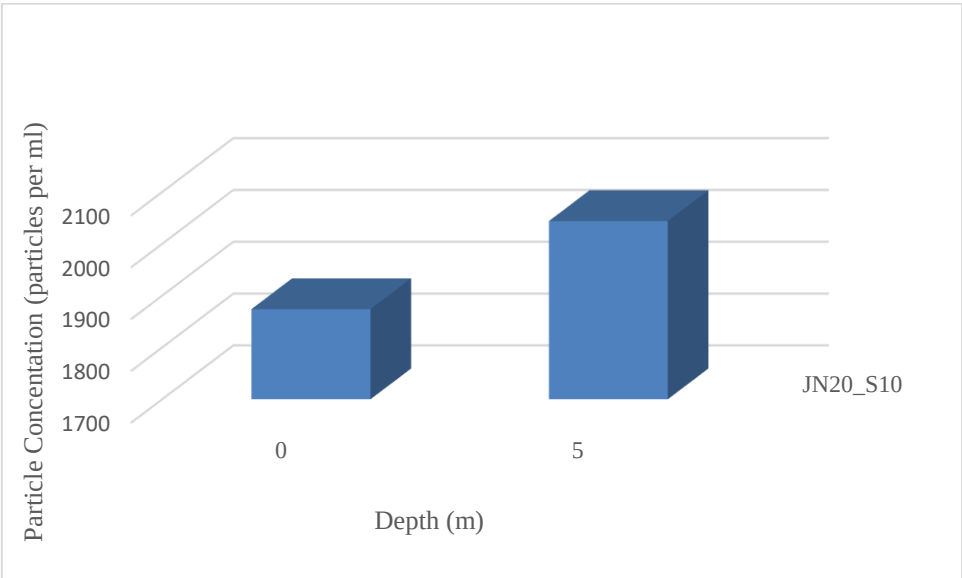

Figure 73. Cu particle Concentration of the Hydrothermal Vent group samples, from OC19.

In a similar case as mentioned right above, the S10 (North Palea Kameni) is the last remaining sampling site from the Hydrothermal Vent samples group. The difference between the two depths is not as striking as the one observed in S12 (~20%), but the trend is the same, exhibiting a higher value for the D005. Like before, this additional information does seem to strengthen the argument over the release of particles around August, but it is not on its own sufficient evidence. As it was mentioned before, the highest particle concentration for S10 has been observed in June 2020, which was also the highest concentration detected among the samples of that batch.

4.2.2. Cu containing particles' mean Cu mass in seawater samples in the proximity of Santorini

Tables 7-10 contain information and the results acquired through the use of the JupyterLab Python Notebook, regarding the mean mass of the detected particles from the samples analyzed for Cu, for 4 different samplings. For the identification of particle pulses, the 5σ threshold criterion has been applied in most cases. Following the process described by Tuoriniemi et al[75], in samples that exhibited, after visual evaluation, significantly low pulses and low background level (i.e, low ''μ'' value), higher thresholds have occasionally been applied (higher number of standard deviations added). As mentioned before, each sample was analyzed 3 times, for five minutes each, leading to 3 technical replicates. In cases when it seemed obvious that the sample didn't contain enough particles to be detected by the system (after visual evaluation of the real time data acquisition), less than three acquisitions have been obtained. In such cases, the corresponding cell in the table appears empty, which it not the same with the cells containing dashes (''-''), in which case the acquisition has been obtained, but the data process did not reveal any event pulses.
any event pulses.

Table 7. Mean Cu mass for the detected nanoparticles of samples analyzed for Cu from October 2019 Sampling

Sample Tag	Sam. Site	Depth (m)	Group	Replicate 1	Replicate 2	Replicate 3	Average	Std
Cu OC19 FLT BLK 2	-	-	Blank	-	-	-		
Cu OC19 P2	Piraeus	Surf	Reference	-				
Cu OC19 P4	Piraeus	Surf	Boats	2.061	1.834	2.447	2.114	0.310
Cu OC19_S02_D000_F10 SeaD	Sea Diamond	Surf	Boats	1.676	1.794	4.049	2.506	1.337
Cu OC19_S02_D005_F10 SeaD	Sea Diamond	5	Boats	0.727	1.478	0.727	0.977	0.434
Cu OC19_S02_D050_F10 SeaD	Sea Diamond	50	Boats	-	-	-		
Cu OC19_S03_D000_F10 Pag	Pagos	Surf	Boats	-	2.407	1.913	2.160	0.349
Cu OC19_S03_D005_F10 Pag	Pagos	5	Boats	1.049	1.083	1.438	1.190	0.215
Cu OC19_S03_D050_F10 Pag	Pagos	50	Boats	1.652	1.676	1.083	1.470	0.336
Cu OC19_S08_D000_F10 NB	North Basin	Surf	Deep Water	5.705	6.116	5.604	5.808	0.271
Cu OC19_S08_D005_F10 NB	North Basin	5	Deep Water	1.438	1.438	7.334	3.403	3.404
Cu OC19_S08_D050_F10 NB	North Basin	50	Deep Water	1.035	0.924		0.980	0.078
Cu OC19_S08_D250_F10 NB	North Basin	250	Deep Water	1.201	1.003		1.102	0.140
Cu OC19_S09_D000_F10 WB	West Basin	Surf	Deep Water	1.498	1.142		1.320	0.252
Cu OC19_S09_D005_F10 WB	West Basin	5	Deep Water	1.083			1.083	
Cu OC19_S09_D050_F10 WB	West Basin	50	Deep Water	1.181	2.15	-	1.666	0.685
Cu OC19_S09_D250_F10 WB	West Basin	250	Deep Water	1.388	-	2.032	1.710	0.455
Cu OC19_S10_D005_F10 NPK	NPK	5	H. Vent	1.26	3.139	3.248	2.549	1.118
Cu OC19_S12_D000_F10 Akrotiri	Akrotiri	Surf	Hotels' Waste	1.913	2.862	1.053	1.943	0.905
Cu OC19_S12_D005_F10 Akro	Akrotiri	5	Hotels' Waste	2.243	1.794	2.645	2.227	0.426
Cu OC19_S12_D050_F10 Akro	Akrotiri	50	Hotels' Waste	-				
Cu OC19_S13_D000_F10 SB	South Basin	Surf	Deep Water	2.21	2.121	3.495	2.609	0.769
Cu OC19_S13_D005_F10 SB	South Basin	5	Deep Water	2.648	2.951	1.705	2.435	0.650
Cu OC19_S13_D050_F10 SB	South Basin	50	Deep Water	1.201	1.794	-	1.498	0.419
Cu OC19_S13_D250_F10 SB	South Basin	250	Deep Water	-				
Cu OC19_S14_D000_F10	Vlychada	Surf	Boats	-				

Table 8. Mean Cu mass for the detected nanoparticles of samples analyzed for Cu from January 2020 Sampling

Sample	Sam. Site	Depth (m)	Group	Replicate 1	Replicate 2	Replicate 3	Average	Std
Cu JA20_FLT2_BLK	-	-	Blank	2.15	1.091		1.621	0.749
Cu JA20_S03_D000_F10 Pag	Pagos	0	Boats	-				
Cu JA20_S03_D005_F10 Pag	Pagos	5	Boats	1.86	2.15	5.329	3.113	1.925
Cu JA20_S03_D050_F10 Pag	Pagos	50	Boats	3.492	19.683	2.433	8.536	9.668
Cu JA20_S10_D000_F10 NPK	NPK	0	H.Vent	6.035	3.775	2.833	4.214	1.646
Cu JA20_S10_D005_F10 NPK	NPK	5	H.Vent	5.47	2.927	-	4.199	1.798
Cu JA20_S13_D005_F10 SB	South Basin	5	Deep Water	20.678	6.53	5.235	10.814	8.567
Cu JA20_S13_D050_F10 SB	South Basin	50	Deep Water	2.221	2.685	7.167	4.024	2.731
Cu JA20_S13_D250_F10 SB	South Basin	250	Deep Water	3.398	33.889	-	18.644	21.560
Cu JA20_S14_D000_F10 Vly	Vlychada	0	Boats	4.481	10.89	4.305	6.559	3.752
Cu JA20_S14_D005_F10 Vly	Vlychada	5	Boats	4.811	7.872	6.6	6.428	1.538
Cu JA20_S17_D000_F10 AgRef	Aegean	0	Reference	2.503	-		2.503	
Cu JA20_S17_D005_F10 AgRef	Aegean	5	Reference	6.813	1.656	1.514	3.328	3.019

Table 9. Mean Cu mass for the detected nanoparticles of samples analyzed for Cu from June 2020 Sampling								
Sample	**Sam. Site**	**Depth (m)**	**Group**	**Replicate 1**	**Replicate 2**	**Replicate 3**	**Average**	**Std**
Cu JN20_FLT_BLK1 MQ	-	-	Blank	-				
Cu JN20_FLT_BLK2 NISK	-	-	Blank	0.878	1.198		1.038	0.226
Cu JN20_S03_D000_F10 Pagos D1	Pagos	0	Boats	0.699	-	1.717	1.208	0.720
Cu JN20_S03_D000_F10 Pag D2	Pagos	0	Boats	2.197	-		2.197	
Cu JN20_S03_D005_F10 Pagos D1	Pagos	5	Boats	-	-			
Cu JN20_S03_D005_F10 Pag D2	Pagos	5	Boats	-	-			
Cu JN20_S03_D050_F10 Pagos D1	Pagos	50	Boats	-	2.197	4.174	3.186	1.398
Cu JN20_S03_D050_F10 Pag D2	Pagos	50	Boats	-	-	-		
Cu JN20_S10_D000_F10 NPK D1	NPK	0	H.Vent	0.759	0.827	-	0.793	0.048
Cu JN20_S10_D005_F10 NPK D1	NPK	5	H.Vent	0.981	1.238	2.077	1.432	0.573
Cu JN20_S13_D000_F10 SB	South Basin	0	Deep Water	1.238			1.238	
Cu JN20_S13_D005_F10 SB	South Basin	5	Deep Water	2.376	2.197		2.287	0.127
Cu JN20_S13_D050_F10 SB	South Basin	50	Deep Water	-				
Cu JN20_S13_D250_F10 SB	South Basin	250	Deep Water	2.316	3.515	3.395	3.075	0.660
Cu JN20_S14_D000_F10 Vly	Vlychada	0	Boats	4.204		5.312	4.758	0.783
Cu JN20_S14_D005_F10 Vly	Vlychada	~2	Boats		11.905	64.38	38.143	37.105
Cu JN20_S16_D000_F10 AgRef	Aegean	0	Reference					
Cu JN20_S16_D005_F10 AgRef	Aegean	5	Reference	2.796			2.796	
Cu JN20_S16_D050_F10 AgRef	Aegean	50	Reference	2.796	4.953		3.875	1.525

Table 10. Mean Cu mass for the detected nanoparticles of samples analyzed for Cu from August 2020 Sampling								
Sample	**Sam. Site**	**Depth (m)**	**Group**	**Replicate 1**	**Replicate 2**	**Replicate 3**	**Average**	**Std**
Cu AU20_FLT_BLK2_F10	-	-	Blank	13.924			13.924	
Cu AU20_S03_D000_F10 D1	Pagos	Surf	Boats	4.898	3.78	6.916	5.198	1.589
Cu AU20_S03_D005_F10 D1	Pagos	5	Boats	1.159			1.159	
Cu AU20_S03_D050_F10 D1	Pagos	50	Boats	1.506	1.775	2.392	1.891	0.454
Cu AU20_S03_D005_F10 D2	Pagos	5	Boats	15.812	3.876	5.579	8.422	6.456
Cu AU20_S03_D050_F10 D2	Pagos	50	Boats	34.924	3.414	9.988	16.109	16.623
Cu AU20_S10_D000_F10	N.P.K.	Surf	H. Vent		10.416	3.356	6.886	4.992
Cu AU20_S10_D005_F10	N.P.K.	Surf	H. Vent	14.423	2.932	4.551	7.302	6.220
Cu AU20_S13_D000_F10	SB	Surf	Deep Water	1.467	1.544	1.93	1.647	0.248
Cu AU20_S13_D005_F10	SB	5	Deep Water	1.66	3.232	4.165	3.019	1.266
Cu AU20_S13_D050_F10	SB	50	Deep Water		2.315	2.7	2.508	0.272
Cu AU20_S13_D250_F10	SB	250	Deep Water	2.315			2.315	
Cu AU20_S14_D000_F10 D1	Vly	0	Boats					
Cu AU20_S14_D000_F10 D2	Vly	0	Boats	2.122			2.122	
Cu AU20_S17_D000_F10	AgRef	0	Reference	5.013	7.044	3.96	5.339	1.568
Cu AU20_S17_D005_F10	AgRef	5	Reference	0.928	0.712		0.820	0.153
Cu AU20_S17_D050_F10	AgRef	50	Reference	0.627	4.705		2.666	2.884

4.2.2.1. General trends concerning Cu containing particles' mean mass

For the same reasons mentioned in the previous section, a choice of samples has been made, in order to show the general trend that is depicted in *Figure 74* (they are correspondent to the ones mentioned in Section 4.2.1). As a reference, 1fg of Cu corresponds to ~$2x10^7$ Cu atoms:

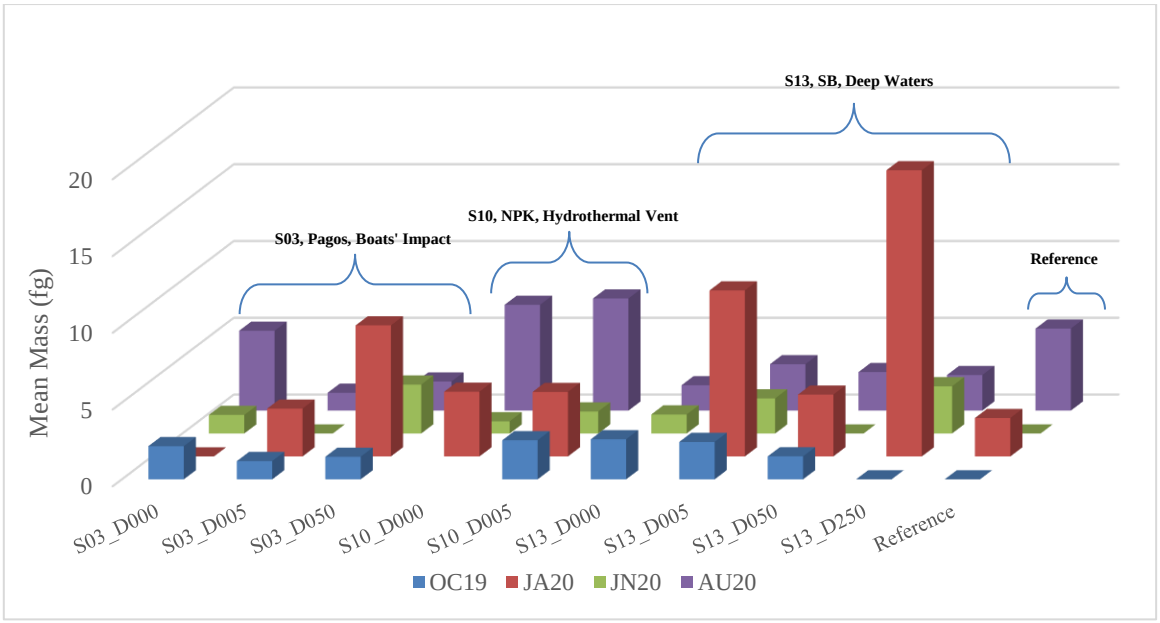

Figure 74. Mean Mass of Cu - containing particles for the different sample groups, from different samplings.

To begin with, it is obvious that the metal content of the particles detected in January and August was overall much higher. Supposing that the detected particles have the same composition in all different time periods, their metal content should be directly proportional to their size. Engineered Cu containing nanomaterial have been reported to rapidly aggregate when in seawater matrix (within minutes), in significant sizes (>1μm).[44]Therefore, it is reasonable to expect that, should the particle concentration is sufficient, the particles detected be larger, rather than numerous.

Not unlike the particle concentration shown in *Figire 69*, the maximum value for the mean mass of the particles seems to not be in the same site for every time period. What is worth noting, also, is that the maximum of the mean mass of a sampling is *not* corresponding to the maximum of the particle concentration of the same sampling. Larger particles seem to be preferably gathered in S13 in January, where the largest particles overall are also observed. June and October exhibit a more or less homogeneous distribution, regarding the size of the particles they contain, while the maximum of August is at the site of the hydrothermal vent.

Regarding the Boats Impact sample group, represented by the S03 (Pagos) sampling site, there is no clear trend shared among the different depths of the site. However, the maximum mean size is in D000 in August and October (although slightly), while it has moved to lower depths in January, and apparently even lower in June. Once again supposing, that this behavior is representative of a repeating yearlong behaviour of the system, the precipitation of the larger Cu particles seems to be suggested, an observation in agreement with previous relative studies on engineered nanoparticles[44]. Should this be the case, taking into account their expected rapid aggregation, the hypothesis regarding the release of the Cu particles in August is supported, as the largest particles are detected on the surface in August, and their sedimentation is observed over time, until June. The relatively lower mean mass for the detected particles in D000 and D005 during June, along with the D050 mean mass being lower than the respective value of January, is an indication for the ongoing sedimentation of larger (heavier) particles in the Boats' Impact group.

Turning to the Hydrothermal Vent sample group, represented by the S10 (North Palea Kameni) sampling site, the maximum mean mass of the detected particles appears in August, while the minimum appears in June. Taking into account the particle concentration chart (*Fig.69*), a very high particle concentration of small particles appears in June, while a slightly lower particle concentration of much larger particles is observed in August. Since this behaviour seems to be opposite to the one the Boats' Impact group exhibit, either the origin of the particles is different in the two sites (maybe a natural release from the hydrothermal vent, opposed to the anthropogenic factor), or the same phenomena (like currents) affect the two sites in the opposite manner.

Finally, the Deep Waters sample group, represented by the S13 (South Basin) sampling site, exhibits the overall maximum mean mass, in the depth of 250 m in January (> 18fg / particle, i.e, > $3{,}7 \times 10^8$ Cu atoms/particle). D250 exhibits the maximum observed mean mass in January and June, and the minimum in October. D005 and D050 exhibit the same behavior across the different time periods, meaning the mean mass increases from October to January, decreases from January to June, and then increases again in August. Taking the overall distribution of the mean masses observed, it seems that larger particles are found more commonly closer to the surface in August and October, and in lower depths in January and June. It is also likely, as it was mentioned before, that larger particles might have precipitated lower than the 250 m mark in June, which would also explain the overall lower particle concentration observed in *Figure 69* as well.

The comparison of the different sample groups versus the time period of their acquisition, was aiming at observing the temporal variations of the samples. A more in-depth study of each individual sample group should provide some insight on the effect of the different depths on the same site, as well as justify the grouping of the samples. The samples chosen are corresponding to the ones studied for their particle concentration in section 4.2.1.

4.2.2.2. Cu mean mass trends concerning the Boats' Impact Group, in October 2019

Figure 75 is a representation of the Cu – containing particles' concentration for the Boats Impact sample group, acquired during October 2019.

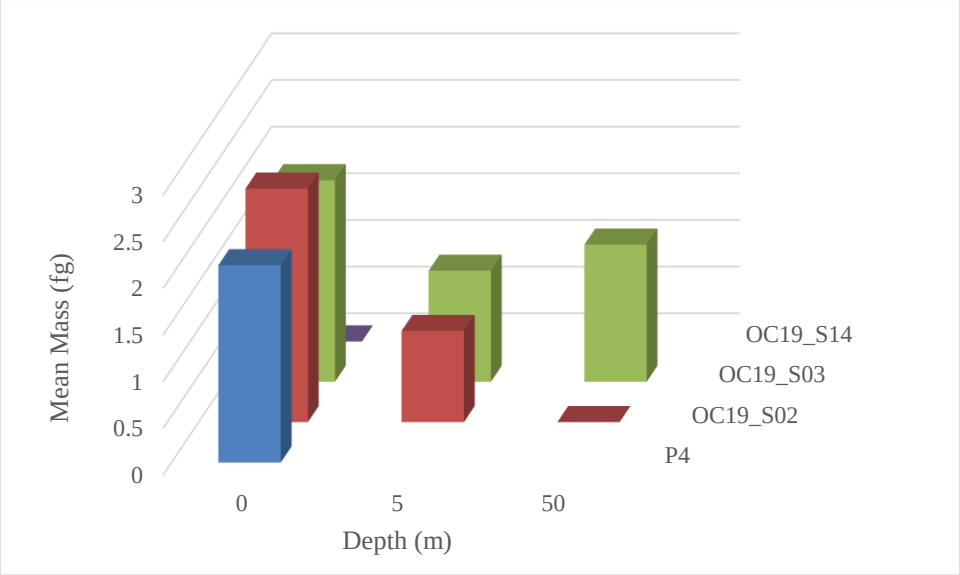

Figure 75. Mean mass of Cu – containing particles for the Boats' Impact group samples, from OC19.

As it was mentioned before, the P4 (Piraeus) sample was only acquired once, to be compared with the samples taken from Santorini. Also, the S14 (Vlychada) sample was only evaluated during this sampling. What is worth noting, is that, In October, all sampling sites (S14 is not included in the comparison duo to the lack of data) exhibit the maximum of their observed mean mass on the surface. In addition, the particles detected in S02 and S03 are apparently larger than the ones detected in the P4 sample. Compared with *Figure 70*, that shows the respective particle concentrations, it becomes apparent that the particles on the surface of S02 and S03 are fewer, but larger, while they shrink but multiply as a function of depth. This is an indication that larger particles released close (prior) to October tend to remain close to the surface. S02 and S02 exhibit similar behavior regarding their particles' mean mass, with the exception of D050, which can be attributed to factors mentioned in section 4.2.1. Those include higher boats activity on S03 than on S02, that also includes higher number of larger ships, S02 being closer to the shore, and of course the presence of the Sea Diamond shipwreck.

4.2.2.3. Cu mean mass trends concerning the Deep Waters Group, in October 2019

Figure 76 is a representation of the Cu – containing particles' concentration for the Deep Waters sample group, acquired during October 2019.

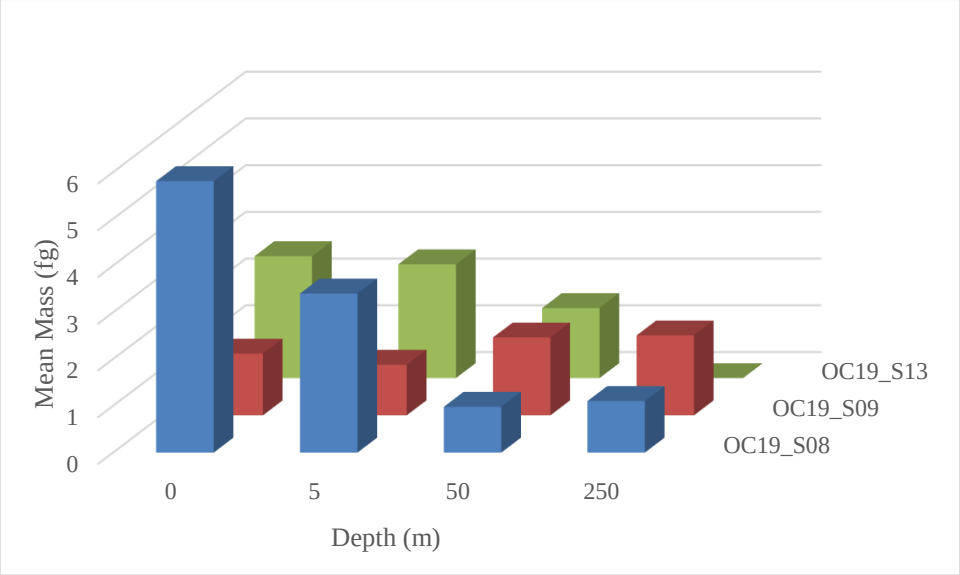

Figure 76. Mean mass of Cu – containing particles for the Deep waters group samples, from OC19.

The maximum mean mass for the Deep Waters group also seems to be closer to the surface in October and June, like the Boats Impact Group, while S09 exhibits a more or less homogeneous distribution of observed mean mass values across the different depths. What is worth noting, is that comparing this chart with *Figure 71*, concerning the particle concentration of the same samples, they both exhibit more or less the same trends between the mean mass and particle concentration. For example, the D000 of the S08 sampling site exhibits both the larger mean mass for its detected particles, as well as the highest number concentration among the different depths. Both of those metrics exhibit similar trends for the rest of the samples in the site, decreasing as a function of depth. The exact same observation can be made for the samples concerning the S13 sampling site. S09 exhibits an opposite trend to the other two sampling sites, but the same trend as the corresponding chart regarding the particle concentration in the site *Figure 71*.

4.2.2.4. Cu mean mass trends concerning the Hotels and Wastes Group, in October 2019

Figure 77 is a representation of the Cu – containing particles' concentration for the Hotels and Wastes sample group, acquired during October 2019.

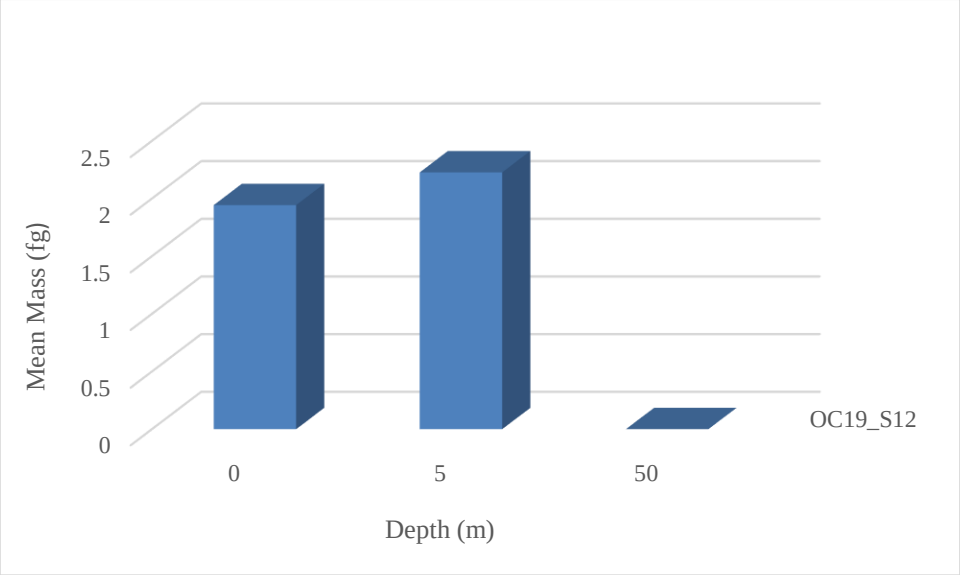

Figure 77. Mean mass of Cu – containing particles for the Hotels and Wastes group samples, from OC19.

Both of the samples where particles have been detected (D000 and D005) for the Hotels and Wastes sample group exhibit relatively low mean mass for the detected particles. Comparing this chart with *Figure 72*, concerning the same samples mean size, they exhibit the same trend between them, meaning that D005 contains both larger, and more particles per ml of sample.

4.2.2.5. Cu mean mass trends concerning the Hydrothermal Vent Group, in October 2019

Figure 78 is a representation of the Cu – containing particles' concentration for the Hydrothermal Vent sample group, acquired during October 2019.

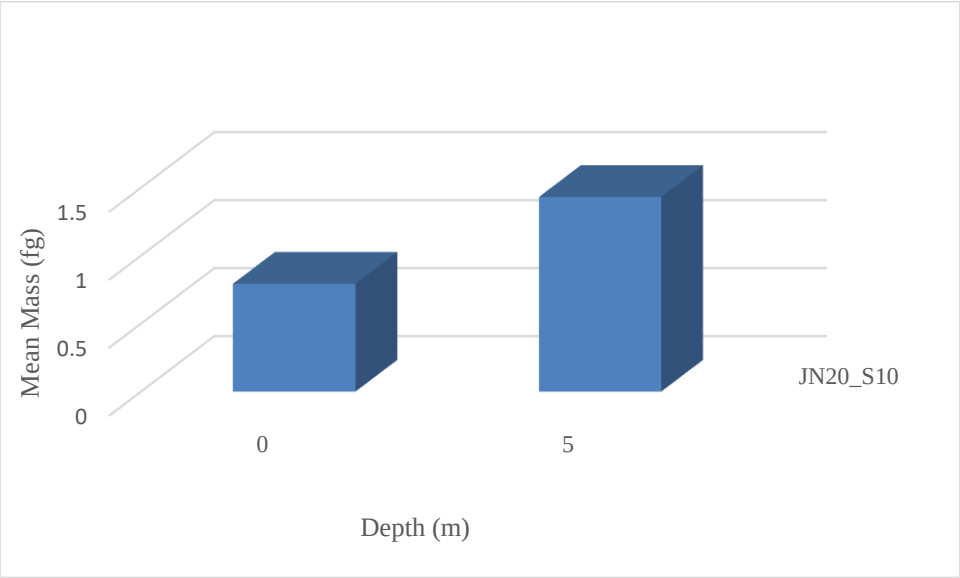

Figure 78. Mean mass of Cu – containing particles for the Hydrothermal Vent group samples, from OC19.

Finally, both of the samples from the hydrothermal vent site exhibit relatively low mean mass for the detected

particles. Comparing this chart with *Figure 73* concerning the same samples mean size, they exhibit the same trend between them, meaning that D005 contains both larger, and more particles per ml of sample.

5. Conclusions

The use of the on – line dilution system for the analysis of seawater samples has been revisited, and evaluated for the analysis of particle suspensions and dissolved analyte solutions. The system exhibited remarkable robustness and continuous analysis capability for more than 10 hours, for a number of months, without significant damage to the equipment (mainly the interface).

5.1. Conclusions for Investigating the Fate of Silver Nanoparticles and Ionic Silver is Seawater Systems (Mesocosm Tanks)

The on – line dilution system has been successfully incorporated in the analysis of seawater samples from mesocosm tanks, spiked with low ppt concentrations of either particulate or ionic Ag, in a collaboration project with the Hellenic Center for Marine Research (HCMR). Overall, the system exhibited high recovery values and robustness, and the results were consistent with the expectations from the literature.

Taking advantage of the known concentrations of particulate and ionic Ag in the AgNP and Ionic Ag treated tanks respectively, the system's capabilities regarding a low dwell time (75 μs per datapoint) have been evaluated, and compared with results from a widely used dwell time (10 ms per datapoint). Also, three different threshold criteria have been applied for the identification of event pulses as single moieties. Two of them are, μ + 3std (3σ) and μ + 5std (5σ), where ''μ'' stands for the average intensity value and std for the standard deviation of the dataset, after a process that is proposed by Pace et al[116] and widely accepted in the single particle analysis. And the third is equal to $\mu + 2.71 + 3.29 * \sqrt{\mu}$, (PG) where ''μ'' stands for the mean intensity of the dataset, as it was mentioned before, a threshold based on the Poisson Statistics. After a comparative study of all the different thresholds versus the different dwell times, both for the ionic Ag and the AgNP treated tanks, the optimal conditions for each analysis where determined: For the analysis of samples from seawater tanks spiked with Ag nanoparticles, analyzed using 10 ms dwell time, the μ + 3std threshold criterion proved suitable, yielding a recovery value of 97.9% ± 66.6%, closely followed by the μ + 5std threshold criterion, with 81.7% ± 20.9%. For the analysis of samples from seawater tanks spiked with Ag nanoparticles, analyzed using 75 μs dwell time, $\mu + 2.71 + 3.29 * \sqrt{\mu}$, was proven more reliable, yielding a recovery value of 79.0% ± 26.1%. For the analysis of samples from seawater tanks spiked with Ionic Ag, analyzed using 10 ms dwell time, both the μ + 3std and μ + 5std threshold criteria performed similarly well, with recovery values of 61.1% ± 22.3% and 64.7% ± 21.2% respectively. And finally, for the analysis of samples from seawater tanks spiked with Ionic Ag, analyzed using 75 μs dwell time, the μ + 5std threshold proved sufficient, with a recovery value of 71.2% ± 27.2, after excluding the datapoints before D2. Close examination of the data regarding the excluded datapoints

revealed the obvious miscalculation, since the recovery value for the dataset was 142.3% ± 180.1%. Moreover, this miscalculation was not an issue for the PG threshold criterion when it was applied on the same data. That means, that the origin of the anomaly was signals of very low intensity, falsely identified as particles.
During the analysis of the samples from the ionic Ag spiked tanks, pulse events usually associated with particles were observed, whose nature and origin have been examined. Cross-referencing of the related observations during the experiment with literature, in addition to a simulation using GEOCHEM – EZ, led to the tentative conclusion that the pulse events were caused by the detection of particles formed, despite the very low silver concentrations. The nature of the detected particles is still under investigation, but the initial results suggest moieties of Ag complexed with Natural Organic Matter, Ag_2S particles, or a combination of both.

5.2. Conclusions for Investigating the Occurrence and metal content (Cu) of Copper – containing particles in seawater samples in the proximity of the Island of Santorini

After the initial evaluation of the technique during the mesocosm experiment, the on – line dilution system has been incorporated in the analysis of seawater samples in the proximity of islands, and more specifically, Santorini, under the ongoing NanoIsland program (ELIDEK). Santorini has been chosen as an ideal site for the study of engineered, incidental and naturally occurring particles, as it is a very popular touristic destination during the summer, and is essentially a still active volcanic site. Samples have been acquired from sites all over the caldera, over a period of two years, so the temporal and spatial variations of the particles occurrence and metal content could be studied. After due consideration of the elements environmental impact, and the probability of their occurrence, a list of 10 elements has been drafted, of which 5 have already been analyzed (Pb, V, Ni, Cu, Fe). For the processing of the acquired data, a python-based script has been developed, using the JupyterLab notebook interface. Of the chosen elements, the results regarding the Cu containing particles have been presented, and their particle concentration and mean mass have been studied. The processing revealed generally higher particle concentration in sites associated with boats activity during the summer period. Also, particles with higher Cu content were generally found in deeper waters, while there have been indications about their precipitation, beginning around the same period as the high particle concentrations observed. Based on the afore mentioned observations, the period of their release was tentatively suggested to be in summer. The correlation with the sites associated with higher boats activity, led to the tentative conclusion that their origin was, at least for the most part, anthropogenic.

6. Future Goals

The present thesis has set the basis for thorough analysis of nanomaterials in natural seawater samples, which is a major concern in modern society, due to the ever-growing use and release of nanomaterial in the

environment. Future aspirations stemming from this work include:

- Further processing of the data concerning the particle – related signals during the analysis of seawater mesocosm tanks spiked with low ppt concentrations, so that their nature can be verified.
- Processing and presentation of the data concerning the rest of the analyzed elements from the NanoIsland program, along with the analysis of the rest of the elements on the list (Ti, As, Ce, Zn, Zr).
- A comparative study could subsequently be conducted, leading to correlations between elements, and revealing information about the detected particles origin and composition.
- Further development of the python – based script, so that it can be used universally in the analysis of samples containing single moieties, as an independent program (graphic user interface). The final program should be able to analyze data from analysis with different dwell time, regardless of the use of CRC (Collision/Reaction Cell), and apply the *appropriate* thresholds for the extraction of case – specific results.

7. Acknowledgments

First and foremost, I would like to thank the Department of Chemistry, of the University of Crete, for providing me with the instruments and materials needed for the experimental work of this thesis to be conducted. Despite the grim situation in Greece, during the period of my studies, the Department of Chemistry has managed to provide me and numerous other students with the opportunity of expanding and deepening our knowledge and expertise on the fields of our interests. The department's stuff cannot, as this point, be mentioned by name, but their hard work and immense contribution in shaping the future of our scientific field cannot go unmentioned. The Hellenic Research for Marine Research is also more than deserving of my gratitude, for the opportunity given to me to work among great scientists of our field from all over the world, on a project of such great importance. Again, all our remarkable colleagues from HCMR cannot be mentioned by name, but their work and their attitude truly make them the ideal collaborators in any project.

There is also a great number of individuals I would like to thank for their help and guidance through my years as an undergraduate and, afterwards, a master's student: My supervising professor and mentor for the better part of the last four years, Dr. Spiros A. Pergantis, for his immense contribution on my education and the shaping of my scientific and academic profile. My close colleague and mentor, (currently) PhD Candidate Manos Mavrakis, for his patience, his guidance, and the countless hours we spent together, working on a number of projects, or conversing on matters of mutual interest, either to promote our work, him passing his hard-earned knowledge to me, or to lighten the mood when circumstances were less than ideal. My close colleague and mentor Dr. Andreas Gondikas, scientific supervisor of the NanoIsland project, for his guidance, his spirit, and the opportunities he gave me through the project, to further my knowledge of the scientific and practical part of our field. The scientific supervisor, and co – supervisor of the laboratory I visited for my Erasmus+ internship

in the University of Oviedo, Dr. Bettmer Jörg, and the deputy dean of the University of Oviedo and co – supervisor of said laboratory, Dr. Maria Montes – Bayon, for their guidance, their attitude, and the great collaboration they offered me, both during my 4 – month stay in their group, and during our joint efforts within the Mesocosms experiment mentioned within the study. Dr. Nikos Daskalakis and Dr. Andreas Hillbol, may he rest in peace, for their invaluable input in teaching me all the basics I needed to develop the python processing tool. And of course, the members of my master's thesis and defence evaluation committee, Dr. Konstantinos Milios, also my professor during my undergraduate and master's studies, and Dr. Manolis Tsapakis, also my colleague during the mesocosm experiment, and A' researcher in the HCMR, for their valuable time and advice. Many more thanks and acknowledgments should go out to my friends and family, whose support was strong and ever – present, without which I doubt I could have reached this point of my academic and scientific career. This being hardly the appropriate time and manner for the expressing of my gratitude to the people closest to me, I simply want to thank each and every individual that believed in me, even when my faith was wavering. To any of them reading this note, I thank you for your patience, your support and your faith, and I apologize for all the times I treated you worse than you deserved.

8. Bibliography

1. Nanomaterials definition matters. *Nat. Nanotechnol.* **14**, 193 (2019).
2. Kreyling, W. G., Semmler-Behnke, M. & Chaudhry, Q. A complementary definition of nanomaterial. *Nano Today* **5**, 165–168 (2010).
3. Hochella, M. F. *et al.* Natural, incidental, and engineered nanomaterials and their impacts on the Earth system. *Science (80-.).* **363**, (2019).
4. Hosnedlova, B. *et al.* Nano-selenium and its nanomedicine applications: A critical review. *Int. J. Nanomedicine* **13**, 2107–2128 (2018).
5. Chhabria, S. & Desai, K. Selenium Nanoparticles and Their Applications. *Encycl. Nanosci. Nantotechnology* 1–32 (2016).
6. Gandin, V., Khalkar, P., Braude, J. & Fernandes, A. P. Organic selenium compounds as potential chemotherapeutic agents for improved cancer treatment. *Free Radic. Biol. Med.* **127**, 80–97 (2018).
7. Menon, S., KS, S. D., Santhiya, R., Rajeshkumar, S. & S, V. K. Selenium nanoparticles: A potent chemotherapeutic agent and an elucidation of its mechanism. *Colloids Surfaces B Biointerfaces* **170**, 280–292 (2018).
8. Zhang, Y. *et al.* Enhancement of cell permeabilization apoptosis-inducing activity of selenium nanoparticles by ATP surface decoration. *Nanomedicine Nanotechnology, Biol. Med.* **9**, 74–84 (2013).
9. Maldonado, C. R., Salassa, L., Gomez-Blanco, N. & Mareque-Rivas, J. C. Nano-functionalization of metal complexes for molecular imaging and anticancer therapy. *Coord. Chem. Rev.* **257**, 2668–2688 (2013).
10. Zhao, Y., Sun, Q., Zhang, X., Baeyens, J. & Su, H. Self-assembled selenium nanoparticles and their application in the rapid diagnostic detection of small cell lung cancer biomarkers. *Soft Matter* **14**, 481–489 (2018).
11. Prasad, K. S., Patel, H., Patel, T., Patel, K. & Selvaraj, K. Biosynthesis of Se nanoparticles and its effect on UV-induced DNA damage. *Colloids Surfaces B Biointerfaces* **103**, 261–266 (2013).
12. Seisenbaeva, G. A. *et al.* Dispersion of TiO2 nanoparticles improves burn wound healing and tissue regeneration through specific interaction with blood serum proteins. *Sci. Rep.* **7**, 1–11 (2017).
13. Hasan, S. A Review on Nanoparticles : Their Synthesis and Types. *Res. J. Recent Sci. Res . J . Recent . Sci . Uttar Pradesh (Lucknow Campus)* **4**, 1–3 (2014).
14. Pant, H. R. *et al.* Antibacterial and photocatalytic properties of Ag/TiO2/ZnO nano-flowers prepared by facile one-pot hydrothermal process. *Ceram. Int.* **39**, 1503–1510 (2013).
15. Batista, C. C. S. *et al.* Antimicrobial activity of nano-sized silver colloids stabilized by nitrogen-containing polymers: The key influence of the polymer capping. *RSC Adv.* **8**, 10873–10882 (2018).
16. Khalid, A. *et al.* Intrinsic fluorescence of selenium nanoparticles for cellular imaging applications. *Nanoscale* **8**, 3376–3385 (2016).

17. Stratakis, M. & Garcia, H. Catalysis by supported gold nanoparticles: Beyond aerobic oxidative processes. *Chem. Rev.* **112**, 4469–4506 (2012).
18. Chaudhary, S. & Mehta, S. K. Selenium Nanomaterials: Applications in Electronics, Catalysis and Sensors. *J. Nanosci. Nanotechnol.* **14**, 1658–1674 (2014).
19. Singh, T., Shukla, S., Kumar, P., Wahla, V. & Bajpai, V. K. Application of nanotechnology in food science: Perception and overview. *Front. Microbiol.* **8**, 1–7 (2017).
20. Fytianos, G. & Rahdar, A. Nanomaterials in Cosmetics : Recent Updates. 1–16 (2020).
21. Sharma, V. K., Filip, J., Zboril, R. & Varma, R. S. Natural inorganic nanoparticles-formation, fate, and toxicity in the environment. *Chem. Soc. Rev.* **44**, 8410–8423 (2015).
22. Keller, A. A. *et al.* Comparative environmental fate and toxicity of copper nanomaterials. *NanoImpact* **7**, 28–40 (2017).
23. Luoma, S. N. *et al.* Effect of cysteine and humic acids on bioavailability of Ag from Ag nanoparticles to a freshwater snail. *NanoImpact* **2**, 61–69 (2016).
24. Lodeiro, P., Browning, T. J., Achterberg, E. P., Guillou, A. & El-Shahawi, M. S. Mechanisms of silver nanoparticle toxicity to the coastal marine diatom Chaetoceros curvisetus. *Sci. Rep.* **7**, 1–10 (2017).
25. Miglietta, M. L., Rametta, G., Manzo, S. & Rocco, A. Lecture Notes in Electrical Engineering: Foreword. *Lect. Notes Electr. Eng.* **91 LNEE**, (2011).
26. Rodriguez-Navarro, C., Di Lorenzo, F. & Elert, K. Mineralogy and physicochemical features of Saharan dust wet deposited in the Iberian Peninsula during an extreme red rain event. *Atmos. Chem. Phys.* **18**, 10089–10122 (2018).
27. Wilson, M. A. *et al.* Nanomaterials in soils. *Geoderma* **146**, 291–302 (2008).
28. Morgado, R. G., Loureiro, S. & González-Alcaraz, M. N. *Changes in soil ecosystem structure and functions due to soil contamination*. *Soil Pollution: From Monitoring to Remediation* (Elsevier Inc., 2017). doi:10.1016/B978-0-12-849873-6.00003-0
29. Patinha, C., Armienta, A., Argyraki, A. & Durães, N. *Inorganic pollutants in soils*. *Soil Pollution: From Monitoring to Remediation* (Elsevier Inc., 2017). doi:10.1016/B978-0-12-849873-6.00006-6
30. Loureiro, S. *et al. Nanomaterials as soil pollutants*. *Soil Pollution: From Monitoring to Remediation* (Elsevier Inc., 2017). doi:10.1016/B978-0-12-849873-6.00007-8
31. Kulmala, M. *et al.* Formation and growth rates of ultrafine atmospheric particles: A review of observations. *J. Aerosol Sci.* **35**, 143–176 (2004).
32. Kerminen, V. M. *et al.* Atmospheric new particle formation and growth: Review of field observations. *Environ. Res. Lett.* **13**, 103003 (2018).
33. Kalivitis, N. *et al.* Formation and growth of atmospheric nanoparticles in the eastern Mediterranean: Results from long-term measurements and process simulations. *Atmos. Chem. Phys.* **19**, 2671–2686 (2019).
34. Lee, S. H. *et al.* New Particle Formation in the Atmosphere: From Molecular Clusters to Global Climate. *J. Geophys. Res. Atmos.* **124**, 7098–7146 (2019).

35. Okada, S. *et al.* The making of natural iron sulfide nanoparticles in a hot vent snail. *Proc. Natl. Acad. Sci. U. S. A.* **116**, 20376–20381 (2019).
36. Yin, Y., Liu, J. & Jiang, G. Sunlight-induced reduction of ionic Ag and Au to metallic nanoparticles by dissolved organic matter. *ACS Nano* **6**, 7910–7919 (2012).
37. Prichard, H. M. & Fisher, P. C. Identification of platinum and palladium particles emitted from vehicles and dispersed into the surface environment. *Environ. Sci. Technol.* **46**, 3149–3154 (2012).
38. Gondikas, A. *et al.* Where is the nano? Analytical approaches for the detection and quantification of TiO2 engineered nanoparticles in surface waters. *Environ. Sci. Nano* **5**, 313–326 (2018).
39. Gondikas, A. P. *et al.* Release of TiO2 nanoparticles from sunscreens into surface waters: A one-year survey at the old danube recreational lake. *Environ. Sci. Technol.* **48**, 5415–5422 (2014).
40. Toncelli, C. *et al.* Silver nanoparticles in seawater: A dynamic mass balance at part per trillion silver concentrations. *Sci. Total Environ.* **601**–**602**, 15–21 (2017).
41. Yang, Y., Long, C. L., Li, H. P., Wang, Q. & Yang, Z. G. Analysis of silver and gold nanoparticles in environmental water using single particle-inductively coupled plasma-mass spectrometry. *Sci. Total Environ.* **563**–**564**, 996–1007 (2016).
42. El Badawy, A. M., Scheckel, K. G., Suidan, M. & Tolaymat, T. The impact of stabilization mechanism on the aggregation kinetics of silver nanoparticles. *Sci. Total Environ.* **429**, 325–331 (2012).
43. Li, X. & Lenhart, J. J. Aggregation and dissolution of silver nanoparticles in natural surface water. *Environ. Sci. Technol.* **46**, 5378–5386 (2012).
44. Conway, J. R., Adeleye, A. S., Gardea-Torresdey, J. & Keller, A. A. Aggregation, dissolution, and transformation of copper nanoparticles in natural waters. *Environ. Sci. Technol.* **49**, 2749–2756 (2015).
45. Gondikas, A. P. *et al.* Cysteine-induced modifications of zero-valent silver nanomaterials: Implications for particle surface chemistry, aggregation, dissolution, and silver speciation. *Environ. Sci. Technol.* **46**, 7037–7045 (2012).
46. El Badawy, A. M. *et al.* Impact of environmental conditions (pH, ionic strength, and electrolyte type) on the surface charge and aggregation of silver nanoparticles suspensions. *Environ. Sci. Technol.* **44**, 1260–1266 (2010).
47. Timerbaev, A. R., Kuznetsova, O. V. & Keppler, B. K. Current trends and challenges in analysis and characterization of engineered nanoparticles in seawater. *Talanta* **226**, 122201 (2021).
48. Stephan, C. NOTE ICP - Mass Spectrometry Rapid Measurement of Nanoparticles in Seawater using Single Particle ICP-MS with All Matrix Solution.
49. Laborda, F. *et al.* Detection, characterization and quantification of inorganic engineered nanomaterials: A review of techniques and methodological approaches for the analysis of complex samples. *Anal. Chim. Acta* **904**, 10–32 (2016).
50. Zucker, R. M., Massaro, E. J., Sanders, K. M., Degn, L. L. & Boyes, W. K. Detection of TiO2nanoparticles in cells by flow cytometry. *Cytom. Part A* **77**, 677–685 (2010).
51. Husen, A. & Siddiqi, K. S. Plants and microbes assisted selenium nanoparticles: Characterization and

application. *J. Nanobiotechnology* **12**, 1–10 (2014).

52. Kamnev, A. A., Mamchenkova, P. V., Dyatlova, Y. A. & Tugarova, A. V. FTIR spectroscopic studies of selenite reduction by cells of the rhizobacterium Azospirillum brasilense Sp7 and the formation of selenium nanoparticles. *J. Mol. Struct.* **1140**, 106–112 (2017).
53. Laborda, F. *et al.* Detection, characterization and quantification of inorganic engineered nanomaterials: A review of techniques and methodological approaches for the analysis of complex samples. *Anal. Chim. Acta* **904**, 10–32 (2016).
54. Moreno-Martin, G., Pescuma, M., Pérez-Corona, T., Mozzi, F. & Madrid, Y. Determination of size and mass-and number-based concentration of biogenic SeNPs synthesized by lactic acid bacteria by using a multimethod approach. *Anal. Chim. Acta* **992**, 34–41 (2017).
55. Mitrano, D. M. *et al.* Silver nanoparticle characterization using single particle ICP-MS (SP-ICP-MS) and asymmetrical flow field flow fractionation ICP-MS (AF4-ICP-MS). *J. Anal. At. Spectrom.* **27**, 1131–1142 (2012).
56. Sötebier, C. A., Weidner, S. M., Jakubowski, N., Panne, U. & Bettmer, J. Separation and quantification of silver nanoparticles and silver ions using reversed phase high performance liquid chromatography coupled to inductively coupled plasma mass spectrometry in combination with isotope dilution analysis. *J. Chromatogr. A* **1468**, 102–108 (2016).
57. Loeschner, K. *et al.* Absorption, distribution, metabolism and excretion of selenium following oral administration of elemental selenium nanoparticles or selenite in rats. *Metallomics* **6**, 330–337 (2014).
58. Gartman, A. *et al.* The role of nanoparticles in mediating element deposition and transport at hydrothermal vents. *Geochim. Cosmochim. Acta* **261**, 113–131 (2019).
59. Wadhwani, S. A. *et al.* Green synthesis of selenium nanoparticles using Acinetobacter sp. SW30: Optimization, characterization and its anticancer activity in breast cancer cells. *Int. J. Nanomedicine* **12**, 6841–6855 (2017).
60. Jiménez-Lamana, J. *et al.* Detection and characterization of biogenic selenium nanoparticles in selenium-rich yeast by single particle ICPMS. *J. Anal. At. Spectrom.* **33**, 452–460 (2018).
61. Álvarez-Fernández García, R. *et al.* Addressing the presence of biogenic selenium nanoparticles in yeast cells: Analytical strategies based on ICP-TQ-MS. *Analyst* **145**, 1457–1465 (2020).
62. Pergantis, S. A., Jones-lepp, T. L. & Heithmar, E. M. Hydrodynamic Chromatography Online with Single Particle- Inductively Coupled Plasma Mass Spectrometry for Ultratrace Detection of Metal-Containing Nanoparticles. (2012).
63. Huynh, K. A., Siska, E., Heithmar, E., Tadjiki, S. & Pergantis, S. A. Detection and Quanti fi cation of Silver Nanoparticles at Environmentally Relevant Concentrations Using Asymmetric Flow Field − Flow Fractionation Online with Single Particle Inductively Coupled Plasma Mass Spectrometry. (2016). doi:10.1021/acs.analchem.6b00764
64. Samontha, A., Shiowatana, J. & Siripinyanond, A. Particle size characterization of titanium dioxide in sunscreen products using sedimentation field-flow fractionation-inductively coupled plasma-mass

spectrometry. *Anal. Bioanal. Chem.* **399**, 973–978 (2011).

65. Carazzone, C., Raml, R. & Pergantis, S. A. Online with Inductively Coupled Plasma-Mass Spectrometry for Sizing Large Proteins , DNA , and Nanoparticles. **80**, 5812–5818 (2008).
66. Size, K. Size and elemental composition of nanoparticles using ion mobility. **27**, (2012).
67. Sötebier, C. A. *et al.* Combination of single particle ICP-QMS and isotope dilution analysis for the determination of size, particle number and number size distribution of silver nanoparticles. *J. Anal. At. Spectrom.* **31**, 2045–2052 (2016).
68. Laborda, F., Bolea, E. & Jiménez-Lamana, J. Single particle inductively coupled plasma mass spectrometry: A powerful tool for nanoanalysis. *Anal. Chem.* **86**, 2270–2278 (2014).
69. Stephan, C. Single Particle ICP-MS. *PerkinElmer* **4**, 88 (2015).
70. Candás-Zapico, S., Kutscher, D. J., Montes-Bayón, M. & Bettmer, J. Single particle analysis of TiO2in candy products using triple quadrupole ICP-MS. *Talanta* **180**, 309–315 (2018).
71. Lim, J. H. *et al.* Detection and characterization of SiO2 and TiO2 nanostructures in dietary supplements. *J. Agric. Food Chem.* **63**, 3144–3152 (2015).
72. Jiménez-Lamana, J. *et al.* Detection and characterization of biogenic selenium nanoparticles in selenium-rich yeast by single particle ICPMS. *J. Anal. At. Spectrom.* **33**, 452–460 (2018).
73. Witzler, M., Küllmer, F. & Günther, K. Validating a Single-Particle ICP-MS Method to Measure Nanoparticles in Human Whole Blood for Nanotoxicology. *Anal. Lett.* **51**, 587–599 (2018).
74. Abad-Alvaro, I., Bolea, E., Laborda, F. & Castillo, J. R. An ICP-MS-based platform for release studies on silver-based nanomaterials. *J. Anal. At. Spectrom.* **32**, 1101–1108 (2017).
75. Tuoriniemi, J., Cornelis, G. & Hassellöv, M. Size discrimination and detection capabilities of single-particle ICPMS for environmental analysis of silver nanoparticles. *Anal. Chem.* **84**, 3965–3972 (2012).
76. Laborda, F., Bolea, E. & Jiménez-Lamana, J. Single particle inductively coupled plasma mass spectrometry for the analysis of inorganic engineered nanoparticles in environmental samples. *Trends Environ. Anal. Chem.* **9**, 15–23 (2016).
77. Tsiola, A. *et al.* Low-dose addition of silver nanoparticles stresses marine plankton communities. *Environ. Sci. Nano* **5**, 1965–1980 (2018).
78. Tsiola, A. *et al.* The impact of silver nanoparticles on marine plankton dynamics: Dependence on coating, size and concentration. *Sci. Total Environ.* **601**–**602**, 1838–1848 (2017).
79. Kadar, E. *et al.* Colloidal stability of nanoparticles derived from simulated cloud-processed mineral dusts. *Sci. Total Environ.* **466**–**467**, 864–870 (2014).
80. Amable, L., Stephan, C., Smith, S. & Merrifield, R. An Introduction to Single Cell ICP-MS Analysis. *White Pap.* 1–5 (2017).
81. Ho, K.-S. & Chan, W.-T. Time-resolved ICP-MS measurement for single-cell analysis and on-line cytometry. *J. Anal. At. Spectrom.* **25**, 1114 (2010).
82. Corte Rodríguez, M., Álvarez-Fernández García, R., Blanco, E., Bettmer, J. & Montes-Bayón, M. Quantitative Evaluation of Cisplatin Uptake in Sensitive and Resistant Individual Cells by Single-Cell

ICP-MS (SC-ICP-MS). *Anal. Chem.* acs.analchem.7b02746 (2017). doi:10.1021/acs.analchem.7b02746

83. Zheng, L. N. *et al.* Quantitative analysis of Gd@C82(OH)22 and cisplatin uptake in single cells by inductively coupled plasma mass spectrometry. *Anal. Bioanal. Chem.* **407**, 2383–2391 (2015).
84. Zheng, L. N. *et al.* Determination of quantum dots in single cells by inductively coupled plasma mass spectrometry. *Talanta* **116**, 782–787 (2013).
85. Tsiola, A. *et al.* Low-dose addition of silver nanoparticles stresses marine plankton communities. *Environ. Sci. Nano* **5**, 1965–1980 (2018).
86. Fouquet, Y. *et al.* Hydrothermal activity and metallogenesis in the Lau back-arc basin. *Nature* **349**, 778–781 (1991).
87. Fouquet, Y. Hydrothermal activity in the Lau back-arc basin: sulfides and water chemistry. *Geology* **19**, 303–306 (1991).
88. Hsu-Kim, H., Mullaugh, K. M., Tsang, J. J., Yucel, M. & Luther, G. W. Formation of Zn- and Fe-sulfides near hydrothermal vents at the Eastern Lau Spreading Center: Implications for sulfide bioavailability to chemoautotrophs. *Geochem. Trans.* **9**, 1–14 (2008).
89. Yücel, M., Gartman, A., Chan, C. S. & Luther, G. W. Hydrothermal vents as a kinetically stable source of iron-sulphide-bearing nanoparticles to the ocean. *Nat. Geosci.* **4**, 367–371 (2011).
90. Gartman, A., Findlay, A. J. & Luther, G. W. Nanoparticulate pyrite and other nanoparticles are a widespread component of hydrothermal vent black smoker emissions. *Chem. Geol.* **366**, 32–41 (2014).
91. Findlay, A. J. *et al.* Iron and sulfide nanoparticle formation and transport in nascent hydrothermal vent plumes. *Nat. Commun.* **10**, 1–7 (2019).
92. Estes, E. R. *et al.* Abiotic synthesis of graphite in hydrothermal vents. *Nat. Commun.* **10**, (2019).
93. Houk, R. S. Inductively Coupled Argon Plasma as an Ion Source for Mass Spectrometric Determination of Trace Elements. *Anal. Chem.* **52**, 2283–2289 (1980).
94. Limbeck, A. *et al.* Recent advances in quantitative LA-ICP-MS analysis: Challenges and solutions in the life sciences and environmental chemistry ABC Highlights: Authored by Rising Stars and Top Experts. *Anal. Bioanal. Chem.* **407**, 6593–6617 (2015).
95. MacHado, R. C. *et al.* Solid sampling: Advantages and challenges for chemical element determination-A critical review. *J. Anal. At. Spectrom.* **35**, 54–77 (2020).
96. Sader, J. A. & Ryan. Advances in ICP-MS Technology and the Application of Multi-Element Geochemistry to Exploration. *Proc. Explor.* **17**, 541–552 (2017).
97. Ohata, M. & Nishiguchi, K. Research progress on gas to particle conversion-gas exchange ICP-MS for direct analysis of ultra-trace metallic compound gas. *Anal. Sci.* **34**, 657–666 (2018).
98. Thomas, R. A beginner's guide to ICP-MS. *Spectrosc. (Santa Monica)* **17**, 36–41 (2002).
99. Thomas, R. Spectroscopy tutorial - A beginner's guide to ICP-MS - Part II: The sample-introduction system. *Spectroscopy* **16**, 56-+ (2001).
100. Miyashita, S. ichi *et al.* High transport efficiency of nanoparticles through a total-consumption sample introduction system and its beneficial application for particle size evaluation in single-particle ICP-MS.

Anal. Bioanal. Chem. **409**, 1531–1545 (2017).

101. Thomas, R. A beginner's guide to ICP-MS - Part III: The plasma source. *Spectroscopy* **16**, 26-+ (2001).
102. Thomas, R. Part IV: The interface region. *Spectrosc. tutorial. A Beginner's Guid. to ICP-MS* **16**, 26–34 (2001).
103. Thomas, R. A Beginner's Guide to ICP-MS - Part V: The Ion Focusing System. *Spectroscopy* **16**, 38–44 (2001).
104. Thomas, R. A Beginner's Guide to ICP-MS Part VI — The Mass Analyzer. *Spectrosc. Tutor.* **16**, 38–42 (2001).
105. Thomas, R. TUTORIAL: A Beginner's Guide to ICP-MS (XIII). *Spectroscopy* **16**, 22–27 (2001).
106. Thomas, R. A Beginner ' s Guide to ICP-MS - Part VII: Mass Analyzers: Time-of-Flight Technology. *Spectroscopy* **17**, 36–41 (2001).
107. Thomas, R. A beginner's guide to ICP-MS: Part X - Detectors. *Spectrosc. (Santa Monica)* **17**, 34–39 (2002).
108. May, T. W., Wiedmeyer, R. H., Survey, U. S. G. & Division, B. R. full-text ICP interferences. *At. Spectrosc.* **19**, 150–155 (1998).
109. Thomas, R. A Beginner's guide to ICP-MS: Part XII - A review of interferences. *Spectrosc. (Santa Monica)* **17**, 24–31 (2002).
110. Bolea-Fernandez, E., Balcaen, L., Resano, M. & Vanhaecke, F. Overcoming spectral overlap: Via inductively coupled plasma-tandem mass spectrometry (ICP-MS/MS). A tutorial review. *J. Anal. At. Spectrom.* **32**, 1660–1679 (2017).
111. Somoano-Blanco, L., Rodríguez-González, P., Pröfrock, D., Prange, A. & Ignacio García Alonso, J. Comparison of different mass spectrometric techniques for the determination of polychlorinated biphenyls by isotope dilution using 37Cl-labelled analogues. *Anal. Methods* **7**, 9068–9075 (2015).
112. Instrument, W. Triple Quadrupole ICP-MS or Single Quadrupole ICP-MS? Which Instrument is Right for Me? 1–5 (2009).
113. Woods, G. & McCurdy, E. Triple-Quadrupole ICP-MS Provides Improved Performance for Difficult Polyatomic and Isobaric Overlaps on Lead Isotopes. *Spectroscopy* **28**, s28–s34 (2013).
114. Mozhayeva, D. & Engelhard, C. A critical review of single particle inductively coupled plasma mass spectrometry-A step towards an ideal method for nanomaterial characterization. *J. Anal. At. Spectrom.* **35**, 1740–1783 (2020).
115. Montaño, M. D., Olesik, J. W., Barber, A. G., Challis, K. & Ranville, J. F. Single Particle ICP-MS: Advances toward routine analysis of nanomaterials. *Anal. Bioanal. Chem.* **408**, 5053–5074 (2016).
116. Pace, H. E. *et al.* Determining Transport Efficiency for the Purpose of Counting and Sizing Nanoparticles via Single Particle Inductively Coupled Plasma Mass Spectrometry (vol 83, pg 9361, 2011). *Anal. Chem.* **84**, 4633 (2012).
117. Laborda, F., Jiménez-Lamana, J., Bolea, E. & Castillo, J. R. Selective identification, characterization and determination of dissolved silver(i) and silver nanoparticles based on single particle detection by

inductively coupled plasma mass spectrometry. *J. Anal. At. Spectrom.* **26**, 1362–1371 (2011).

118. Lee, S. *et al.* Nanoparticle size detection limits by single particle ICP-MS for 40 elements. *Environ. Sci. Technol.* **48**, 10291–10300 (2014).
119. Franze, B., Strenge, I. & Engelhard, C. Single particle inductively coupled plasma mass spectrometry: Evaluation of three different pneumatic and piezo-based sample introduction systems for the characterization of silver nanoparticles. *J. Anal. At. Spectrom.* **27**, 1074–1083 (2012).
120. Degueldre, C., Favarger, P. Y. & Wold, S. Gold colloid analysis by inductively coupled plasma-mass spectrometry in a single particle mode. *Anal. Chim. Acta* **555**, 263–268 (2006).
121. Laborda, F., Bolea, E. & Jiménez-Lamana, J. Single particle inductively coupled plasma mass spectrometry: A powerful tool for nanoanalysis. *Anal. Chem.* **86**, 2270–2278 (2014).
122. Laborda, F., Jiménez-Lamana, J., Bolea, E. & Castillo, J. R. Critical considerations for the determination of nanoparticle number concentrations, size and number size distributions by single particle ICP-MS. *J. Anal. At. Spectrom.* **28**, 1220–1232 (2013).
123. Abad-Álvaro, I. *et al.* Evaluation of number concentration quantification by single-particle inductively coupled plasma mass spectrometry: microsecond vs. millisecond dwell times. *Anal. Bioanal. Chem.* **408**, 5089–5097 (2016).
124. Gundlach-Graham, A., Hendriks, L., Mehrabi, K. & Günther, D. Monte Carlo Simulation of Low-Count Signals in Time-of-Flight Mass Spectrometry and Its Application to Single-Particle Detection. *Anal. Chem.* **90**, 11847–11855 (2018).
125. Tanner, M. Shorter signals for improved signal to noise ratio, the influence of Poisson distribution. *J. Anal. At. Spectrom.* **25**, 405–407 (2010).
126. Spectrometry, M. ICP – Mass Spectrometry. 3–4
127. Toncelli, C., Mylona, K., Tsapakis, M. & Pergantis, S. A. Flow injection with on-line dilution and single particle inductively coupled plasma-mass spectrometry for monitoring silver nanoparticles in seawater and in marine microorganisms. *J. Anal. At. Spectrom.* **31**, 1430–1439 (2016).
128. Chronakis M.I, Mavrakis E, Perganis S.A, García, R. R. Á. & Stephan, C. Monitoring the Fate of Silver Nanoparticles in Seawater Using Single Particle ICP-MS, PerkinElmer (2019).
129. Shaff, J. E., Schultz, B. A., Craft, E. J., Clark, R. T. & Kochian, L. V. GEOCHEM-EZ: A chemical speciation program with greater power and flexibility. *Plant Soil* **330**, 207–214 (2010).
130. Weiss, C. J. A Creative Commons Textbook for Teaching Scientific Computing to Chemistry Students with Python and Jupyter Notebooks. *J. Chem. Educ.* (2021). doi:10.1021/acs.jchemed.0c01071
131. Mozhayeva, D. & Engelhard, C. A quantitative nanoparticle extraction method for microsecond time resolved single-particle ICP-MS data in the presence of a high background. *J. Anal. At. Spectrom.* **34**, 1571–1580 (2019).
132. Adegboyega, N. F. *et al.* Enhanced formation of silver nanoparticles in Ag+-NOM-iron(II, III) systems and antibacterial activity studies. *Environ. Sci. Technol.* **48**, 3228–3235 (2014).
133. Adegboyega, N. F. *et al.* Interactions of aqueous Ag+ with fulvic acids: Mechanisms of silver

nanoparticle formation and investigation of stability. *Environ. Sci. Technol.* **47**, 757–764 (2013).

134. Hou, W. C., Stuart, B., Howes, R. & Zepp, R. G. Sunlight-driven reduction of silver ions by natural organic matter: Formation and transformation of silver nanoparticles. *Environ. Sci. Technol.* **47**, 7713–7721 (2013).
135. Li, L., Zhou, Q., Geng, F., Wang, Y. & Jiang, G. Formation of nanosilver from silver sulfide nanoparticles in natural waters by photoinduced Fe(II, III) redox cycling. *Environ. Sci. Technol.* **50**, 13342–13350 (2016).
136. Michael E.Q. Pilson, *An introduction to the Chemistry of the Sea*, second edition (1981).
137. Kuwabara, J. S., Van Geen, A., McCorkle, D. C. & Bernhard, J. M. Dissolved sulfide distributions in the water column and sediment pore waters of the Santa Barbara Basin. *Geochim. Cosmochim. Acta* **63**, 2199–2209 (1999).
138. Adeleye, A. S., Oranu, E. A., Tao, M. & Keller, A. A. Release and detection of nanosized copper from a commercial antifouling paint. *Water Res.* **102**, 374–382 (2016).
139. Malhotra, N. *et al.* Review of copper and copper nanoparticle toxicity in fish. *Nanomaterials* **10**, 1–28 (2020).
140. Yang, L. & Wang, W. X. Comparative contributions of copper nanoparticles and ions to copper bioaccumulation and toxicity in barnacle larvae. *Environ. Pollut.* **249**, 116–124 (2019).
141. Van Den Berg, C. M. G. Determination of copper complexation with natural organic ligands in seawater by equilibration with MnO2 II. Experimental procedures and application to surface seawater. *Mar. Chem.* **11**, 323–342 (1982).
142. Batley, G. E. & Florence, T. M. Determination of the chemical forms of dissolved cadmium, lead and copper in seawater. *Mar. Chem.* **4**, 347–363 (1976).